Institute for Marine and Atmospheric Research Utrecht (IMAU)
at Utrecht University

Master's Thesis in Climate Physics (M.Sc.)

Impact of Climate Change on Summertime Air Quality in the Netherlands

An Analysis of Changes in Ozone, Fine Particulate Matter, and Ammonia between now and 2050 under the High Climate Change Scenario RCP8.5 using WRF and EMEP4NL

by Johanna Knauf
Student ID: 5017831

December 7, 2022

Supervised by:
Prof. Dr. Guus Velders

Abstract

Air quality depends both on the emission of air pollutants and on local meteorological conditions. Climate change could therefore affect air quality on local to global scales through changes in meteorology. This study aims to determine the regional impact of climate change on summertime air quality for the Netherlands and to compare it to the effect of air pollutant emission reductions. The focus is on changes in ozone, fine particulate matter, and ammonia concentrations.

By nudging a weather model (WRF) with the output of a high climate change scenario (HadGEM2-ES RCP8.5), high resolution meteorology fields are obtained for a recent (2008-2017) and future (2050-2059) climate. It is shown that in this scenario climate change leads to a 2.5-fold increase in the number of stagnant days and to an increase in the daytime mixing layer height in the simulated summer period.

Simulations are performed with these two meteorological datasets and two emission datasets. The emissions are based on reported air pollutant emissions from 2008-2017 and on a maximum feasible reduction scenario for 2050 (ECLIPSE V6b MFR). Different combinations of the meteorology and emissions are then used as input for a nested chemical transport model (EMEP4NL). For a high future climate change scenario the simulations show an increase of 11% in the daily maximum 8-hour mean of ozone and a decrease of 6% in daily mean ammonia and of 25% in daily mean fine particulate matter concentrations in the Netherlands. Emission reduction measures alone lead to a decrease of 20% in ammonia and of 48% in fine particulate matter concentrations and to a shift in the ozone formation regime and local increases of ozone in urban areas. The combination of climate change and emission reduction measures reinforces the reductions in ammonia (-28%) and fine particulate matter (-59%) concentrations. For ozone, climate change has a detrimental effect on the benefit of emission reduction measures, but emission reduction measures half the mean effect of climate change on ozone concentrations in the Netherlands.

Contents

All shell scripts and python codes written for this thesis can be requested from the author.

Acknowledgements

Thanks to the World Climate Research Programme's working group on coupled modelling which coordinated CMIP5 and to the funding agencies who support CMIP5. I thank the HadGEM2-ES modelling group for their work and for making their model output publicly available. I recognize the work of the Earth System Grid Federation (ESGF) which maintains the corresponding data centres. I would like to thank the development team of WRF. In addition, I would like to thank the EMEP modelling groups at MSC-W for developing the EMEP CTM and CEIP for coordinating the emission reports. I would also like to recognize the efforts of IIASA to make GAINS emission data available. Many thanks to the developers of the Climate Data Operator (cdo) software, of the NCAR command language (ncl), and of the matplotlib, cartopy, pandas, numpy, scipy, seaborn, and netCDF4 python packages.

This study would not have been possible without the support, patience, and expertise of my supervisor Guus Velders, both at IMAU and RIVM. Thank you for believing in me when the modelling took longer than planned, for giving me the freedom to make my own decisions, and for always taking the time to meet up and discuss my progress and obstacles.

Special thanks to Eric van der Swaluw at RIVM for your patience about the nudging settings in WRF, for always pointing me to the right person for my questions, and for helping me to understand the changes in nitrogen. Thank you to Wilco de Vries at RIVM for helping me with the technical set-up to run WRF and EMEP simulations and for trusting me with large computational resources.

I would like to thank Ruben Verweij and Shelley van der Graaf at RIVM for taking the time to explain WRF and EMEP to me and for helping me to solve technical issues. I could not have done this without you! Thank you to Sebastiaan Hazelhorst at RIVM for your help with the emissions.

This thesis project was incorporated into the framework of an internship at RIVM. There I had the honour of getting to know people from different groups within the department for environmental quality (MIL), to get some insights into their work and to be included as an equal member. Thank you for showing me your work, for answering my questions, and for being patient with my Dutch skills.

The APCG group at IMAU showed me the practical side of atmospheric chemistry and gave me some insights about how the job of a researcher looks like. You have made me eager to continue on this path myself.

I am grateful for the advice from Xiaodong Chen at PNNL and Massimo Vieno at CEH about using climate scenario output as input for WRF in the beginning of the project and for the discussion of results with William Collins at the University of Reading.

Thank you to my friends and the other master's students for relaxing together in breaks, for shared laughs, and for having an open ear for me. Lastly, I would like to thank my family for buffering my frustrations and listening to my enthusiasm during the project.

Acronyms

APCG	Atmospheric Physics and Chemistry Group.
ARW	Advanced Research WRF solver.
CEH	UK Centre for Ecology and Hydrology.
CEIP	EMEP Centre on Emission Inventories and Projections.
CMIP5	5th Climate Model Intercomparison Project.
CTM	Chemical Transport Model.
ECLIPSE	Evaluating the CLimate and Air Quality ImPacts of Short-livEd Pollutants project.
EMEP	European Monitoring and Evaluation Programme for Transboundary Long-Range Transported Air Pollutants.
EMEP4NL	EMEP model configuration for the Netherlands.
EU	European Union.
HadGEM2-ES	Earth System configuration of the Hadley Centre Global Environment Model version 2.
IIASA	International Institute for Applied System Analysis.
IMAU	Institute for Marine and Atmospheric Research Utrecht.
JJA	June to August.
KNMI	Koninklijk Nederlands Meteorologisch Instituut.
MACC_III	Monitoring Atmospheric Composition and Climate Inventory version 3.
MFR	Maximum Feasible Reduction scenario.
MIL	Centrum Milieukwaliteit.
MSC-W	Meteorological Synthesizing Centre-West.
PNNL	Pacific Northwest National Laboratory.
RCP	Representative Concentration Pathway.
RIVM	Dutch National Institute for Public Health and the Environment.
SNAP	Selected Nomenclature for reporting of Air Pollutants.
TNO	Netherlands Organisation for Applied Scientific Research.
WMO	World Meteorological Organization.
WPS	WRF Preprocessing System.
WRF	Weather Research and Forecasting model.

Chemical Formulas

Chemical formula	Name
CH_4	Methane
CO	Carbon Monoxide
CO_2	Carbon Dioxide
CO_2-EQ	Carbon Dioxide Equivalent (the amount of CO_2that would have the same global warming potential as all greenhouse gases combined)
HNO_3	Nitric Acid
H_2SO_4	Sulphuric Acid
HO_2	Hydroperoxyl Radical
H_2O_2	Hydrogen Peroxide
N_2	Molecular Nitrogen
NH_3	Ammonia
NH_4^+	Ammonium
NO	Nitric Oxide
NO_2	Nitrogen Dioxide
NO_x	Nitrogen Oxides (NO + NO_2)
NO_3^-	Nitrate
O_2	Molecular Oxygen
O_3	Ozone
OH	Hydroxyl Radical
SO_2	Sulphur Dioxide
SO_x	Sulphur Oxides
SO_4^{2-}	Sulphate
VOC	Volatile Organic Compound
HFCs	Hydrofluorocarbons
$PM_{2.5}$	Particulate Matter $< 2.5\mu m$
PM_{10}	Particulate Matter $< 10\mu m$

Table 1: Chemical formulas and names

1 Introduction and Motivation

Since Wu et al. (2008) introduced the concept of a "climate change penalty" for air quality, there has been a growing field of research about the impact of climate change on air quality under different climate and emission scenarios with varying results (e.g., Jacob and Winner, 2009; Colette et al., 2015; Lacressonnière et al., 2016; Watson et al., 2016). Reasons for this lie in the high spatial and temporal variability of air pollutant concentrations, the dependence on assumptions about emission and climate changes, and difficulties in including all relevant chemical processes for the formation, reaction, and deposition of air pollutants. The aim of this study is to determine the regional impact of climate change on summertime air quality in comparison to the effects of air pollutant emission reductions using the EMEP model configuration for the Netherlands (EMEP4NL: van der Swaluw et al., 2021) under the climate change scenario RCP 8.5 (Riahi et al., 2011).

This chapter introduces the topics of climate change (Section 1.1) and air pollution (Section 1.2), reviews the literature about the impact of climate change on air quality (Section 1.3), outlines the scope and research questions of this thesis (Section 1.4), and gives an overview of the structure of this study (Section 1.5).

1.1 Climate Change

Ongoing emissions of greenhouse gases by humankind induce a radiative forcing to the Earth's climate system. The current state of knowledge about changes in the climate system and a range of future scenarios can be found in the IPCC Sixth Assessment Report (IPCC, 2021). Since 1850–1900 climate change has already increased global mean temperatures by about 1.1°C (WMO, 2022). In the Netherlands annual mean temperatures have increased by 2.1 ± 0.6°C in the last century (CLO, 2020). These changes in the mean state of the climate are partly hidden from human perception by natural variability and become more apparent in the extremes. One example for this is that 31% of the burden of heat-related mortality in the Netherlands from 1991 to 2018 can be attributed to climate change (Mitchell, 2021).

1.2 Air Pollution

Ground level ozone (O_3), nitrogen dioxide (NO_2), and particulate matter (PM) are widely recognised as unhealthy for human health, so that both the World Health Organization (WHO, 2021) and the European Union (EU, 2022) have set air quality standards to limit exposure to these pollutants (Table 2). Particulate matter is an umbrella term for suspended solid particles and liquid droplets in air and is often referred to as "aerosol" (Seinfeld and Pandis, 2016). It consists of inorganic and organic compounds which can be emitted directly from anthropogenic and natural sources or formed from precursor gases. It can be further divided into PM_{10} and $PM_{2.5}$ for sizes smaller than 10 and 2.5 µm.

Both particulate matter and NO_2 concentrations are influenced by ammonia concentrations. NH_3 serves as a nutrient for plants but affects their diversity at high concentrations. Heathlands, for example, are adversely affected from annual and monthly mean concentrations of 8 µg/m^3 and 23 µg/m^3, respectively (van der Eerden et al., 1991). While $PM_{2.5}$ and NO_2 standards are typically defined for daily and yearly mean concentrations, ozone air quality standards usually define a threshold for the daily maximum 8-hour mean. This standard takes the photochemical formation of ozone during the day and the persistence of high concentrations over several hours into account (Rombout et al., 1986).

	Averaging period	EU	WHO
O_3	8 hours	120 µg/m^3	100 µg/m^3
NO_2	1 year 1 day	40 µg/m^3	10 µg/m^3 25 µg/m^3
$PM_{2.5}$	1 year 1 day	20 µg/m^3	5 µg/m^3 15 µg/m^3

Table 2: Overview of ambient air quality standards (EU, 2022; WHO, 2021).

99% of the world's population are breathing air that contains unhealthy levels of $PM_{2.5}$ and NO_2 (WHO, 2022). In the European Union, 96% of the urban population was exposed to levels of $PM_{2.5}$, 95% to levels of O_3, and 89% to levels of NO_2 in 2020 that are above the WHO guidelines (EEA, 2022). In the Netherlands, air quality has improved significantly over the past decades as a result of emission reductions. The loss of life expectancy from air pollution decreased from 48 months in 1980 to 12 months in 2015 (Velders et al., 2020). If no air pollutant reduction policies would have been implemented, the loss of life expectancy could have reached 85 months (Velders et al., 2020). This implies that air quality policies increased life expectancy by around 6 years. To improve air quality further, the EU has launched a "Zero Pollution Action Plan" which includes a target to reduce premature deaths caused by air pollution by 55% until 2030 (EC, 2022).

1.3 Air Quality in a Changing Climate

Climate change and air pollution are interconnected in several ways. Some air pollutants and air pollutant precursors (e.g., methane, black carbon, HFCs) contribute a positive radiative forcing to the climate system and lead to warming, while others (e.g., NO_x, SO_2, organic carbon, NH_3) contribute a negative radiative forcing associated with cooling (Figure 6.12 in IPCC, 2021). Some of the latter components can contribute indirectly to warming through their chemical reactions with other species. For example, higher NO_x concentrations lead to the formation of tropospheric ozone which has a positive radiative impact (Lammel and Graßl, 1995). Climate change in turn affects local meteorological fields which change the mixing, transport, reaction speed, and deposition of air pollutants. Additionally, climate change can lead to changes in biogenic emissions of precursor gases. The importance of this interdependence has recently been recognised by the WMO which

started publishing a yearly "Air Quality and Climate Bulletin" in 2021 (WMO, 2021; WMO, 2022).

Wu et al. (2008) defined the difference between emission controls needed to reach an ozone air quality target in a present-day climate versus a future climate as the "climate change penalty". This term, sometimes also referred to as "climate penalty", evolved to be used not only for the detrimental effect of climate change on the effectiveness of measures to reduce ozone levels but also on the effectiveness of ammonia (Skjøth and Geels, 2013) and $PM_{2.5}$ (Westervelt et al., 2016) controls. Most studies agree that the climate penalty is small compared to the benefits of emission reduction measures for air quality (e.g., in Tagaris et al., 2007; Colette et al., 2013; Watson et al., 2016). For cases in which climate change leads to less air pollution, the term "climate benefit" is used.

Ozone

The results of previous studies analysing the impact of climate change on ozone concentrations vary widely in magnitude but largely agree on an increase of ozone in a warmer climate. The results of Watson et al. (2016) lie on the lower end. They analyse the effect of climate change on ozone concentrations by comparing a scenario with 2°C of warming with the climate of 1971-2000 both with constant emissions of a 2050 scenario based on current legislation. Climate change is not found to have a statistically significant effect, with up to 0.8 ppb of ozone increase in summer. This means that the air quality improvements induced by emission reduction policies would not be threatened by climate change. In Colette et al. (2015) the robustness of the ozone climate penalty for Europe is assessed. They conclude that the penalty across models and simulations is robust and stress the importance of biogenic isoprene emissions for its magnitude. The results indicate an increase of summertime ozone due to climate change of at most 5 ppb by the end of the century. On the upper end, Lacressonnière et al. (2014) find an increase in O_3 of 12.7 µg/m^3 (approximately 6.4 ppb) in western Europe in summer (June to September), when modelling the combined effect of warming under RCP8.5 and emission changes until 2050. These changes are mostly caused by an increase of the stratosphere-troposphere transport of ozone in a future climate which outweighs the changes in the chemical budget of ozone. According to Jacob and Winner (2009), the increased probability for persistent and stagnant weather patterns over the mid-latitudes could lead to higher concentrations of ozone. They find that the increase of ozone in a future climate is largely due to warming and could be exacerbated in high-pollution events. In a study by Doherty et al. (2013), ozone increases strongly in polluted areas through the effect of climate change. This leads to the need of reducing precursor emissions by up to 60% in western Europe to offset the increase of ozone by climate change until the end of this century.

Ammonia

Hole and Engardt (2008) study the effect of climate change on wet and dry deposition of oxidised and reduced nitrogen species for northern Europe. They find a spatially variable pattern depending on the local prominence of precipitation or of temperature changes for the deposition of nitrogen species. Sutton et al. (2013) describe the climate sensitivity of NH_3 deposition and NH_3 emission and find an increase of NH_3 in a warmer climate. This finding is supported by Skjøth and Geels (2013). The dependence of nitrogen deposition on meteorological variable fields is included in this study. The dependence of NH_3 emissions on meteorological parameters is not taken into account and could lead to biased results (Section 6.1.3).

$PM_{2.5}$

Lacressonnière et al. (2016) model the influence of 2°C of warming on $PM_{2.5}$ concentrations in Europe. They conclude that the projected changes are not robust but likely small and caused by changes in dust, sea salt, and biogenic VOC emissions. In a study by Park et al. (2020), the impact of climate change under scenario RCP8.5 by the end of this century is analysed with seven models. They find a likely increase in the annual mean of $PM_{2.5}$ in most regions of the world but a decrease for the Netherlands.

1.4 Scope of this Thesis and Research Questions

Most previous studies focused on large-scale air quality changes due to climate change. The impact of climate change on air quality could manifest differently for a smaller region like the Netherlands with its high population density and large fraction of agriculturally used areas. This study aims to fill this gap. As a first approach, it investigates a maximum possible impact of climate change and air pollutant reductions on summertime air quality in the Netherlands in northwestern Europe by using the high emission climate change scenario RCP8.5 and the ECLIPSE Maximum Feasible Reduction scenario (MFR) for 2050 (Stohl et al., 2015; Klimont et al., 2017; IEA, 2018; IIASA, 2019; Klimont et al., 2022).

The spatial and temporal resolution of the Earth System configuration of the Hadley Centre Global Environment Model version 2 (HadGEM2-ES: Jones et al., 2011; Martin et al., 2011) scenario RCP8.5 (Riahi et al., 2011) output is not high enough for a regional air quality analysis. Therefore, the Weather Research and Forecasting model (WRF: Skamarock et al., 2008) is nudged by HadGEM2-ES data to derive hourly fields of future meteorology with a resolution of around 5 km. These meteorological fields and two emission datasets are then used as input for the nested Chemical Transport Model (CTM) EMEP4NL. The use of two emission datasets, one of recently reported emissions and one of a maximum feasible reduction scenario for 2050, allows for a comparison of the effects

of climate change with the effects of emission regulations on air quality, as well as an assessment on the impact of climate change on the effectiveness of air pollutant emission reductions.

Research Questions

This study first serves as a feasibility study for acquiring future meteorology by nudging WRF with climate scenario output and aims to assess the validity of acquiring air quality information by nudging EMEP4NL with these data. This leads to the first two research questions:

1. Is nudging WRF with HadGEM2-ES RCP8.5 output suitable to generate meteorological input that is in alignment with observations for the past years?

2. Is nudging EMEP4NL with these meteorological fields a valid approach to study concentrations of air pollutants?

Following this, it aims to quantify the effect of climate change and emission reduction measures on air quality in the Netherlands. This analysis is guided by the these three research questions:

3. How are summertime levels of ozone, $PM_{2.5}$, and ammonia affected by climate change under the RCP8.5 scenario in the Netherlands until the 2050s?

4. How does the effect of climate change compare to the effect of strong air pollutant emission reductions on summertime air quality?

5. How is the effect of emission controls influenced by climate change and what is the effect of emission controls in a changing climate?

Based on the literature in Section 1.3, the following hypotheses are formed:

Related to 3.: Climate change alone leads to an increase in summertime ozone which is strongest in the more polluted areas. Changes in $PM_{2.5}$ are expected to behave inversely to changes in the frequency of precipitation. Ammonia is expected to increase with temperature and to be inversely related to the frequency of precipitation.

Related to 4.: The magnitude in changes for ozone, $PM_{2.5}$, and ammonia in a strong climate change scenario is smaller than in a strong air pollutant emission reductions scenario.

Related to 5.: The effectiveness of air pollutant emission reduction measures to decrease ozone concentrations weakens. The effect of climate change on ozone concentrations is mitigated when air pollutant emissions are reduced in addition. For ammonia and $PM_{2.5}$ this depends on the sign of changes due to climate change (see "Related to 3.").

1.5 Structure of this Study

Chapter 2 addresses conversions between units and types of humidity (Section 2.1), the formation of ozone (Section 2.2), the nitrogen cycle (Section 2.3), the formation of particulate matter (Section 2.4), and gives the theoretical background of air quality climate interactions (Section 2.5). Chapter 3 starts by outlining the simulations performed for this study (Section 3.1). This is followed by a description of the models WRF (Section 3.3) and EMEP4NL (Section 3.5) and the datasets for climate (Section 3.2), emissions (Section 3.4), and model validation (Section 3.6). The chapter concludes with an outline of the analysis methods (Section 3.7). The validity of the model results is assessed and discussed along research questions 1 and 2 in Chapter 4. In Chapter 5, the changes in the meteorological fields with climate change are analysed first (Section 5.1), then the effect of climate change on air quality (Section 5.2), the effect of air pollutant emission reductions on air quality (Section 5.3), and their combined influence (Section 5.4) is studied. These results are interpreted, discussed, and put into the context of previous studies along research questions 3 to 5 in Section 6. This chapter also includes an assessment of the methodological strengths and weaknesses of this study. The study ends with suggestions for further research (Section 7) and the conclusions (Section 8).

2 Theory

This chapter provides an overview of the general theoretical background for this thesis. It starts by providing formulas for the conversion between different ways to describe the amount of pollutants in the air and between different measures for humidity (Section 2.1). The section continues by outlining the formation of ozone (Section 2.2), the nitrogen cycle (Section 2.3), and the formation of $PM_{2.5}$ (Section 2.4). It concludes with the theoretical impact of climate change on air pollutant concentrations and their deposition (Section 2.5).

2.1 Conversions

Mixing Ratio and Concentrations

In this study ozone levels are given as a mixing ratio r_X or as a concentration c_X. The unit conversion is as follows (Seinfeld and Pandis, 2016):

$$c_X = \frac{p \cdot M_X \cdot r_X}{R \cdot T} \tag{1}$$

with Temperature T in K, the universal gas constant $R = 8.31 \frac{\text{Nm}}{\text{molK}}$, the surface atmospheric pressure $p = 1013$ hPa, and molar mass (M_X). For surface conditions at 20°C, for example, that means that 1 ppb of ozone translates to 1.99 µg/m^3.

Water Vapour Mixing Ratio and Specific Humidity

Water vapour mixing ratio (q) and specific humidity (hus) are used interchangeably in this study. This simplification is valid for most conditions because specific humidity and water vapour mixing ratio relate as follows (Mölders and Kramm, 2014):

$$hus = \frac{q}{1+q}. \tag{2}$$

With water vapour mixing ratios of up to 10^{-2} kg/kg this leads to deviations of up to 1% of the absolute value.

Water Vapour Mixing Ratio and Relative Humidity

The water vapour mixing ratio (q) is used as a measure for humidity in this study. Relative humidity ($h_{relative}$), which is a more important indicator for precipitation, also depends on temperature and pressure in the following way (WMO, 1966; Murray, 1967):

$$\epsilon = \frac{M_w}{M_{air}} \tag{3}$$

$$\text{Teten's equation} : e_s(T) = 6.11\text{hPa} \cdot e^{\frac{17.27 \cdot T}{T + 237.29\text{K}}} \tag{4}$$

$$r_w(p,T) = \frac{\epsilon \cdot e_s(T)}{p - e_s(T)} \tag{5}$$

$$h_{relative}(T,q,p) = 100 \cdot \frac{q}{r_w(p,T)} \cdot \frac{\epsilon + r_w(p,T)}{\epsilon + q} \tag{6}$$

with ϵ as the ratio of the molecular weights of water M_w and dry air M_{air}, the saturation vapour pressure e_s, the saturation water mixing ratio r_w in kg/kg, Temperature T in °C, pressure p in the same units as e_s, q as the water vapour mixing ratio in kg/kg, and the relative humidity $h_{relative}$ in %.

2.2 Ozone Formation

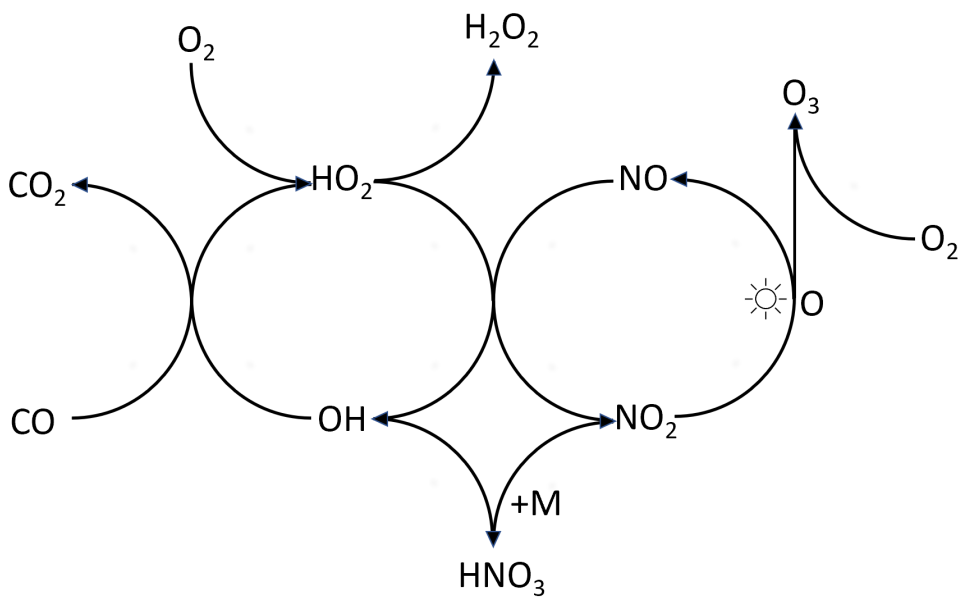

Figure 1: Chemical reactions involved in tropospheric ozone formation, based on Jacob (1999).

Ozone (O_3) is characterised as an air pollutant because it oxidises biological tissue and therefore harms human and ecosystem health (Jacob, 1999). It is formed in the atmosphere in the presence of carbon monoxide (CO) or precursors such as methane (CH_4) and volatile organic compounds (VOC) that lead to the formation of hydroperoxyl radicals (HO_2). CO reacts with an hydroxyl radical (OH) to carbon dioxide (CO_2) and atomic hydrogen (H), which forms HO_2 by reacting with molecular oxygen (O_2). In the presence of nitric oxide (NO), OH can be recovered in the reaction $NO+HO_2 \rightarrow NO_2+OH$. Nitrogen dioxide ($NO_2$) can then be photolysed to NO and atomic oxygen (O) which reacts with O_2 to O_3 (Jacob, 1999).

This cycle is limited in two ways: If NO_x concentrations are low, peroxyl radicals react with each other instead of with NO ($HO_2 + HO_2 \rightarrow H_2O_2 + O_2$). If NO_x concentrations are high, OH reacts with NO_2 to nitric acid ($OH + NO_2 + M \rightarrow HNO_3 + M$). Therefore ozone levels can be limited either by VOCs or by NO_x. Since the relationship of NO_x and VOC concentrations to ozone concentrations is not linear, it is important to know

whether the ozone formation is limited by NO_x or VOCs to understand changes in ozone concentrations (Jacob, 1999; Seinfeld and Pandis, 2016). In this study a ratio of 8:1 of VOC in ppbC to NO_x in ppb (Dodge, 1977) is used to differentiate between NO_x-limited (higher ratio) ozone formation and VOC-limited (lower ratio) ozone formation.

2.3 Nitrogen Cycle

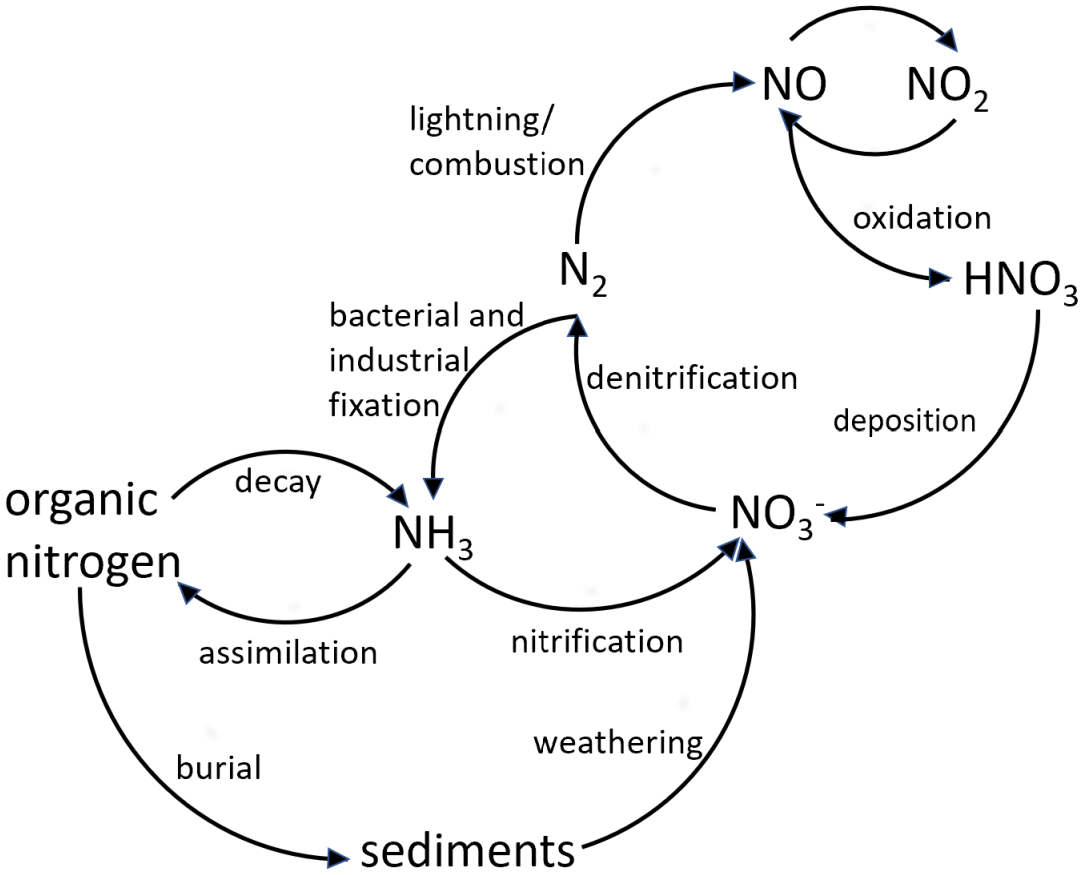

Figure 2: Processes involved in the nitrogen cycle, based on Jacob (1999).

The nitrogen cycle plays a role not only for levels of ammonia (NH_3) and nitrogen dioxide (NO_2) in the atmosphere, but also for the formation of ozone (Section 2.2) and $PM_{2.5}$ (Section 2.4). This section describes the main processes in the nitrogen cycle.

Atmospheric molecular nitrogen (N_2) is reduced to NH_3 by bacteria and industrial processes (Seinfeld and Pandis, 2016). NH_3 can then be oxidised to nitrate (NO_3^-) under aerobic conditions or forms ammonium which can be assimilated by plants. This organic nitrogen is either buried on the ocean floor and incorporated in sediments, or becomes biologically available again as NH_3 and ammonium (NH_4^+) by decay (Jacob, 1999). Additionally, molecular nitrogen forms NO in lightning and combustion processes, which is rapidly cycled with NO_2. Hence NO and NO_2 are often described jointly as NO_x. To-

gether with OH, NO_x can form nitric acid (see Section 2.2), which contributes to NO_3^- when washed out of the atmosphere. In anaerobic conditions bacteria use NO_3^- for the oxidation of organic components which leads to a release of N_2 back to the atmosphere. The deposition of reduced nitrogen (e.g. NH_3 and NH_4^+) and of oxidised nitrogen (e.g. NO_3^-) increases the nutrient content and lower pH of the soil (Jacob, 1999).

2.4 Particulate Matter Formation

$PM_{2.5}$ is differentiated into primary and secondary aerosols, depending on their formation processes. Primary aerosols, such as sea salt and dust, are directly emitted into the atmosphere by wind. Secondary aerosols are formed from precursor gases such as NH_3 and sulphuric acid (H_2SO_4). When these gases condensate and coagulate they form fine particulate matter (Jacob, 1999).

2.5 Effect of Climate Change on Air Quality

Climate change affects local meteorological conditions including temperature, wind, humidity, precipitation, cloud cover, and mixing layer height. Annual mean temperatures in northwestern Europe, for example, are expected to increase with climate change in the coming decades and summer (JJA) temperatures are expected to increase more strongly than winter temperatures across different scenarios (Figure 4.19 and 4.20 in IPCC, 2021). Projected summertime precipitation changes are not robust but tend to be negative for northwestern Europe in summer (Figure 4.13 and 2.24 in IPCC, 2021). According to Varotsos et al. (2013), the mixing layer height in Europe could increase slightly in western Europe until 2050.

These changes can affect air pollutant concentrations and the deposition in several ways. This section gives an overview of some of the main theoretical influences.

The Arrhenius expression describes the temperature dependence of rate coefficients for most bimolecular reactions (Akimoto, 2016):

$$k_r(T) = A \cdot e^{-E_a/RT}$$

with k_r as the rate constant, a pre-exponential factor A, the activation energy E_a, the universal gas constant R, and temperature T. This equation indicates that chemical reactions could speed up in a warmer climate.

Isoprene emissions increase with temperatures of up to around 40°C (Guenther et al., 1993). This could lead to an increase in VOCs in a future climate.

The equilibrium between ammonium nitrate and ammonia and nitric acid ($NH_4NO_3 \rightleftharpoons NH_3 + HNO_3$) is temperature dependent (Stelson et al., 1979). At higher temperatures the equilibrium shifts towards higher concentrations of NH_3.

Dry deposition of nitrogen depends on wind speed, humidity, wetness of the surface, and solar heating. It is therefore indirectly influenced by climate change (Finlayson-Pitts and Pitts, 1999). Changes in precipitation amount and frequency have a direct effect on wet deposition of nitrogen compounds which in turn can effect both ozone and particulate matter formation. Changes in wind speed and mixing height leads to changes in the transport of air pollutants (Simpson et al., 2012).

Atmospheric chemistry constitutes a complex system due to its dependencies with meteorology and interdependent chemical reaction cycles between different components. This includes the effect of changes in cloud cover. The sign or magnitude of changes can therefore rarely be calculated analytically but is most often modelled based on explicit solvers or empirical parameterizations. Jacob and Winner (2009) give an overview of the correlations of ozone and particulate matter concentrations in polluted regions with meteorological variables based on perturbation studies. For ozone they find a strong positive correlation with temperature and regional stagnation, generally negative correlations with wind speed and cloud cover, and weak or variable correlations with mixing depth, humidity, and precipitation. For particulate matter they find strong positive correlations with regional stagnation, strong negative correlations with mixing depth and precipitation, and generally negative correlations with temperature, wind speed, and cloud cover. Geiß et al. (2017) analyse the correlation of mixing height with air pollutant concentrations. Based on field measurements in Berlin, they find a positive correlation with surface ozone concentrations due to downward mixing, a negative correlation for NO_x, and spatially differing correlations of mixing height with PM_{10}.

3 Methods, Models, and Data

The challenge in modelling air quality in a future climate lies in the need for high spatial and temporal resolutions of meteorological fields for chemistry transport models. The grid spacing of climate models is usually larger than 0.5° (Taylor et al., 2012). This corresponds to more than 30 km for the Netherlands which does not suffice for air quality modelling and analysis. In this study, a resolution of around 5 km is achieved by using the output of the global climate model scenario HadGEM2-ES (Jones et al., 2011; Martin et al., 2011) RCP8.5 (Riahi et al., 2011) to nudge the model WRF (Skamarock et al., 2008). Its output and emission data are then used as input for EMEP4NL (van der Swaluw et al., 2021) (see Figure 3). In this set-up the spatial variability of air pollutant concentrations resolves the spatial differences between urban and rural environments.

This chapter first gives an overview of the performed simulations (Section 3.1). Then the HadGEM2-ES climate model and the RCP 8.5 scenario are introduced, and the methods described to make the climate scenario output compatible with WRF are outlined (Section 3.2). Section 3.3 introduces WRF, includes a description of the model domains and resolutions, and gives an overview of the different model components and settings. For the emissions two different emission datasets are used (Section 3.4): the reported emissions from 2008-2017 (Hoogerbrugge et al., 2019; CEIP, 2022) and the ECLIPSE V6b MFR emission scenario 2050 (Stohl et al., 2015; Klimont et al., 2017; IEA, 2018; IIASA, 2019; Klimont et al., 2022). Section 3.5 introduces EMEP4NL, its boundary and initial conditions, and the processing of the emission and meteorological input fields. The data used for model validation are described in Section 3.6. The chapter concludes with the description of some metrics for data analysis in Section 3.7.

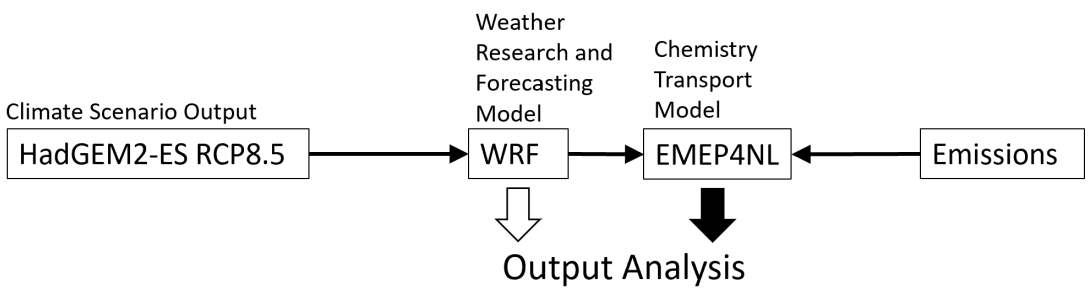

Figure 3: Overview of the modelling approach used in the simulations.

3.1 Overview of Performed Simulations

To answer the research questions outlined in Section 1.4, four simulations are performed. Each of them covers 10 years of data for the months June to August (JJA). 10 years are chosen as a compromise between the computational cost and the need to reduce the

effect of interannual variability on the results. Each WRF and EMEP4NL simulation is performed with 4 days of spin-up time at the end of May. This seems to be sufficient for short-lived airborne chemical components to reach concentrations that are in agreement with the input fields in EMEP4NL.

EMEP_recent (see Table 3) which is based on the HadGEM2-ES RCP8.5 data for 2008-2017 processed with WRF and the dataset of reported emissions from 2008 to 2017, is used as a base scenario both for model validation and for comparison to the three other scenarios in this study. In **EMEP_mitigation** the emission dataset is changed to the ECLIPSE V6b Maximum Feasible Reduction scenario (MFR) for 2050, so that the effect of emission reduction measures alone by mid-century can be studied. With **EMEP_climate**, which is based on HadGEM2-ES RCP8.5 data for 2050-2059 and the reported emissions from 2008-2017, the effect of climate change on air quality can be isolated. In **EMEP_future** both the meteorological input and the air pollutant emissions are changed to the respective future scenario, therefore the combined effect can be determined. By comparing EMEP_mitigation with EMEP_future the influence of climate change on the effect of emission reduction measures and by comparing EMEP_climate with EMEP_future the effect of emission reduction measures in a future climate can be assessed.

	Climate Data	Meteorological Data	Emission Data	Simulation Name
1	HadGEM2-ES RCP8.5 2008-2017	WRF_recent 2008-2017	Dataset 2008-2017	EMEP_recent
2			ECLIPSE MFR 2050	EMEP_mitigation
3	HadGEM2-ES RCP8.5 2050-2059	WRF_future 2050-2059	Dataset 2008-2017	EMEP_climate
4			ECLIPSE MFR 2050	EMEP_future

Table 3: Overview of simulations and their corresponding input datasets

3.2 HadGEM2-ES RCP8.5 Model Output

EMEP4NL requires a temporal and spatial resolution of meteorological fields that is not available for a future climate scenario. Therefore, the output of the HadGEM2-ES RCP8.5 simulation is used to nudge WRF (Section 3.3). The output of WRF is then used as input of EMEP4NL (Section 3.5).

3.2.1 HadGEM2-ES Model

For this study the climate output of the Earth System configuration of the Hadley Centre Global Environment Model version 2 (HadGEM2-ES: Jones et al., 2011; Martin et al., 2011) was used. Its atmospheric component has 38 vertical layers up to 40 km altitude with a horizontal resolution of 1.25° x 1.875°. The oceanic component has 40 unevenly spaced vertical levels and a zonal and meridional resolution of 1° with the meridional resolution increasing from 1° to 1/3° between 30° and the equator.

The model configuration HadGEM2-ES includes dynamic vegetation, tropospheric chemistry, and ocean biology (Martin et al., 2011). HadGEM2-ES is part of the 5th Climate Model Intercomparison Project (CMIP5: Taylor et al., 2012). In this context, simulations were performed with the corresponding prescribed boundary conditions for RCP8.5. The model output is available at the CMIP5 archive (DKRZ, 2015).

3.2.2 RCP8.5 Climate Change Scenario

In the set of Representative Concentration Pathways (RCPs), RCP8.5 is the high greenhouse gas emission scenario and does not include climate change mitigation policies (Riahi et al., 2011). It is therefore sometimes considered as a business-as-usual scenario. RCP8.5 is named after its corresponding radiative forcing at the end of the century ($8.5\frac{\mathrm{W}}{\mathrm{m}^2}$). Table 4 gives an overview of the radiative forcing, CO_2 and CO_2-EQ concentrations in RCP8.5 compared to observed values and RCP2.6, which includes strong mitigation efforts. RCP8.5 was chosen for this study in order to estimate a potential maximum impact of climate change on air quality in the Netherlands until the middle of the century.

	Observed	RCP8.5		RCP2.6
	recent: 2008 - 2017		future: 2050 - 2059	
Radiative forcing	[a] 2.07 W/m^2	2.30 W/m^2	5.02 W/m^2	2.90 W/m^2
CO_2 concentration	393.3 ppm	395.5 ppm	567.9 ppm	442.5 ppm
CO_2-EQ concentration	477.1 ppm	452.2 ppm	727.8 ppm	502.0 ppm

Table 4: Overview of observed and RCP scenario forcings and concentrations (Hofmann et al., 2006; Meinshausen et al., 2011; Miller et al., 2021)

[a] This radiative forcing is based on historical values for 2008-2014 and on SSP2-4.5 for 2015-2017

3.2.3 Use and Preprocessing of HadGEM2-ES RCP8.5 Data

The HadGEM2-ES RCP8.5 scenario output (specified in Table 5) is used both for a 10-year period in the recent past (2008-2017) and for a 10-year period in the middle of this century (2050-2059). The two periods are referred to as "recent" and "future" in the following.

In order to generate the meteorological input files in grb format for the use in WRF, the following preprocessing steps are necessary:

The variable files for ensemble member "r1i1p1" are downloaded in netcdf format from the CMIP5 archive (DKRZ, 2015). Then the monthly datasets are interpolated to daily resolution. The summer months of all datasets are selected and the calendar is adjusted in a way that the dates from 26th of May to 2nd of September on a 360-day calendar are squeezed together to the dates from the 27th of May to the 31st of August on a 365-day calendar. This generates the 31st of May, July, and August which are missing in the original dataset on a 360-day calendar without disturbing the persistence of weather patterns. The soil layer data are split into four layers and their corresponding height is

assigned. For the soil moisture a unit transformation from kg/m^2 to kg/kg is performed. To the near-surface datasets the corresponding height levels (2 m and 10 m) are assigned. The 3-dimensional temperature, specific humidity, wind, and geopotential height datasets are interpolated to fill missing values below surface pressure levels down to 1000 hPa and then interpolated to 26 pressure levels. Then all variable files are transformed to grib 1 format and their level type and grib1 parameter is assigned. These files are then readable by the preprocessing system WPS of WRF (see Section 3.3.2).

Variable	Unit	Time Step	Vertical Coordinate	Long Variable Name
ps	Pa	monthly	1 surface	Surface Air Pressure
ts	K			Surface Temperature
tsl	K	monthly	4 depths below sea (0.05 - 2 m)	Temperature of Soil
mrlsl	kg/m^2			Moisture of Soil Layer
psl	Pa	daily	1 surface	Sea Level Pressure
tos	K	daily	1 surface	Sea Surface Temperature
hus	1	daily	8 pressure levels (100000 - 1000 Pa)	Specific Humidity
ta	K			Air Temperature
va	m/s			Northward Wind
ua	m/s			Eastward Wind
zg	m			Geopotential Height
huss	1	daily	1 height (2 m)	Near-Surface Spec. Hum.
tas	K			Near-Surface Air Temp.
vas	m/s		1 height (10 m)	Near-Surface Northw. Wind
uas	m/s			Near-Surface Eastw. Wind

Table 5: Climate scenario output variable fields from the HadGEM2-ES model used as input for WRF

3.3 WRF Model

The Weather Research and Forecasting model (WRF) version 3.8 with the Advanced Research WRF solver (ARW) (Skamarock et al., 2008; NCAR, 2017) constitutes a fully compressible, Eulerian non-hydrostatic model that can be used both for idealised and real data simulations.

3.3.1 Model Domains

The simulations in WRF were performed in three one-way nested domains (Figure 4). Domain 1 covers Europe in a horizontal resolution of 1/2° in latitudinal and longitudinal direction. For domain 2 and domain 3 the resolution increases threefold compared to the respective parent domain. This leads to a resolution of $1/18° \approx 0.06°$ in domain 3, which corresponds to grid cells of around 3.5-4.0 km resolution in longitudinal and 6.2 km in latitudinal direction. Vertically WRF has 22 irregularly spaced eta levels.

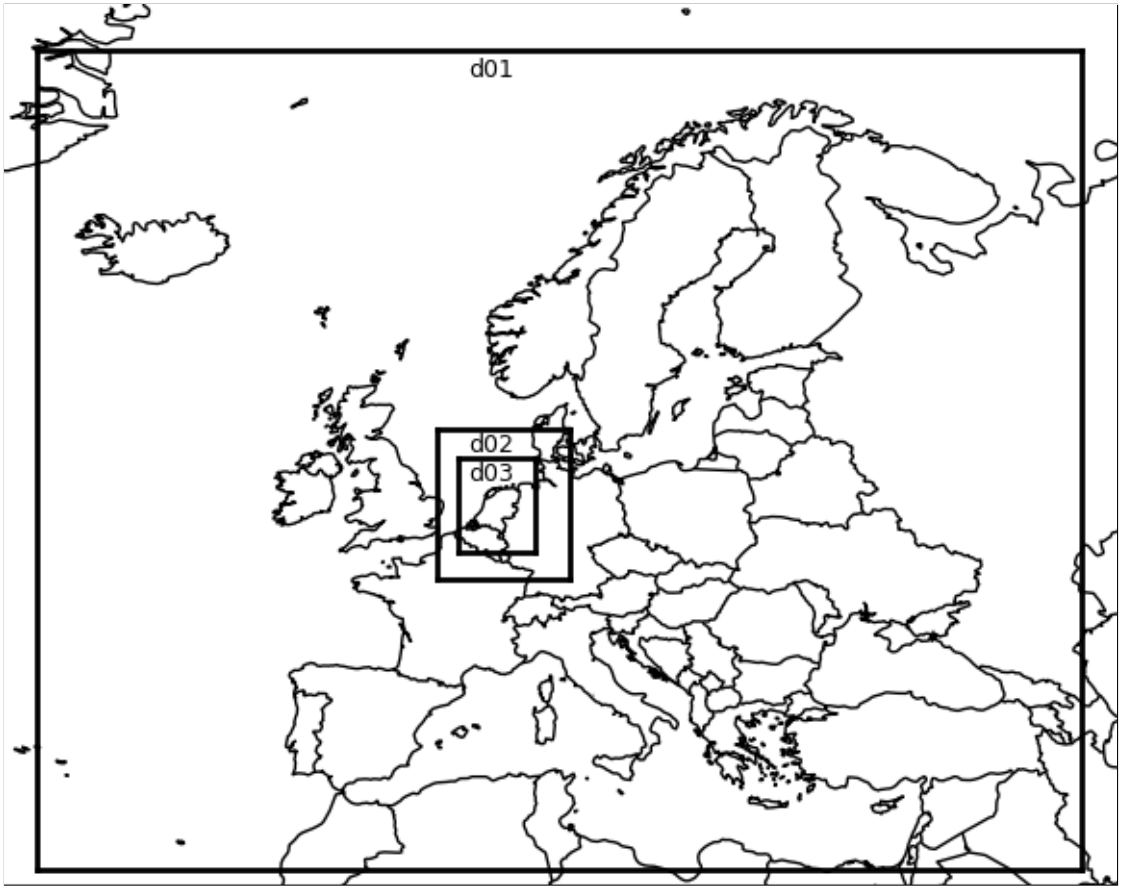

Figure 4: Extents of the the three domains used for the WRF and EMEP4NL model: d01: 31-73°N, 27.25°W- 47.15°E, d02: 48.5-56.5°N, 1.25-10.75°E, d03: 50-55°N, 2.75-8.25°E.

3.3.2 WPS Model

The model includes the WRF preprocessing system (WPS) which consists of three components: ungrib.exe, geogrid.exe, and metgrid.exe. Ungrib retrieves the meteorological fields from the input data (here: preprocessed HadGEM2-ES output), geogrid defines the model domains and resolutions and interpolates the static data (e.g. terrain and land-use type) to these grids, and metgrid interpolates the meteorological input data to this grid. Table 6 shows the corresponding Vtable.

3.3.3 WRF-ARW

WRF itself consists of real.exe and wrf.exe. real.exe generates the initial conditions and lateral boundary condition. wrf.exe then performs the numerical integrations using the ARW dynamics solver. The time and grid settings in WRF are the same as for WPS. Only one-way nesting is performed and the inner grids do not influence their parent grids.

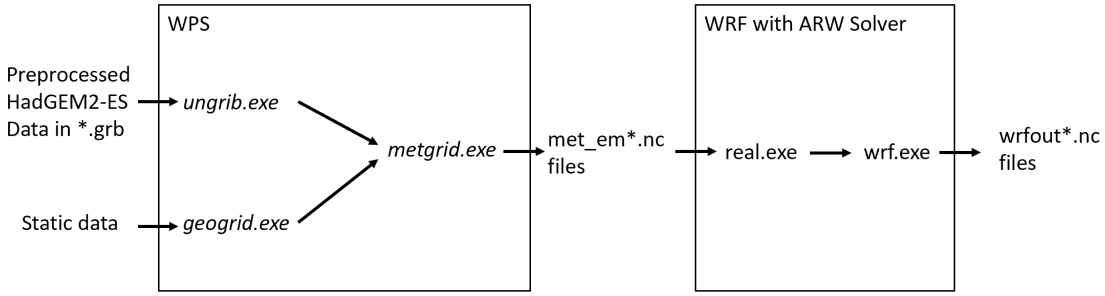

Figure 5: Components of WRF with input and output files

GRIB1 Param	Level Type	From Level1	To Level2	Metgrid Name	Metgrid Units	Metgrid Description
1	01	0		PSFC	Pa	Surface Air Pressure
11	01	0		SKINTEMP	K	Surface Temperature
2	102	0		PMSL	Pa	Sea Level Pressure
11	01	0		SST	K	Sea Surface Temperature
52	100	*		SPECHUMD	1	Specific Humidity
11	100	*		TT	K	Air Temperature
34	100	*		VV	m/s	Northward Wind
33	100	*		UU	m/s	Eastward Wind
07	100	*		GHT	m	Geopotential Height
52	105	2 m		SPECHUMD	1	Near-Surface Spec. Hum.
11	105	2 m		TT	K	Near-Surface Air Temp.
34	105	10 m		VV	m/s	Near-Surface Northw. Wind
33	105	10 m		UU	m/s	Near-Surface Eastw. Wind
11	112	0 cm	5 cm	ST000010	K	Temperature Soil Layer 1
11	112	5 cm	25 cm	ST010040	K	Temperature Soil Layer 2
11	112	25 cm	100 cm	ST040100	K	Temperature Soil Layer 3
11	112	100 cm	200 cm	ST100200	K	Temperature Soil Layer 4
144	112	0 cm	5 cm	SM000010	fraction	Soil Moisture Layer 1
144	112	5 cm	25 cm	SM010040	fraction	Soil Moisture Layer 2
144	112	25 cm	100 cm	SM040100	fraction	Soil Moisture Layer 3
144	112	100 cm	200 cm	SM100200	fraction	Soil Moisture Layer 4

Table 6: Vtable specifying the input variables for WPS

3.3.4 Boundary and Initial Conditions

The boundary condition control in WRF is set to the standard settings with specified boundary conditions for domain 1 and the boundary conditions of domain 2 and 3 determined by the parent domain. The initial conditions are determined by WPS, hence the list of required variable input fields is more extensive than just temperature and wind which are used for nudging.

3.3.5 Model Settings

Physics

WRF itself includes different physics options. For microphysics the Lin and Colle (2011) scheme is used which is suitable for real-data simulations due to its ability to model graupel, snow, and ice processes. The Rapid Radiative Transfer Model (Mlawer et al.,

1997) scheme and the Dudhia scheme (Dudhia, 1989) calculate the longwave and shortwave radiation. For the surface layer, the model relies on the Monin-Obukhov Similarity scheme (Jiménez et al., 2012). The land surface temperature and moisture is modelled in 4 layers with the Noah Land-Surface Model (Niu et al., 2011). Cumulus processes are modelled with the former Kain-Fritsch scheme (Kain and Fritsch, 1993). Additionally, the SST update option is turned on to include changes in sea-surface temperature over the course of a simulation (Appendix A).

Nudging

Grid nudging is set to "on" for all three domains for every 1440 minutes i.e. once per day at 12:00. The nudging coefficients are set to 0.0003 s^{-1} for zonal and meridional wind and temperature but is set to 0.0000/"off" for nudging of specific humidity. The effect of humidity nudging is assessed further in Appendix B.

3.4 Emission Data

SNAP 1	Combustion in energy and transformation industries
SNAP 2	non-industrial combustion plants
SNAP 3	Combustion in manufacturing industry
SNAP 4	Production processes
SNAP 5	Extraction and distribution of fossil fuels and geothermal energy
SNAP 6	Solvent use and other product use
SNAP 7	Road transport
SNAP 8	Other mobile sources and machinery
SNAP 9	Waste treatment and disposal
SNAP 10	Agriculture

Table 7: SNAP sector definitions (EMEP/EEA, 1999)

In addition to hourly input of meteorological fields generated with WRF, EMEP4NL requires input of emissions of the air pollutants SO_x, NO_x, CO, VOC, NH_3, $PM_{2.5}$, and PM_{10}. These emissions are split into total annual values per country and per Selected Nomenclature for reporting of Air Pollutants (SNAP) sector. The 10 SNAP sectors are shown in Table 7. In order to assess the effect of emission reduction scenarios, the reported emissions from 2008-2017 are used for EMEP_recent and EMEP_climate and a Maximum Feasible Reduction scenario (MFR) for 2050 is used for EMEP_mitigation and EMEP_future.

3.4.1 Reported Emissions 2008-2017

For European countries not including the Netherlands, the official EMEP emissions provided in the Webdab emission database (CEIP, 2022) are used. The annual emissions for the years 2008 to 2017 are each related to a base emission netcdf emission file for 2014 by deriving a scaling factors for each country, SNAP sector and air pollutant. The 2014

emission field is based on the CEIP emissions and regridded to the TNO-MACC_III spatial distribution to 1/8° longitude x 1/16° latitude (≈ 7km x 7km over Europe). For the Netherlands the emissions are based on more detailed inventories (Hoogerbrugge et al., 2019).

3.4.2 Emission Scenario 2050

The Evaluating the CLimate and Air Quality ImPacts of Short-livEd Pollutants project (ECLIPSE) scenarios (Stohl et al., 2015; Klimont et al., 2017; IEA, 2018; IIASA, 2019; Klimont et al., 2022) are developed to determine the role of short-lived climate forcers, such as ozone and aerosols. One of the ECLIPSE scenarios is the Maximum Feasible Reduction scenario (MFR) of ECLIPSE Version 6b scenario output for 2050. It is based on the World Energy Outlook for 2018 (IEA, 2018).

The total emissions per country (for EU-28: UK + EU countries), SNAP sector, and pollutant are divided by the total emissions for 2014 to create scaling factors, that are then read in by EMEP4NL in the same way as for 2008-2017. Emissions from countries and regions not included in EU-28 are kept constant at their reported values from 2017.

Following the argument in Section 3.2.2 aiming to study a potential maximum impact of climate change on air quality by choosing RCP8.5, MFR was chosen in order to study a maximum possible impact of emission reduction measures on air quality. Although RCP8.5 does not include greenhouse gas emission reductions, it does include present and planned air pollutant emission reductions until 2030 and increased efforts afterwards (Riahi et al., 2011), but the reductions are weaker than in MFR (shown for 2030 in Amann et al., 2013). It is therefore noted, that using both RCP8.5 and ECLIPSE V6b MFR 2050 in EMEP_future does not constitute a fully consistent combination.

3.5 EMEP4NL

The EMEP model configuration for the Netherlands (EMEP4NL: van der Swaluw et al., 2021) is a configuration of version rv4.36 of the Chemical Transport Model (CTM) EMEP by the Meteorological Synthesizing Centre-West (MSC-W) (MET Norway, 2020). EMEP is an acronym for the European Monitoring and Evaluation Programme for Transboundary Long-Range Transported Air Pollutants. EMEP was set up in 1977 as a joint European effort to address the problem of acid deposition. The MSC-W is one of EMEP's modelling centres, focusing on photo oxidants and aerosol modelling. The EMEP CTM is used both for scientific and policy contexts. It is designed to calculate the concentrations of acidifying and eutrophying compounds such as sulphur and nitrogen oxides, sulphates, nitrates, and ammonium, of surface level ozone, and of particulate matter (Simpson et al., 2012). The set-up of EMEP4NL (van der Swaluw et al., 2021) is based on EMEP4UK (Vieno et al., 2010).

EMEP4NL shares the horizontal and vertical grid specification with WRF (Section 3.3.1) but does not include domain 2. Instead, the horizontal resolution is increased ninefold from domain 1 to domain 3.

3.5.1 Boundary and Initial Conditions

NH_4^+, SO_x, and NO_x boundary and initial conditions for domain 1 are based on past records and future projections. The trend factor for NO_x, specifying the temporal change of NO_x emissions, is applied to several nitrogen species (HNO_3, NO, NO_2, NO_3^-, and PAN). The boundary conditions are updated every month. For ozone not only the boundary conditions but the three-dimensional background field is updated every month. The values are based on measured O_3 values in Mace Head, Ireland, and trajectories based on observational dara from past years. For future years they are based on a trend of (MET Norway, 2020; BoundaryConditions_mod of EMEP):

$$t_{O3} = e^{0.01*(year-2000)}$$

which corresponds to a factor of 1.6 for 2050 and 1.8 for 2059 in background ozone. This factor is applied to the mean background concentrations from 1998-2010. Monthly scaling factors are applied. Methane concentrations increase from 2008 to 2010 from 1860 ppb to 1870 ppb and then stay constant, which might not represent realistic conditions for a future climate.

3.5.2 Processing of Emission Input

The emissions used in EMEP4NL are separated into total annual values per pollutant (SO_x, NO_x, CO, VOC, NH_3, $PM_{2.5}$, PM_{10}), per country, and per SNAP sector.

For each of these sectors, the temporal distribution of emissions is determined with time factors. The time factors distribute the total annual emissions per air pollutant and sector according to monthly, daily, and hourly emission patterns. They are kept the same for all simulations. This is a simplification since not only the total emissions but also the distribution of energy use over the seasons and throughout the day could change with a shift of energy production to renewable energy sources and a transformation of industrial processes and the transport sector until the 2050s (Hendriks et al., 2015).

3.5.3 Processing of Meteorology Input

The meteorology input is read in every hour. Interpolation is used to calculate the meteorological variable fields for every advection time step (every 20 minutes). The impact of meteorological variable fields include, but are not limited to (Simpson et al., 2012):

- Absolute temperature influencing rate coefficients of chemical reactions and the emissions of biogenic volatile organic compounds such as isoprene.

- Specific humidity determining water availability for chemical reactions and influencing dry deposition.
- Horizontal and vertical winds driving the advection of air pollutants.
- Soil moisture altering dry deposition and dust emission.
- Sea surface temperature and wind speeds controlling the production of sea salt aerosols.
- Surface pressure, specific humidity and absolute temperature determining air density

3.5.4 Definition of Mixing Layer Height

The mixing layer height is defined in EMEP as the lowest height for which a modified Richardson number is greater than 0.25 (Ri $>$ 0.25) and issynonymously used as the boundary layer height.

3.6 Data for Model Validation

In order to assess the validity of the approach chosen in this study, EMEP_recent is compared to observed station data from RIVM stations (RIVM, 2022). The hourly measurements of meteorological values correspond to the nearest KNMI station with 75% coverage of data (KNMI, 2022).

3.7 Analysis Methods

Land Mask and Population Density

All mean values for the Netherlands are obtained with the land mask in Figure 6. The exposure of the population to harmful levels of air pollutants is calculated by multiplying the map of the number of days in which the respective air quality standard is exceeded with the population density map of 2021 (CBS, 2022) for all years. This number is then divided by the total number of inhabitants (17.4 million).

Boxplots

The boxplots in Section 3.6 display a box from the 25th to the 75th percentile with a line at the median and a mark at the mean. The whiskers extend to 1.5 times of the range between these percentiles from the edge of the box. Values outside of this range are displayed as dots.

Calm Days

Based on Manders et al. (2012), a calm day is defined as a day with less than 0.5 mm of precipitation, daily mean wind speeds of less than 2 m/s and a daily maximum temperature

higher than 25°C. These conditions are considered as favourable for high concentrations of air pollution.

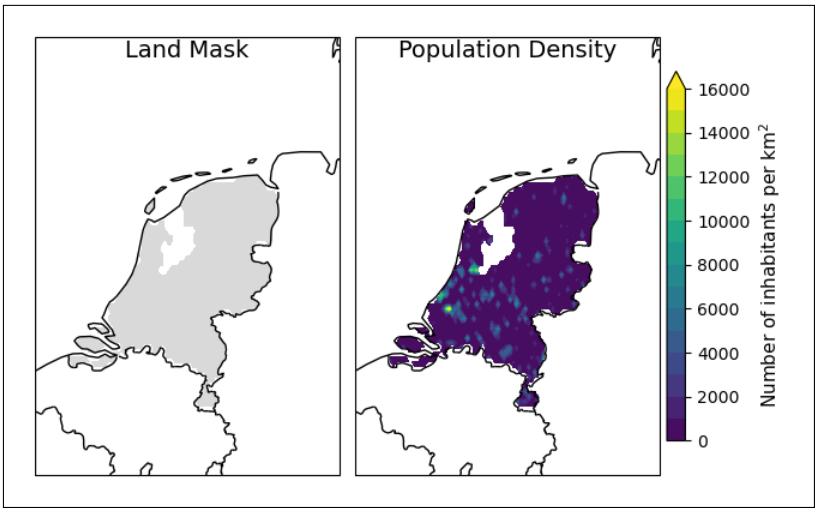

Figure 6: Land Mask and Population Density Map for the Netherlands.

4 Model Validation

In order to assess the validity of the simulation results, the output of temperature, wind, and concentrations of O_3, NH_3, and $PM_{2.5}$ are compared to the observed values at eight RIVM air quality stations distributed over the Netherlands, in Section 4.1. Research question 1 (Is nudging WRF with HadGEM2-ES RCP8.5 output suitable to generate meteorological input that is in alignment with observations for the past years?) and research question 2 (Is nudging EMEP4NL with these meteorological fields a valid approach to study concentrations of air pollutants?) are then discussed on the basis of these results in Section 4.2.

4.1 Results

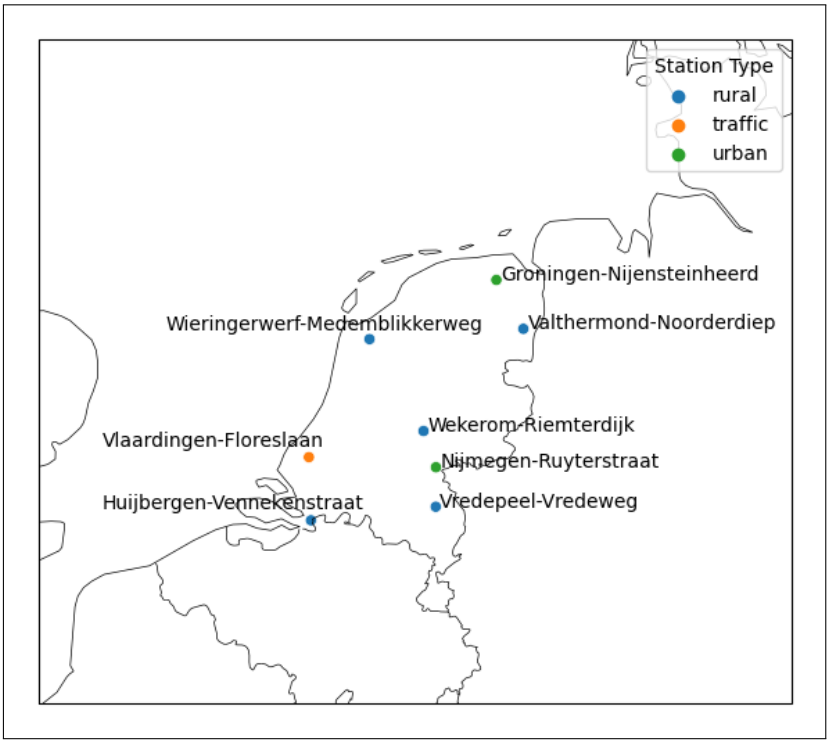

Figure 7: Location and type of the RIVM air quality stations whose data are used in this section.

For near-surface air temperature (Figure 8) there is a mean positive bias of 2.1°C both in the mean and in the median in WRF_recent compared to observations at the eight air quality stations averaged for 2008 to 2017. In WRF_future the temperatures increase by 2.4°C compared to WRF_recent. There is a good agreement for the individual stations Vlaardingen-Floreslaan and Nijmegen-Ruyterstraat and a positive bias at the remaining stations in WRF_recent (Appendix C: Figure 57). Near-surface air temperatures in WRF_future are higher than both the observations and WRF_recent at all stations.

Near surface winds (Figure 9) are underestimated by 0.7 m/s in the median and 0.8 m/s in the mean in the model compared to observations. This underestimation is robust at all stations (Appendix C: Figure 58). In both WRF_recent and WRF_future there are more

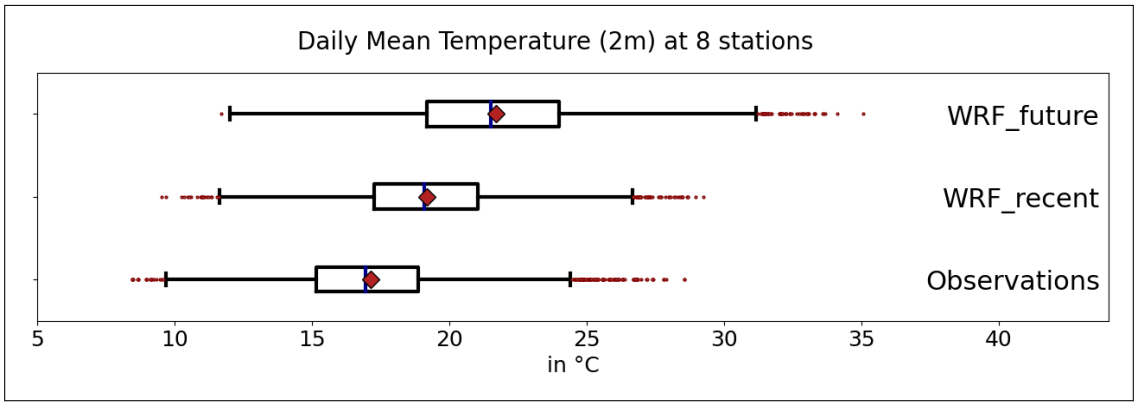

Figure 8: Boxplots of 10-years of daily mean temperatures in summer (JJA) in °C at KNMI stations close by the eight respective RIVM air quality stations (Figure 7) and at the respective locations in WRF_recent (2008-2017) and WRF_future (2050-2059). The box extends from the 25th to the 75th percentile with a line at the median and a mark at the mean. The whiskers length is 1.5 times this range. Dots indicate values outside the extent of the whiskers.

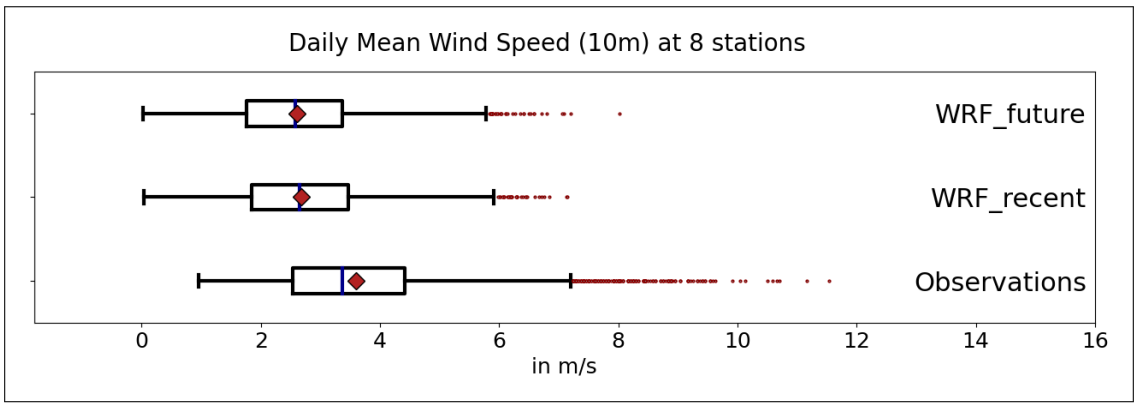

Figure 9: Boxplots of 10-years of daily mean wind speeds in summer (JJA) in m/s at KNMI stations close by the eight respective RIVM air quality stations (Figure 7) and at the respective locations in WRF_recent (2008-2017) and WRF_future (2050-2059).

days with the daily mean wind speed below 2 m/s, which is one of the indicators for a calm day, than in the observations at the respective stations. In the observations there are also more outliers with high wind speeds.

Not only the wind speed but also the wind direction differs between observations and WRF_recent. From 1991-2020 the wind in the Netherlands came predominantly from the southwest and west (KNMI, 2021). In WRF_recent the wind comes predominantly from north-north-west (Figure 13: Row 3, Column 3).

Daily mean ozone concentrations (Figure 10) have a positive bias in EMEP_recent compared to observations of 11.4 µg/m^3 in the median and 10.5 µg/m^3 in the mean. This positive bias is robust for all stations except for Groningen-Nijensteinheerd (Appendix C: Figure 59). Surface ozone concentrations in the other simulations are higher both in terms of the mean and of the median than in EMEP_recent. The spread in daily mean ozone

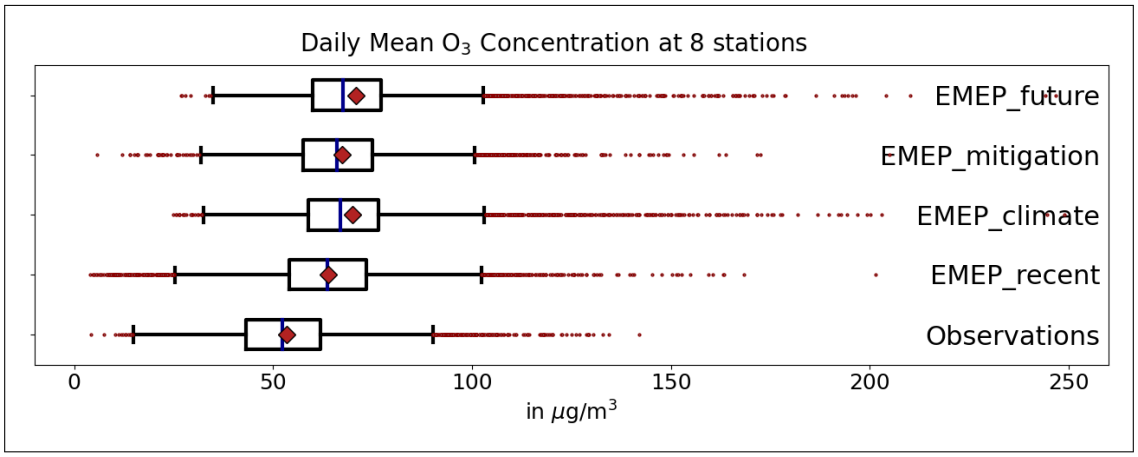

Figure 10: Boxplots of 10-years of daily mean ozone (O_3) concentrations in µg/m^3 in summer (JJA) at the eight RIVM air quality stations (Figure 7) and at the respective locations in EMEP_recent, EMEP_climate, EMEP_mitigation, and EMEP_future.

concentrations in EMEP_recent is similar to the spread in the observations but with more outliers in the model.

For the ammonia (NH_3) concentrations at the five rural stations there is a negative bias in the simulations of 2.9 µg/m^3 in the median and 4.2 µg/m^3 in the mean (Figure 11). Both the concentration and its bias varies strongly between the stations (Appendix C: Figure 60). The largest positive bias is found in Wekerom-Riemterdijk with a median of 16.6 µg/m^3 in the observations versus 3.7 µg/m^3 in the EMEP_recent. The largest negative bias is found in Valthermond-Noorderdiep with 4.9 µg/m^3 in the observations and 10.1 µg/m^3 in EMEP_recent.

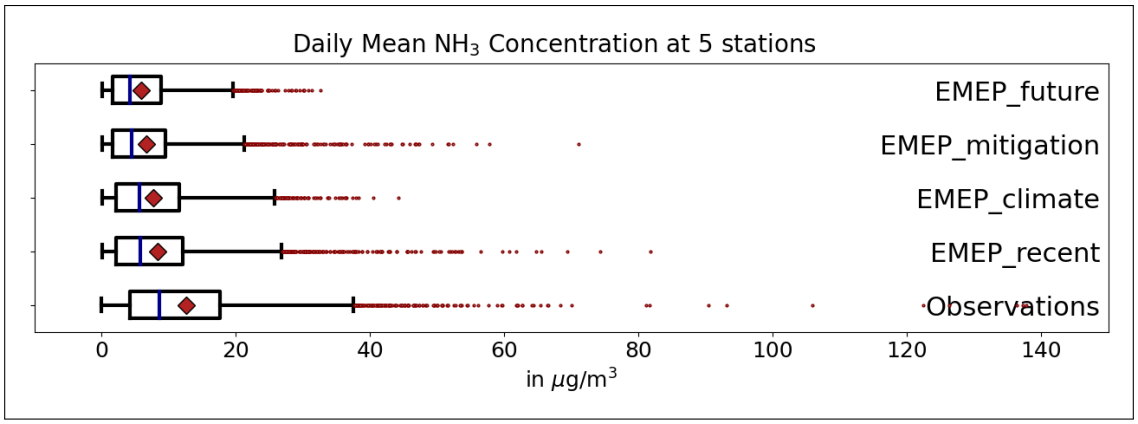

Figure 11: Boxplots of 10-years of daily mean ammonia (NH_3) concentrations in µg/m^3 in summer (JJA) at the five rural RIVM air quality stations (Figure 7) and at the respective locations in EMEP_recent, EMEP_climate, EMEP_mitigation, and EMEP_future.

For fine particulate matter ($PM_{2.5}$) there is a positive bias in EMEP_recent compared to observations at six locations where $PM_{2.5}$ is measured (Figure 12). Additionally, there are more outliers at the higher end of the concentrations in EMEP_recent. The median of the

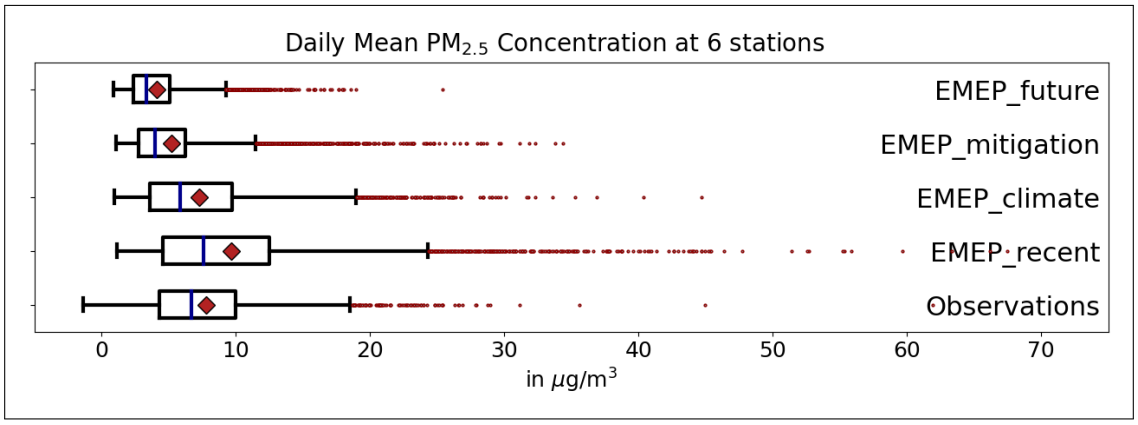

Figure 12: Boxplots of 10-years of daily mean fine particulate matter ($PM_{2.5}$) concentrations in µg/m^3 in summer (JJA) at six RIVM air quality stations (Vredepeel-Vredeweg, Vlaardingen-Floreslaan, Wieringerwerf-Medemblikkerweg, Wekerom-Riemterdijk, Nijmegen-Ruyterstraat, Groningen-Nijensteinheerd) and at the respective locations in EMEP_recent, EMEP_climate, EMEP_mitigation, and EMEP_future.

observations lies in between the median of EMEP_recent and EMEP_climate data with a bias of minus and plus 0.9 µg/m^3 respectively. The agreement of the observations with EMEP_recent and EMEP_climate varies between stations (Appendix C: Figure 61).

4.2 Discussion

All analyses in Section 4.1 are based on a comparison of the statistics in the daily mean values for temperature, wind speed, and O_3, NH_3, and $PM_{2.5}$ concentrations from a point-like station measurement to the modelled value of an approximately 4 km x 6 km grid cell. This leads to innate biases caused by spatial variations within a few kilometres that are independent of the input used for the EMEP4NL.

Research question 1: Is nudging WRF with HadGEM2-ES RCP8.5 output suitable to generate meteorological input that is in alignment with observations for the past years?

Using the climate output of RCP8.5 to nudge WRF leads to an overestimation of the temperature in 2008-2017 in WRF_recent compared to observations and an underestimation of the winds. Both the bias in temperature and wind likely also lead to a positive bias in calm days. Therefore, the climatology in WRF_recent is not in alignment with the real historical climatology. The use an ensemble of models or a regional climate scenario output, such as one of the KNMI'14 scenarios (KNMI, 2015), could lead to better results.

Research question 2: Is nudging EMEP4NL with these meteorological fields a valid approach to study concentrations of air pollutants?

The approach of using WRF data as input for a high resolution version of the EMEP CTM

to evaluate air quality has been chosen before by Lin and Colle (2011). They conclude that this method is suitable for air pollution epidemiology and identify the inaccuracy of emission data as the main cause of biases. In this study the use of climate scenario output for WRF adds more biases. The overestimation of ozone, for example, is likely an effect of the positive bias in temperature and of a positive bias in calm days. The large-scale concentration maps of NH_3 for 2021 (RIVM, 2022) show higher concentrations locally around the station Wekerom-Riemterdijk. This spatial variability is not captured by the model which explains the underestimation of NH_3 concentrations in this area. Additionally, the concentrations of NH_3 and $PM_{2.5}$ are influenced by the wet deposition through precipitation. The average amount of precipitation (Figure 14) and its interannual variability in the Netherlands is realistic in the model (KNMI, 2022) but the spatial variability might differ and lead to biases both in NH_3 and $PM_{2.5}$. This means that while using EMEP4NL for air quality analysis is a valid approach to study air quality, the output is highly influenced by both biases and emissions which leads to skewed results in this study.

Conclusion

The absolute values in the results of this thesis are not representative for the real world climate in the Netherlands. However, the differences to observations for all considered values except for $PM_{2.5}$ are smaller in WRF_recent and EMEP_recent than for the other simulations in which the effect of climate and/or emission changes are analysed. For this reason the sign and relative importance of those changes might still be valid. In addition, this study can give a general overview on which processes are important for air quality changes in the Netherlands. Based on the results and the biases in this study, recommendations for further studies on this topic are given in Section 7.

5 Results

In this chapter the results from the output analyses of the simulations are presented. Section 5.1 focuses on the changes in meteorology between WRF_recent and WRF_future and aims to specify the climate signal between these simulations. In section 5.2 changes in air quality with unchanged emissions (2008-2017) in a changing climate are presented: i.e., the difference between EMEP_recent and EMEP_climate. Section 5.3 then shows the effect of air pollutant emission reductions on summertime air quality in an unchanged climate (2008-2017), i.e. the difference between EMEP_recent and EMEP_mitigation. Section 5.4 concludes the chapter with an analysis of the combined effect of meteorology and emission changes on air quality, i.e. the difference between EMEP_recent and EMEP_future.

5.1 Changes in Meteorology

When nudging the WRF model with temperature and wind fields of the HadGEM2-ES RCP8.5 scenario output (Figure 13), the spatial variability of the variable output fields increases compared to the input due to the underlying maps of land-use and topography. Figure 13 shows higher temperatures and lower water vapour mixing ratios in urban areas than in rural areas both for WRF_recent and WRF_future. In the Netherlands examples for this are the Rotterdam - The Hague metropolitan area, Amsterdam, Eindhoven and Utrecht. The same effect occurs around Brussels, Antwerp, and Ghent in Belgium and in the Rhine-Ruhr metropolitan area in Germany. Generally, there is a north-south gradient and a land-sea gradient in temperatures with higher near-surface temperatures in the south of the domain and over land, excluding the Eifel, Ardennes, and Sauerland at higher altitudes. The water vapour mixing ratio and winds are higher over the North Sea than over land.

The difference in temperatures between WRF_recent and WRF_future is highest in urban areas that are not along the coast and lowest over the North Sea. On average near-surface temperatures increase by 2.5°C in the Netherlands under this scenario. Water vapour mixing ratios increase by $8{\cdot}10^{-4}$ kg/kg on average for the Netherlands which corresponds to an increase of 9.3%. The increase is stronger over the North Sea and lower in the Rhine-Ruhr metropolitan area. In spite of this increase in the water vapour mixing ratio, relative humidity is projected to decrease from 63% (WRF_recent) to 59% (WRF_future) because the effect of the temperature increase on relative humidity outweighs the effect of the water vapour mixing ratio increase in this case (calculations based on quations 3-6 in Section 2.1 with p=1013 hPa and the mean temperature and water vapour mixing ratio of both simulations). The wind speed slightly decreases and changes from a north-north-west wind of 2.8 m/s on average for WRF_recent in the Netherlands to a north wind of 2.7 m/s on average for WRF_future. The wind speed decreases most strongly northwest of Texel over the North Sea.

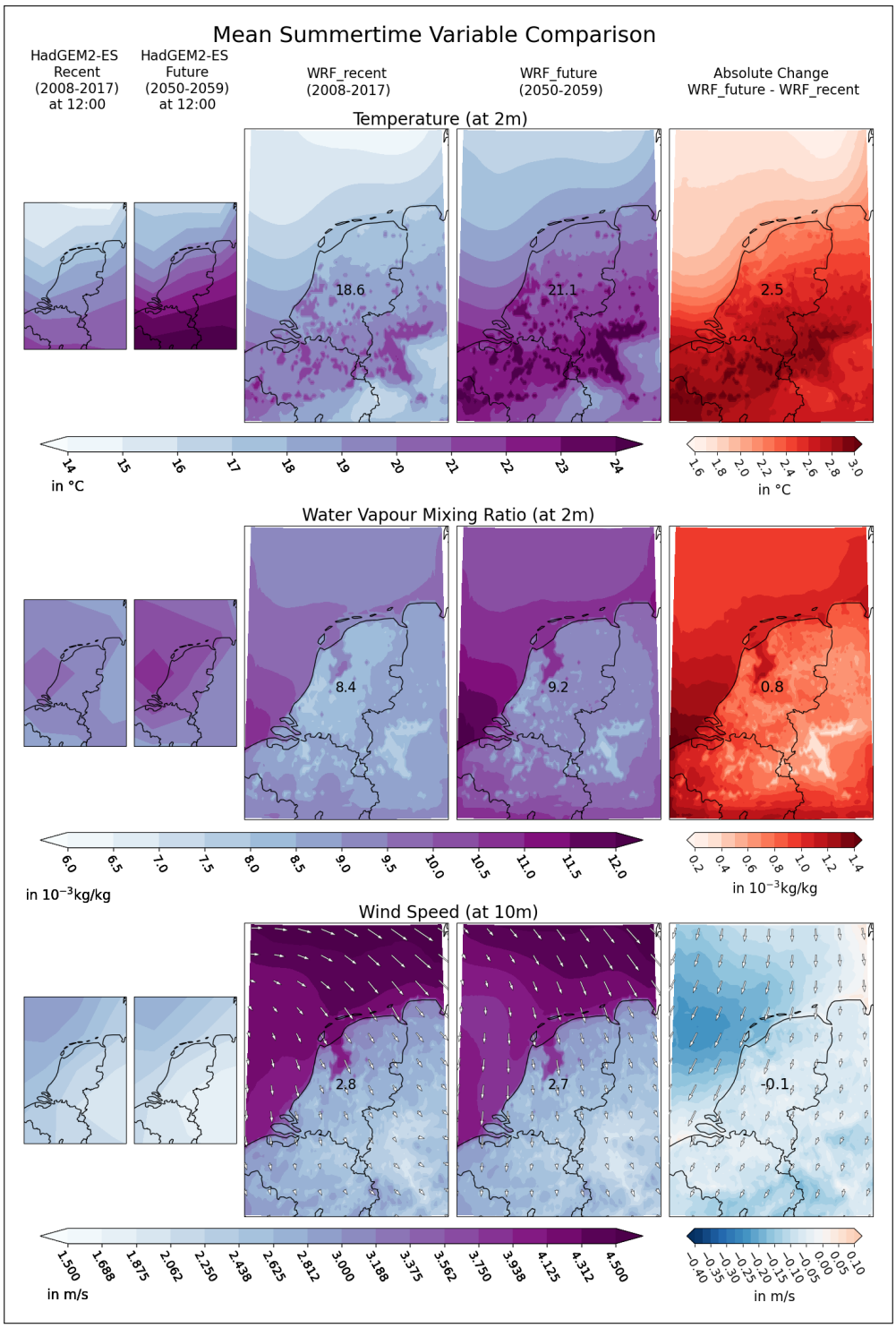

Figure 13: 10-year summertime (JJA) mean of near-surface variable fields for domain 3. Columns 1 and 2 show low resolution HadGEM2-ES RCP8.5 output for 2008-2017 (recent) and 2050-2059 (future). Columns 3 and 4 display the corresponding higher resolution WRF output (WRF_recent and WRF_future) with nudging temperature and winds from HadGEM2-ES data. Column 5 shows the difference between WRF_future and WRF_recent. The first row displays temperature at 2 m in °C, the second row shows the water vapour mixing ratio at 2 m in 10^{-3}kg/kg, and the third row displays the wind speed at 10 m in m/s. The arrows in row 3 indicate the wind direction (Column 3 and 4) and wind direction change (Column 5). The numbers in the centre represent the respective means for the Netherlands in the same units.

The average total precipitation per summer (Figure 14) is higher over land than over the North Sea and higher in Belgium than in the Netherlands. In the Netherlands the mean precipitation per summer decreases by 20% or 55 mm per summer in WRF_future compared to WRF_recent. The average number of days with more precipitation than 0.5 mm decreases from 21.5 days with an average amount of 13.0 mm each to 19.2 days with 11.7 mm each.

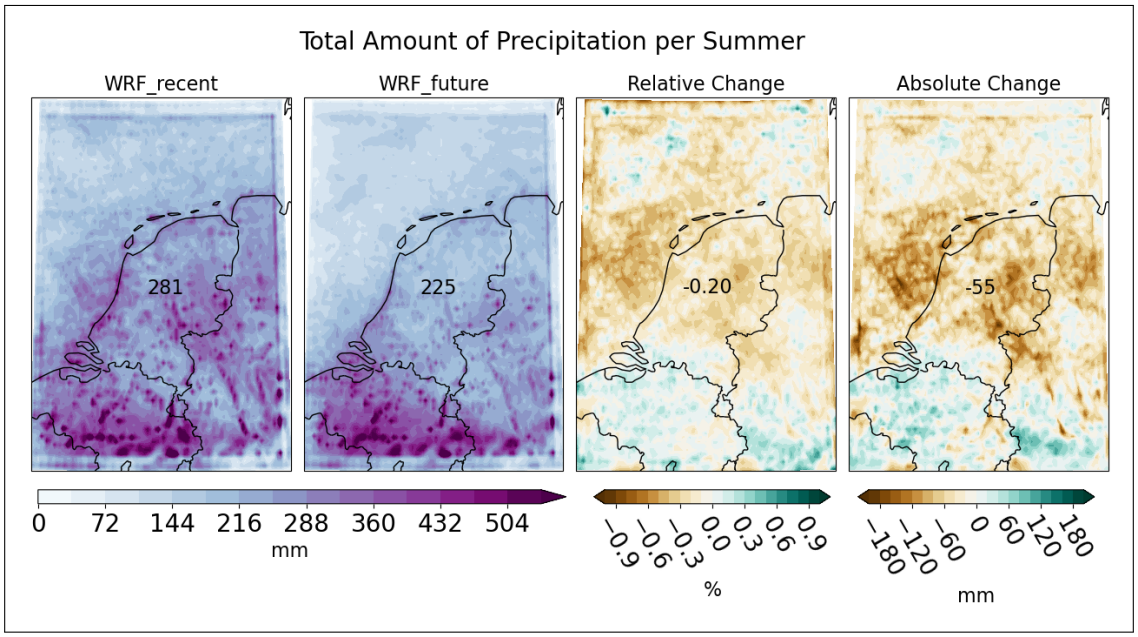

Figure 14: 10-year mean of total summertime (JJA) precipitation in mm as output for domain 3. Panel 1 displays WRF_recent (2008-2017), panel 2 displays WRF_future (2050-2059). In panel 3 the relative and in panel 4 the absolute difference between WRF_recent and WRF_future are shown. The numbers in the centre represent the respective means for the Netherlands in the same units.

The mixing layer height builds up during the day and decreases during the night (Table 8). Figure 15 shows the increase in the mixing layer height at its maximum during the afternoon (12 p.m. to 6 p.m.) in a future climate. In WRF_future this mixing height is increased by 63 m or 10.3% on average over the Netherlands compared to WRF_recent. The mixing layer height during the night stays nearly constant which also leads to an increase in the difference between the mixing layer height during the night and the afternoon by 20.4% (Appendix D.1: Figures 62 and 63). In the Rhine-Ruhr area, the mixing layer increases during the night by a similar magnitude as during the day. Hence, the increase in the daily range in this area is small (Appendix D.1: Figure 63).

The fraction of calm days in summer (Section 3.7) is displayed in Figure 16 for WRF_recent and WRF_future. Over land the number of calm days is highest in urban clustered areas further inland and at low altitudes. The number of calm days increases by a factor of 2.5 between WRF_recent and WRF_future.

	WRF_ recent	WRF_ future	Relative Change	Difference
Daily Mean	459.5 m	485.9 m	+5.8 %	+26.4 m
12 a.m. - 6 a.m. Mean (Night)	286.9 m	282.7 m	-1.4 %	-4.2 m
12 p.m. - 6 p.m. Mean (Afternoon)	613.9 m	677.1 m	+10.3 %	+63.2 m
Difference: Afternoon - Night	327.1 m	394.4 m	+20.4 %	+67.3 m

Table 8: 10-year mean of summertime (JJA) mixing layer heights in m averaged over the Netherlands. Column 1 and 2 show the respective means for WRF_recent and WRF_future, column 3 and 4 show the respective relative changes and total differences. The rows display different periods of the day for averaging.

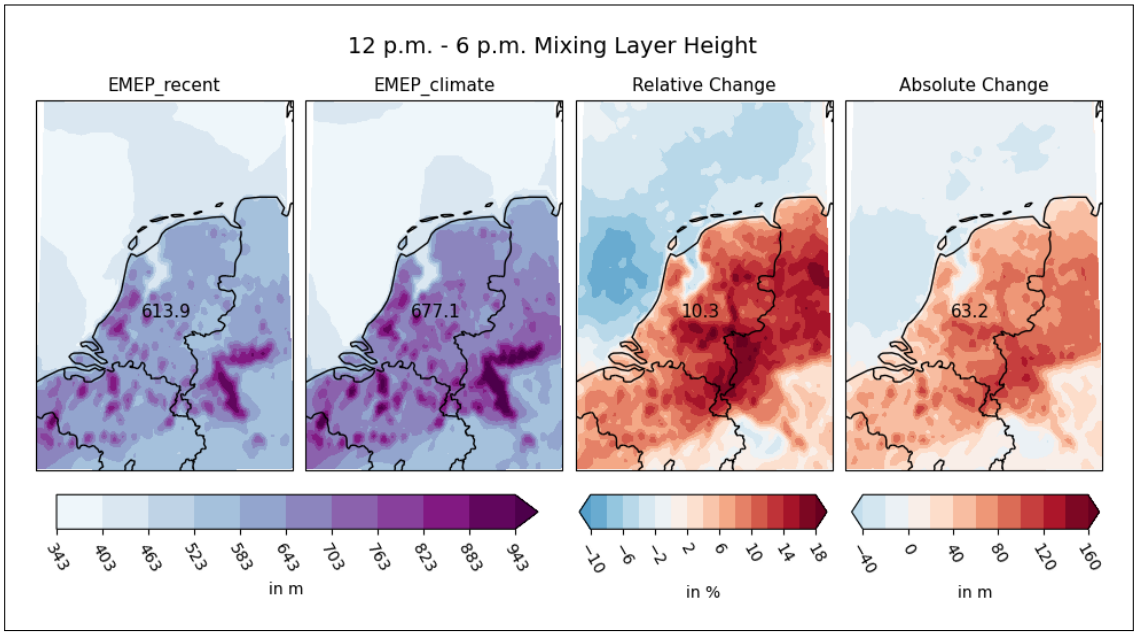

Figure 15: 10-year summertime (JJA) average of the mixing layer height in m between 12 p.m. and 6 p.m. in the afternoon as output for domain 3. The first panel shows EMEP_recent (based on WRF_recent: 2008-2017). The second panel shows EMEP_climate (based on WRF_future: 2050-2059). The third panel shows the relative and the fourth panel shows the absolute change between EMEP_recent and EMEP_climate. The numbers in the centre represent the respective means for the Netherlands in the same units.

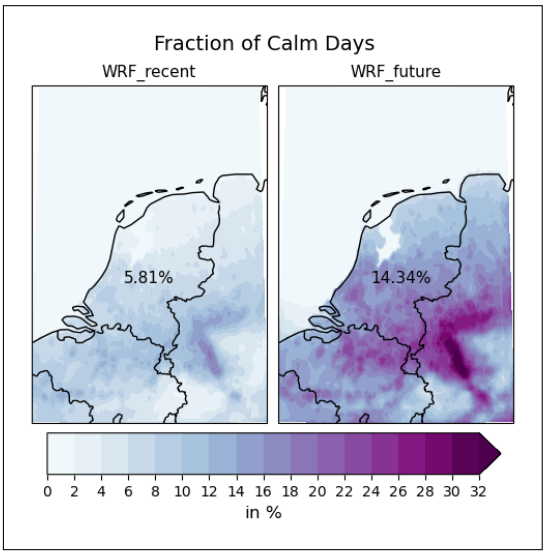

Figure 16: Fraction of calm days in 10-years of summertime (JJA) simulations. The left panel shows WRF_recent and the right panel shows WRF_future. A calm day is defined as a day with a daily maximum temperature > 25°C, daily mean wind speed < 2 m/s and daily total precipitation < 0.5 mm/m^2. The numbers in the centre represent the mean fraction of calm days for the Netherlands.

5.2 Effect of Climate Change on Air Quality

In this section the effect of climate change on air quality is analysed by comparing the output of EMEP_recent with the output of EMEP_climate. Both simulations share the same emission data input based on reported emissions for 2008-2017 (Section 3.4.1) and differ in their meteorological input as shown in Section 5.1. Where useful, results from a comparison of EMEP_mitigation and EMEP_future are added to show the effect of climate change on air pollutants under the low emission scenario ECLIPSE V6b MFR for 2050. The results in this section form the basis to discuss research question 3 (How are summertime levels of ozone, $PM_{2.5}$ and ammonia in the Netherlands affected by climate change under the RCP8.5 scenario until the 2050s?) in Section 6.2.1.

5.2.1 Ozone

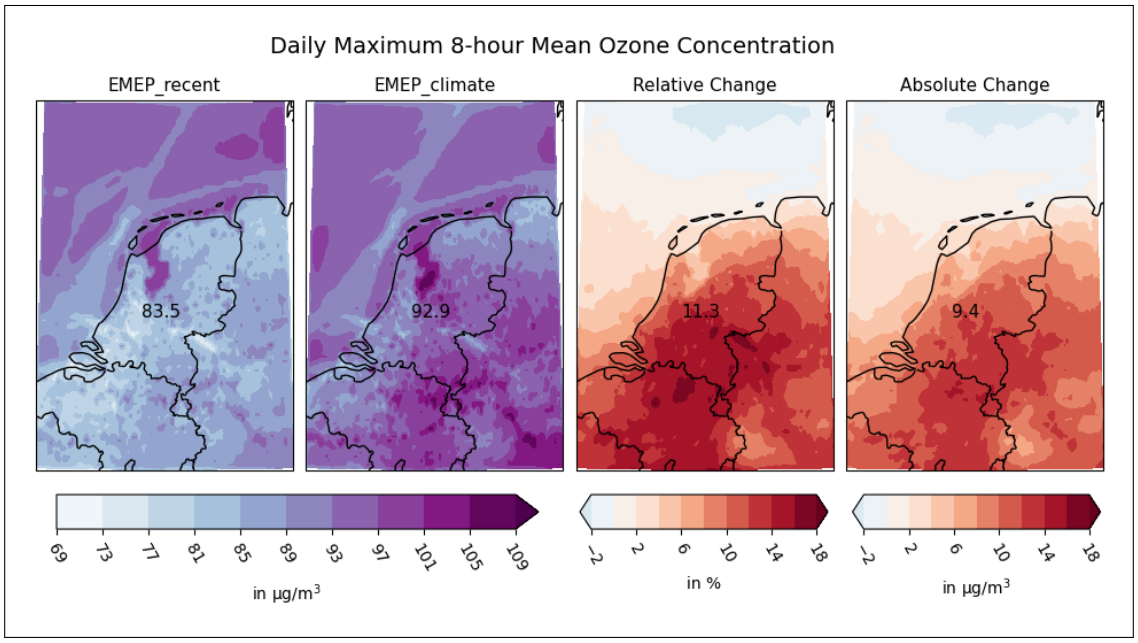

Figure 17: 10-year summertime (JJA) average of daily maximum 8-hour mean surface ozone concentrations in µg/m^3 as output for domain 3. The first panel shows EMEP_recent (based on WRF_recent 2008-2017 meteorology), the second panel shows EMEP_climate (based on WRF_future 2050-2059 meteorology under RCP8.5) output, both simulations are based on reported emissions for 2008-2017. The third panel shows the relative and the fourth panel shows the absolute change between EMEP_climate and EMEP_recent. The numbers in the centre represent the respective means for the Netherlands in the same units.

The daily maximum 8-hour mean ozone surface concentration (Figure 17) is highest over the North sea except for its shipping routes than over the Netherlands in EMEP_recent. The lowest ozone concentrations are found in the lower Rhine region on the Dutch-German border and the Rhine-Meuse-Scheldt delta. The mean daily maximum 8-hour ozone concentration is projected to increase in most of domain 3 in a future climate except for a slight projected decrease north of the West Frisian islands. In the Netherlands daily maximum 8-hour mean surface concentrations increase by 11.3% from 83.5 µg/m^3 (EMEP_recent) to

92.9 µg/m^3 (EMEP_climate). This increase is weaker along the coast than farther inland.

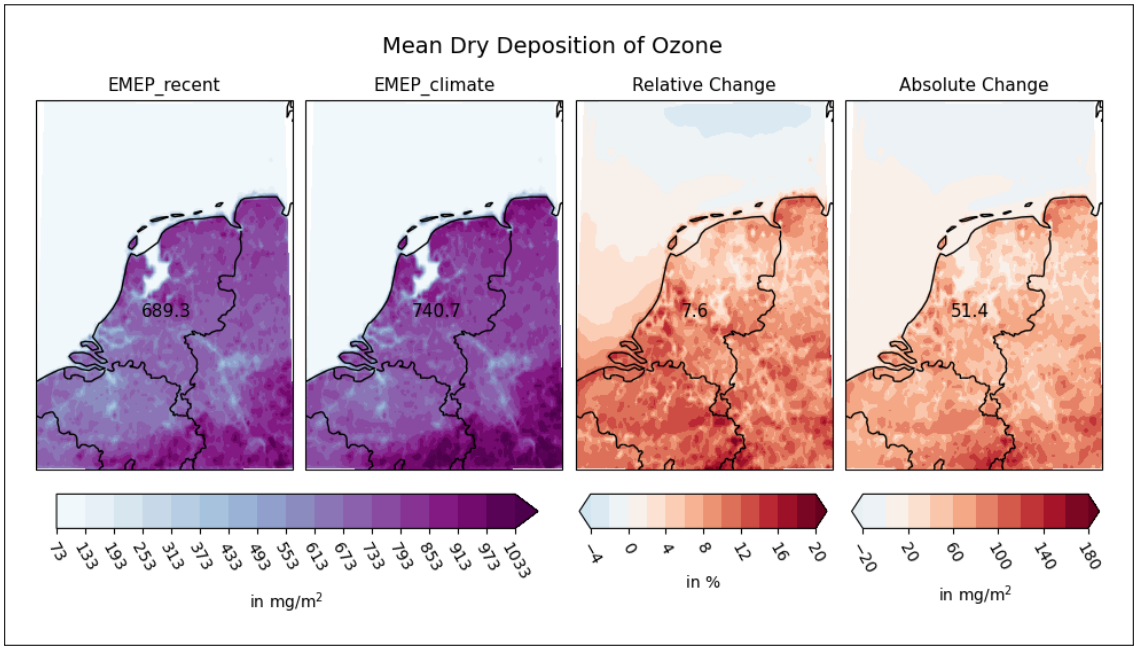

Figure 18: 10-year summertime (JJA) average of total monthly dry deposition of ozone in mg/m^2 as output for domain 3. The first panel shows EMEP_recent (based on WRF_recent 2008-2017 meteorology), the second panel shows EMEP_climate (based on WRF_future 2050-2059 meteorology under RCP8.5) output, both simulations are based on reported emissions for 2008-2017. The third panel displays the relative change and the fourth panel the absolute change between EMEP_climate and EMEP_recent. The numbers in the centre represent the respective means for the Netherlands in the same units.

Dry deposition of ozone (Figure 18) is highest along the northern coasts, in the Ardennes, the Eifel, and the Sauerland regions and lowest in the urban areas Rhine-Ruhr, Rotterdam, The Hague, Antwerp, and Brussels. Dry deposition in the Netherlands increases in EMEP_climate compared to EMEP_recent by 7.7 % with lower increases in the north than in the south of the country.

The average number of days per summer in which the WHO standard for ozone (Section 1.2: Table 2) is exceeded in the Netherlands is 15.5 days in EMEP_recent and 24.5 days in EMEP_climate (Figure 19). This increase is lower than average close to the coasts and higher in the province of Limburg in the south. The average exposure of the population to concentrations of ozone above the WHO standard is 17.2 days per summer in EMEP_recent and increases by 52% in a future climate (Section 5.4: Table 12).

The mean increase of ozone scaled by the increase in temperature (Figure 20) is with on average 1.4 ppb/K between EMEP_recent and EMEP_climate larger than with on average 0.8 ppb/K between EMEP_future and EMEP_mitigation which include emission controls.

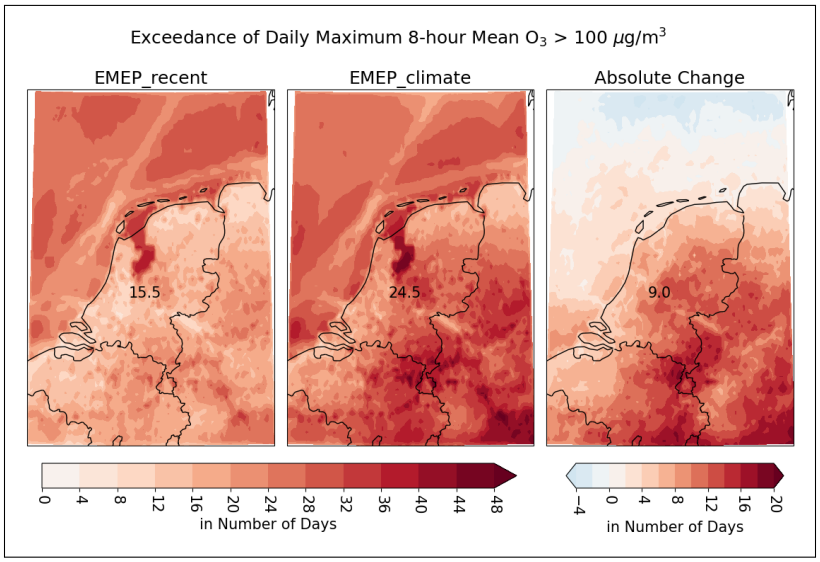

Figure 19: 10-year mean of number of days in summer with daily surface maximum 8-hour mean ozone concentrations higher than the 100 µg/m^3 WHO daily ozone threshold. Panels 1 and 2 show the number of exceedance days for EMEP_recent (based on WRF_recent 2008-2017 meteorology) and EMEP_climate (based on WRF_future 2050-2059 meteorology under RCP8.5) respectively. Both simulations are based on reported emissions for 2008-2017. Panel 3 displays the absolute change. The numbers in the centre represent the respective mean for the Netherlands.

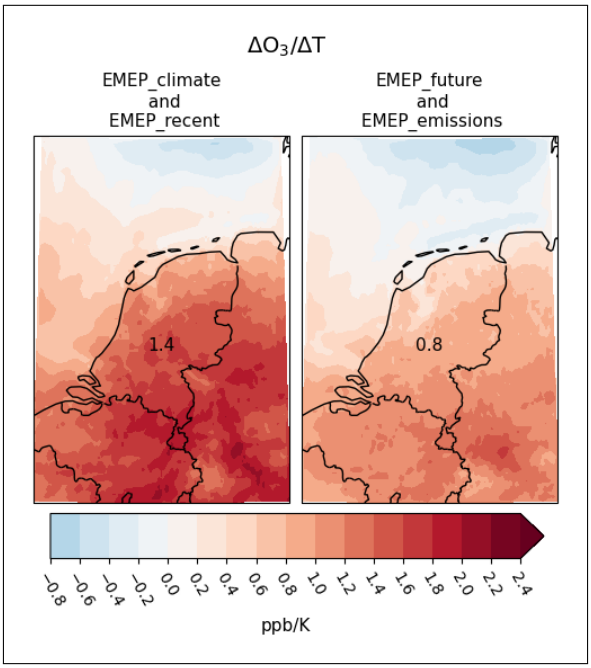

Figure 20: 10-year mean of summertime (JJA) ozone increase per temperature increase in ppb/K. In panel 1 the difference in surface ozone mixing ratios between EMEP_climate and EMEP_recent (both based on reported emissions from 2008-2017) and in panel 2 their difference between EMEP_future and EMEP_mitigation (both based on ECLIPSE MFR 2050) is divided by the temperature increase between WRF_recent and WRF_future. The numbers in the centre represent the respective mean for the Netherlands.

5.2.2 Reduced and Oxidised Nitrogen

The 10-year mean of surface ammonia (NH_3) concentrations (Figure 21) is highest in western Lower Saxony in Germany, in West Flanders in Belgium and in the southern provinces Limburg and North Brabant in the Netherlands. The lowest NH_3 concentrations are found along the coast in the Netherlands. In a future climate, its mean NH_3 summertime concentration is projected to decrease by 5.9% from 8.9 µg/m^3 (EMEP_recent) to 8.3 µg/m^3

(EMEP_climate). NH_3 concentrations increase slightly in parts of the Southern Bight west of the Netherlands and the southeastern parts of domain 3 in Germany.

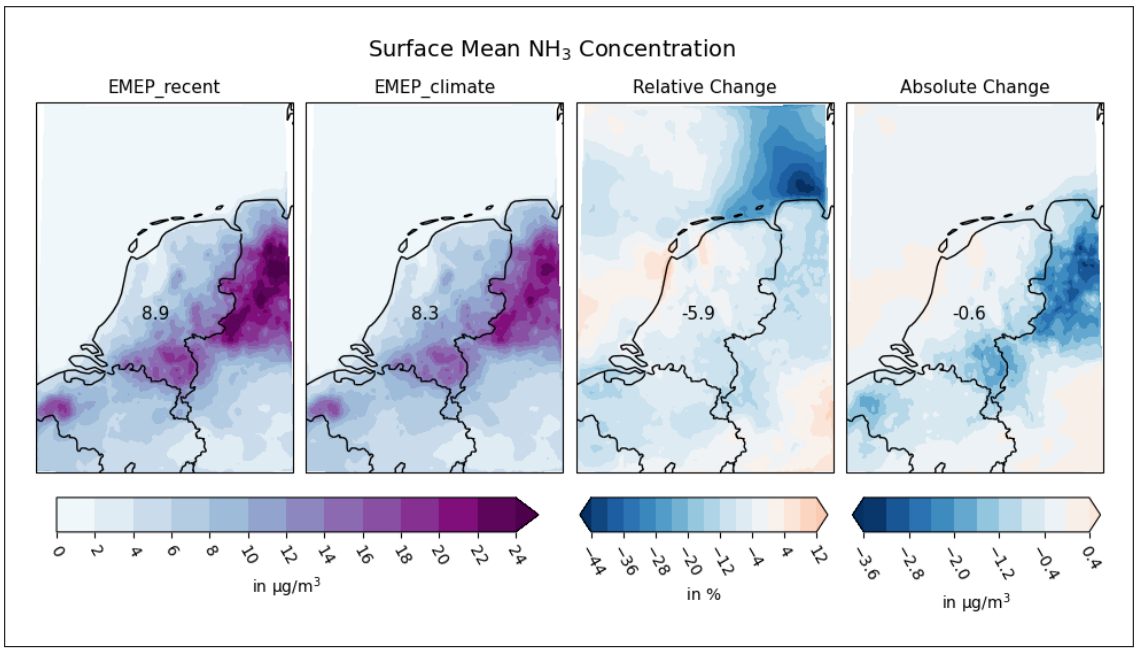

Figure 21: 10-year summertime (JJA) average of daily mean surface ammonia (NH_3) concentrations in µg/m^3 as output for domain 3. The first panel shows EMEP_recent (based on WRF_recent 2008-2017 meteorology), the second panel shows EMEP_climate (based on WRF_future 2050-2059 meteorology under RCP8.5) output, both simulations are based on reported emissions for 2008-2017. The third panel shows the relative and the fourth panel shows the absolute change between EMEP_climate and EMEP_recent. The numbers in the centre represent the respective means for the Netherlands in the same units.

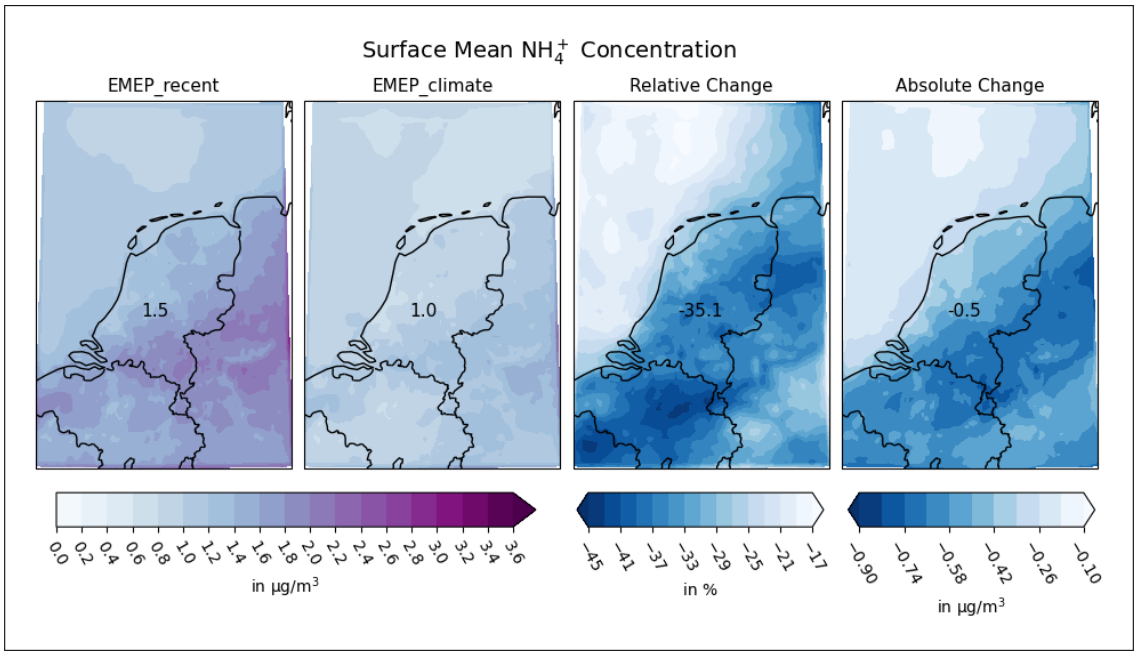

Figure 22: Same as in Figure 21 for ammonium (NH_4^+) in µg/m^3.

Ammonium (NH_4^+) concentrations (Figure 22) show a similar pattern to NH_3 concentrations but the decrease in concentrations from EMEP_recent to EMEP_climate is more pronounced with an average decrease by 35.1% in the Netherlands. NH_4^+ decreases in all of domain 3, including the regions in which NH_3 slightly increases. The absolute decrease in the Netherlands follows a north-west to south-east gradient with the lowest decrease along the coast, where concentrations are low.

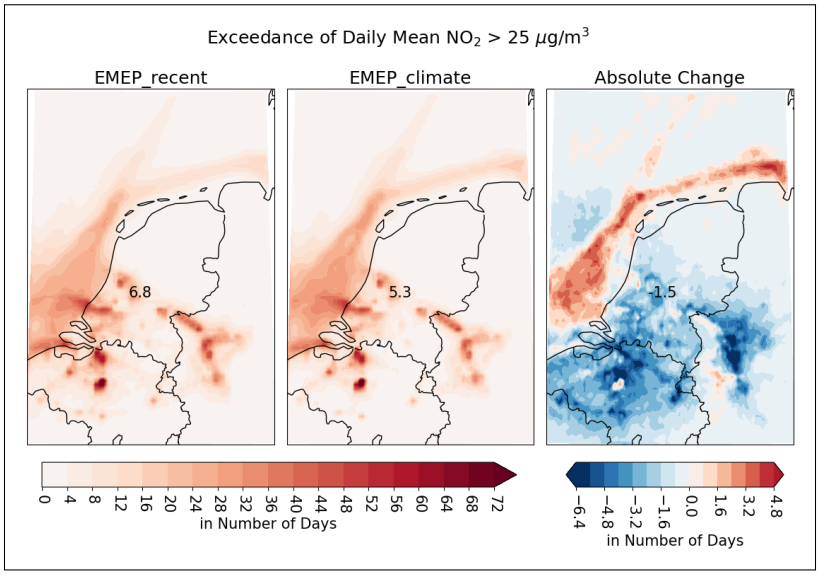

Figure 23: 10-year mean of number of days in summer with surface mean NO_2 concentrations higher than the 25 µg/m^3 WHO daily NO_2 threshold. Panels 1 and 2 show the number of exceedance days for EMEP_recent (based on WRF_recent 2008-2017 meteorology) and EMEP_climate (based on WRF_future 2050-2059 meteorology under RCP8.5) respectively. Both simulations are based on reported emissions for 2008-2017. Panel 3 displays the absolute change. The numbers in the centre represent the respective mean for the Netherlands.

The average number of days per summer in which WHO air quality standard (Section 1.2: Table 2) for nitrogen dioxide (NO_2) is exceeded (Figure 23) is reduced from 6.8 days (EMEP_recent) to 5.3 days (EMEP_climate). The decrease is highest in the most polluted areas over land. In EMEP_recent the each inhabitant is on average exposed to 14.5 days per summer of harmful levels of NO_2. This exposure decreases by 15% in a future climate (Section 5.4: Table 12).

The 10-year summertime average of total monthly nitrogen deposition (Figure 24) is highest in the south-east of the Netherlands and in parts of Lower Saxony and Belgium. In the Netherlands it correlates strongly with the distance to the coast. From EMEP_recent to EMEP_climate total deposition of nitrogen species decreases by 9.4 % in the Netherlands. This decrease is accompanied by a strong decrease of nitrogen deposition in Lower Saxony and an increase of nitrogen deposition in western Belgium and southern North-Rhine Westphalia with the strongest increase of domain 3 in the Eifel. The monthly amount of deposited nitrogen decreases for all processes except for the dry deposition of oxidised nitrogen which increases slightly by 3.5% (Table 9). The decrease of wet deposition of re-

duced nitrogen accounts for 56% of the total decrease, 44% of which are due to a reduction in the wet deposition of NH_3.

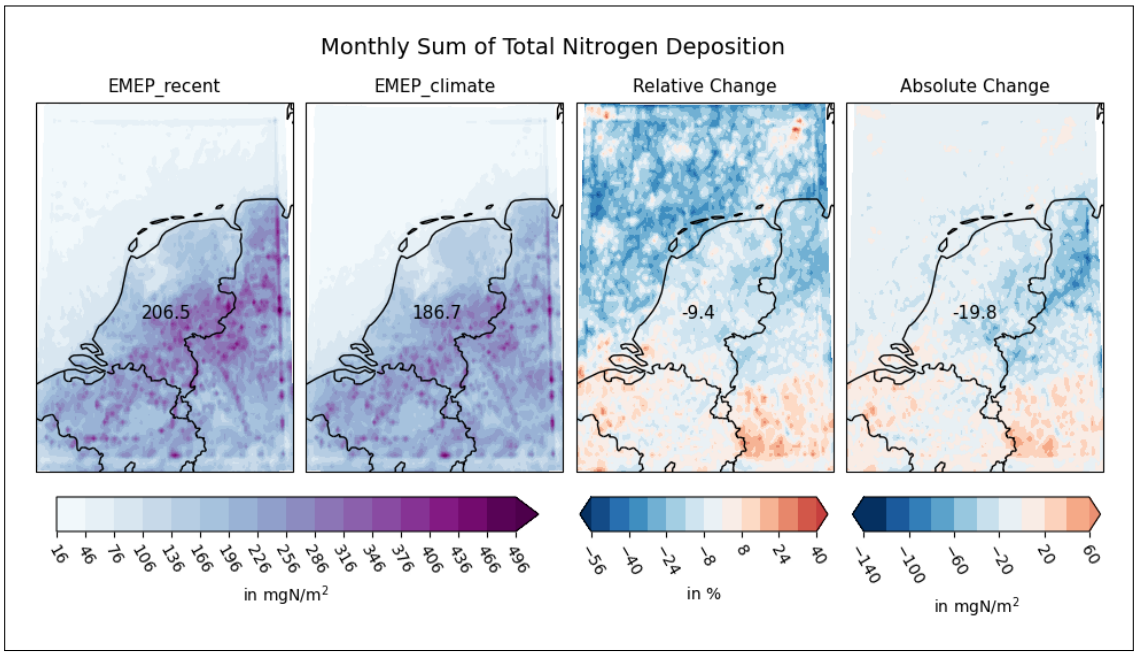

Figure 24: 10-year summertime (JJA) average of monthly sums of wet and dry deposition of reduced and oxidised nitrogen in mgN/m^2 as output for domain 3. The first panel shows EMEP_recent (based on WRF_recent 2008-2017 meteorology), the second panel shows EMEP_climate (based on WRF_future 2050-2059 meteorology under RCP8.5) output, both simulations are based on reported emissions for 2008-2017. The third panel displays the relative change and the fourth panel the absolute change between EMEP_climate and EMEP_recent. The numbers in the centre represent the respective means for the Netherlands in the same units.

	EMEP_recent	EMEP_climate		
	Mean in mgN/m^2	Mean in mgN/m^2	Relative Change in %	Absolute Change in mgN/m^2
Wet deposition of NH_3	50.9	42.1	-16.8	-8.8
Wet deposition of NH_4^+	14.1	11.8	-14.7	-2.3
Wet deposition of reduced nitrogen	65.0	53.9	-16.5	-11.1
Dry deposition of reduced nitrogen	63.7	57.4	-10.4	-6.3
Wet deposition of oxidised nitrogen	35.9	32.0	-10.7	-3.9
Dry deposition of oxidised nitrogen	41.9	43.5	3.5	1.6
Total deposition of nitrogen	206.5	186.7	-9.4	-19.8

Table 9: Overview of the 10-year summertime (JJA) mean of monthly sums of nitrogen deposition for the land surface of the Netherlands in its different forms for EMEP_recent and EMEP_climate, their relative, and absolute change.

5.2.3 Fine Particulate Matter

In EMEP_recent the mean fine particulate matter ($PM_{2.5}$) concentrations follow a gradient with low concentrations over the North Sea in the northwest of domain 3 and high

concentrations in the southeast of domain 3 (Figure 25). An exception to the low concentrations over the North Sea are the shipping routes close to Rotterdam and The Hague. The mean concentrations are highest in the Ruhr region in Germany. From EMEP_recent to EMEP_climate $PM_{2.5}$ concentrations decrease in the entire domain and by 25% on average in the Netherlands.

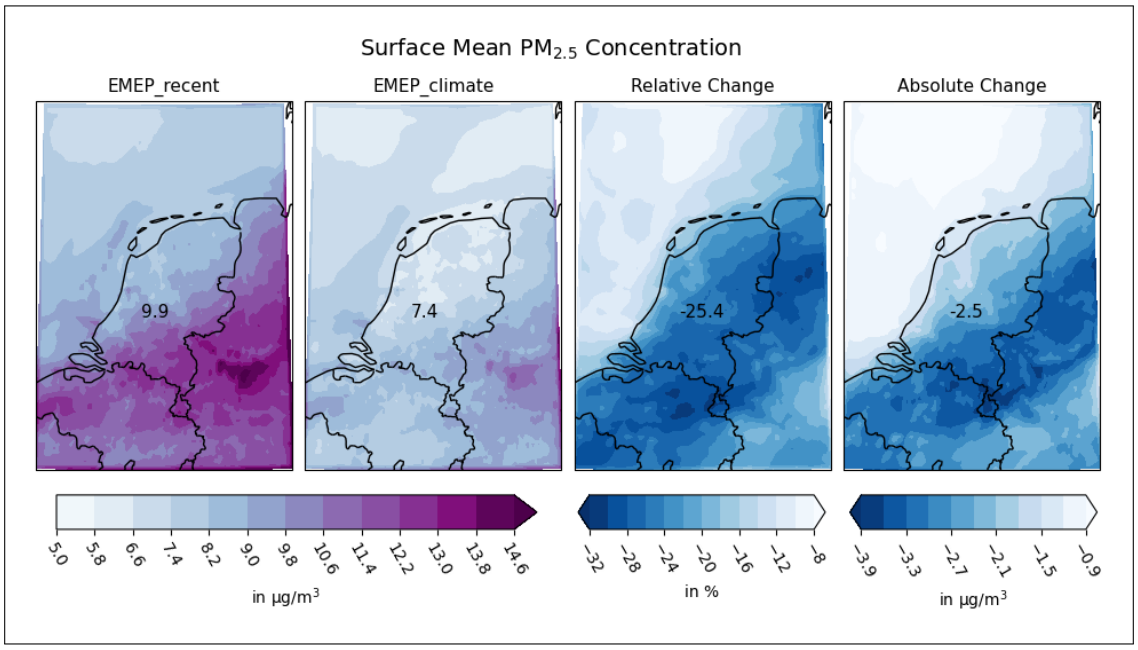

Figure 25: 10-year summertime (JJA) average of daily mean surface $PM_{2.5}$ concentrations in µg/m^3 as output for domain 3. The first panel shows EMEP_recent (based on WRF_recent 2008-2017 meteorology), the second panel shows EMEP_climate (based on WRF_future 2050-2059 meteorology under RCP8.5) output, both simulations are based on reported emissions for 2008-2017. The third panel shows the relative and the fourth panel shows the absolute change between EMEP_climate and EMEP_recent. The numbers in the centre represent the respective means for the Netherlands in the same units.

This decrease in $PM_{2.5}$ concentrations leads to a decrease of the numbers of days per summer in which the WHO air quality threshold (Section 1.2: Table 2) is exceeded from 17.1 days (EMEP_recent) to 8.2 days (EMEP_climate) per summer for the Netherlands (Figure 26). For domain 3 the decrease is most pronounced on the border of Lower Saxony and North-Rhine Westphalia in Germany and the northeast of Belgium. The exposure of the population is 16.4 days on average in EMEP_recent and decreases by 55% solely as an effect of climate change (Section 5.4: Table 12).

The composition of $PM_{2.5}$ changes in a future climate (Figure 27). Nitrate (NO_3^-) constitutes the largest fraction in both simulations but halves from EMEP_recent to EMEP_climate. Ammonium (NH_4^+) also decreases by approximately one third. All other components decrease slightly except for particulate organic matter, which increases slightly from 1.62 µg/m^3 (EMEP_recent) to 1.73 µg/m^3 (EMEP_climate).

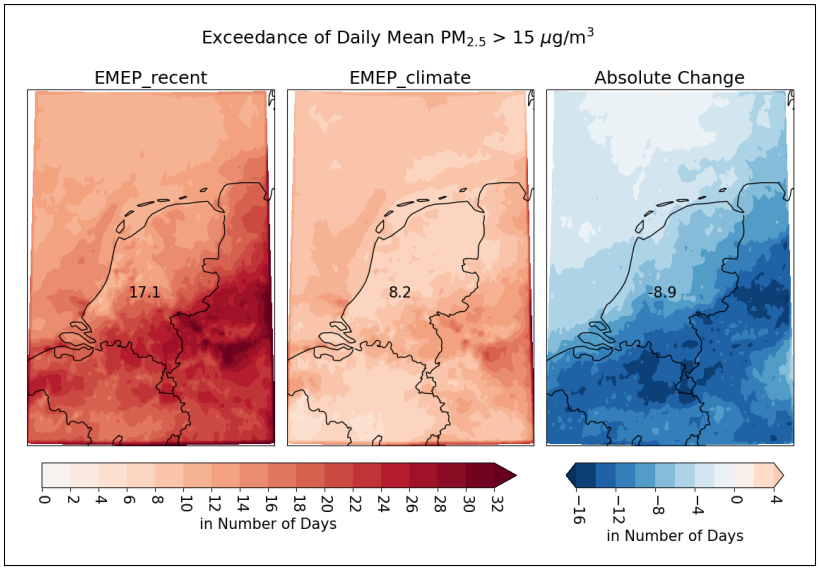

Figure 26: 10-year mean of number of days in summer (JJA) with surface $PM_{2.5}$ concentrations higher than 15 µg/m^3 WHO daily ozone threshold. Panels 1 and 2 show the number of exceedance days for EMEP_recent (based on WRF_recent 2008-2017 meteorology) and EMEP_climate (based on WRF_future 2050-2059 meteorology under RCP8.5) respectively. Both simulations are based on reported emissions for 2008-2017. Panel 3 displays the absolute change. The numbers in the centre represent the respective mean for the Netherlands.

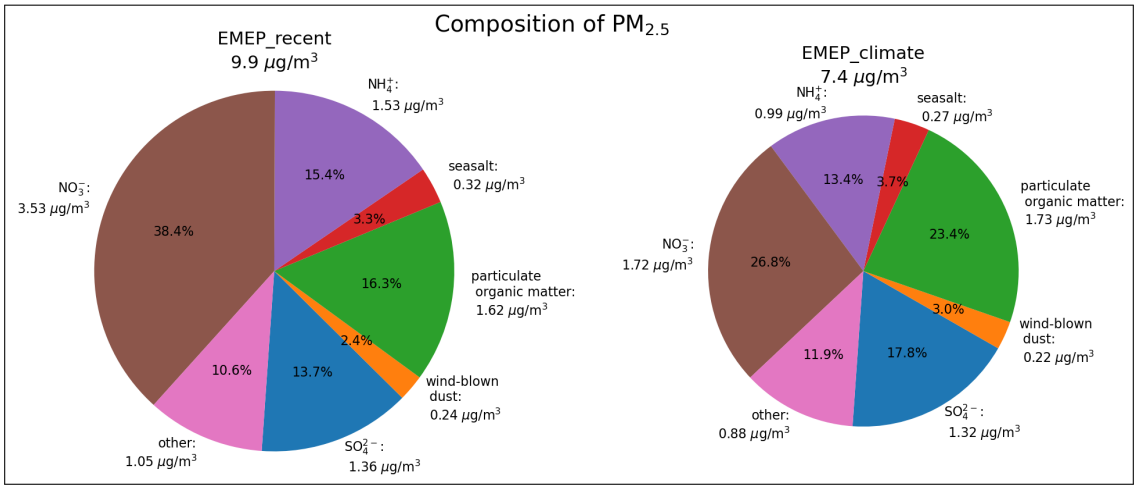

Figure 27: 10-year summertime (JJA) average composition of $PM_{2.5}$ over the Netherlands. The left panel shows the composition for EMEP_recent (based on WRF_recent 2008-2017 meteorology), the right panel shows EMEP_climate (based on WRF_future 2050-2059 meteorology under RCP8.5) output, both simulations are based on reported emissions for 2008-2017.

5.3 Effect of Emission Reduction Measures on Air Quality

In this section the effect of emission reduction measures on air quality is analysed by comparing the output of EMEP_recent with the output of EMEP_mitigation. Both share the same meteorological fields of WRF_recent (2008-2017) and differ in their emission input. EMEP_recent is based on reported emissions of 2008-2017 (Section 3.4.1) and EMEP_mitigation is based on the ECLIPSE V6b Maximum Feasible Reduction scenario for 2050 (Section 3.4.2). Where useful, the effect of emission reductions in a future climate between EMEP_climate and EMEP_future (both based on WRF_future) is analysed in addition.

A comparison of the results in this section with the results of Section 5.2 forms the basis for a discussion of research question 4 (How does the effect of climate change compare to the effect of strong air pollutant emission reductions on summertime air quality?) in Section 6.2.2.

5.3.1 Ozone

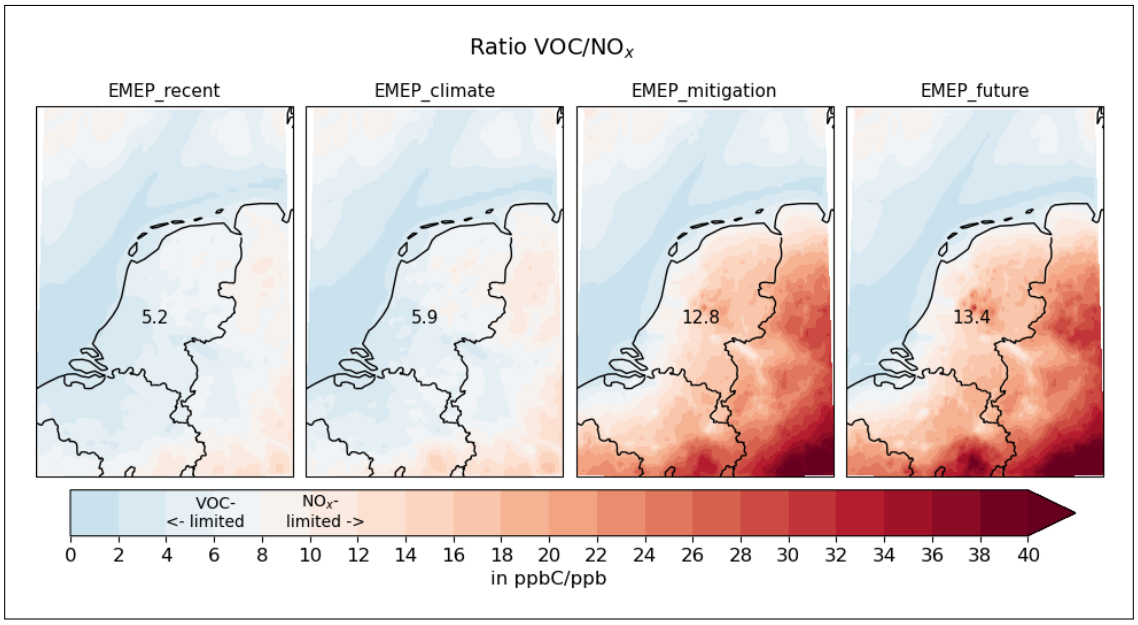

Figure 28: Summertime (JJA) 10-year mean ratio of VOCs in ppbC and NOx in ppb, blue marks VOC-limited areas and red marks NO_x-limited areas for EMEP_recent in panel 1, EMEP_climate in panel 2, EMEP_mitigation in panel 3 and EMEP_future in panel 4. The number in the centre represents the respective mean ratio for the Netherlands in ppbC/ppb.

Figure 28 shows the shift in photochemical regimes for ozone production based on the ratio of VOC in ppbC and NO_x in ppb (Section 2.2). It shows that the Netherlands are dominated by a VOC-limited ozone production regime under the scenarios with 2008-2017 emission data with mean VOC/NO_x ratios of 5.2 ppbC/ppb (EMEP_recent) and 5.9 ppbC/ppb (EMEP_climate). In the scenarios with reduced emissions, the regime changes to an NO_x-limited regime with 12.8 ppbC/ppb (EMEP_mitigation) and 13.4 ppbC/ppb

(EMEP_future). Over Belgium the regimes are similar to the ones for the Netherlands for each simulation respectively. In Germany the ratio increases to the southeast of the domain. The photochemical ozone production regime is VOC-limited for all simulations over the shipping routes of in the North Sea (with unchanged emissions in all simulations).

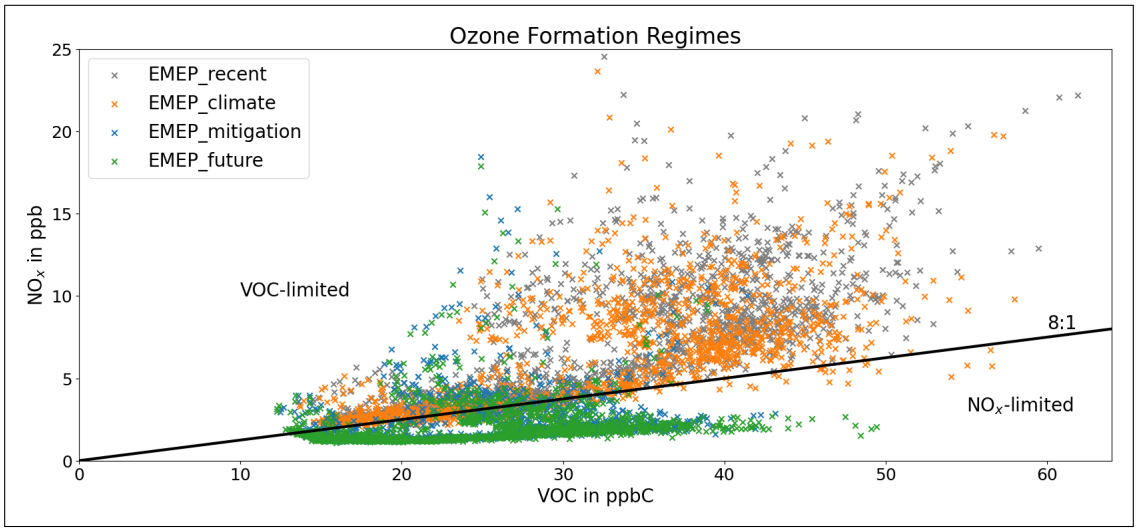

Figure 29: Summertime 10-year mean surface concentrations of VOC in ppbC and NO_x in ppb per gridpoint in domain 3 within the Netherlands for EMEP_recent (grey), EMEP_climate (orange), EMEP_mitigation (blue) and EMEP_future (green), the black line marks a ratio of 8:1 (VOC in ppbC : NOx in ppb)

EMEP_recent and EMEP_climate (Figure 29) have a higher spatial spread in surface mixing ratios of NO_x and of VOC than EMEP_mitigation and EMEP_future. With reduced emissions in EMEP_mitigation and EMEP_future, the NO_x mixing ratio and its spatial spread decrease strongly and the spatial spread in VOC mixing ratios decreases with much less grid points with mixing ratios larger than 40 ppbC compared to EMEP_recent and EMEP_climate.

The daily maximum 8-hour mean ozone concentrations (Figure 30) are projected to decrease by 0.9% on average for the Netherlands with emission reductions but the local changes range from -12% to +28% in domain 3 with ozone increasing mostly in the metropolitan areas and in the shipping areas of the Lower Rhine and the Rhine-Meuse-Scheldt delta and decreasing in the north of the Netherlands. Both VOCs and NO_x decrease in those areas with a stronger relative change in NO_x (Appendix D.3: Figure 66 and 67).

Dry deposition of ozone (Figure 31) increases by 1.4% on average for the Netherlands from EMEP_recent to EMEP_mitigation. The increase is limited to the southern half of the Netherlands and urban areas. In the norther half dry deposition decreases.

The average number of days in the Netherlands for which the WHO air quality standard for ozone (Section 1.2: Table 2) is exceeded (Figure 32) decreases from 15.5 days

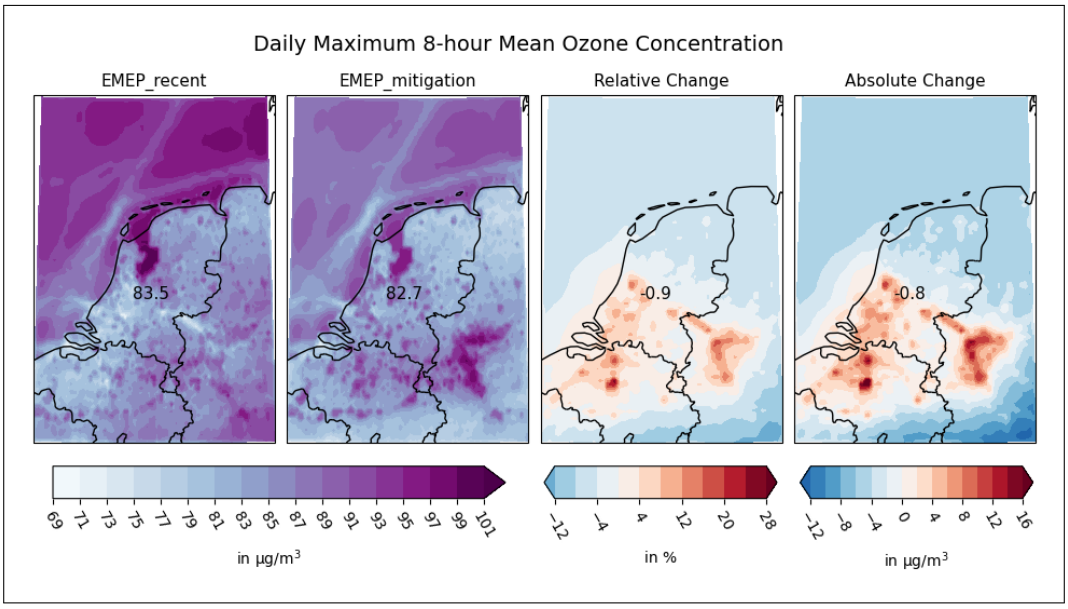

Figure 30: 10-year summertime (JJA) average of daily maximum 8-hour mean surface ozone concentrations in µg/m^3 as output for domain 3. The first panel shows EMEP_recent (based on reported emission for 2008-2017), the second panel shows EMEP_mitigation (based on ECLIPSE V6b MFR 2050 emissions) output, both simulations are based on WRF_recent (2008-2017) meteorology. The third panel shows the relative and the fourth panel shows the absolute change between EMEP_mitigation and EMEP_recent. The numbers in the centre represent the respective means for the Netherlands in the same units.

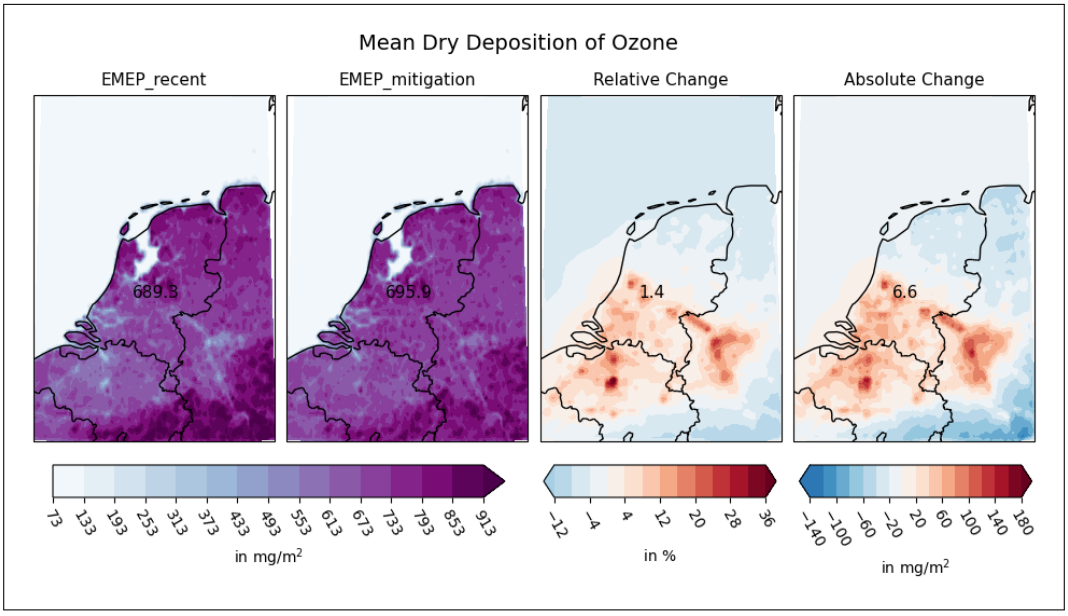

Figure 31: 10-year summertime (JJA) average of total monthly dry deposition of ozone in mg/m^2 as output for domain 3. The first panel shows EMEP_recent (based on reported emission for 2008-2017), the second panel shows EMEP_mitigation (based on ECLIPSE V6b MFR 2050 emissions) output, both simulations are based on WRF_recent (2008-2017) meteorology. The third panel displays the relative change and the fourth panel the absolute change between EMEP_mitigation and EMEP_recent. The numbers in the centre represent the respective means for the Netherlands in the same units

(EMEP_recent) per summer to 12.6 days (EMEP_mitigation). The number of days decreases in most parts of the domain, except for the urban centres. The average exposure to harmful levels of O_3 therefore stays nearly constant with a 1% increase in EMEP_mitigation from the base level of 17.2 days in EMEP_recent (Section 5.4: Table 12).

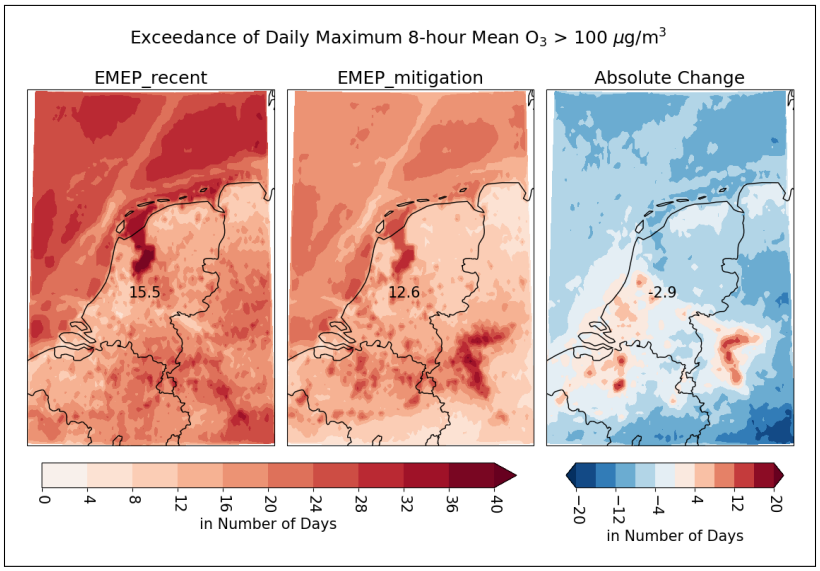

Figure 32: 10-year mean of number of days in summer with surface ozone concentrations higher than 100 µg/m^3 WHO daily ozone threshold. Panels 1 and 2 show the number of exceedance days for EMEP_recent (based on reported emission for 2008-2017) and EMEP_mitigation(based on ECLIPSE V6b MFR 2050 emissions) output, both simulations are based on WRF_recent (2008-2017) meteorology. Panel 3 displays the absolute change. The numbers in the centre represent the respective mean for the Netherlands.

5.3.2 Reduced and Oxidised Nitrogen

With the Maximum Feasible Reduction scenario for emission reductions surface ammonia (NH_3, Figure 33) concentrations decrease most strongly in Lower Saxony by up to 50%. In the Netherlands NH_3 concentrations decrease by 20.7% on average. The relative change is similar for all provinces with around -20% including the southern provinces Limburg and North Brabant, in which ammonia concentrations are the highest.

Ammonium (NH_4^+) decreases more strongly than ammonia by an average of 60.9% for the Netherlands (Figure 34). The spatial pattern shows less correlation with agricultural land-use and more correlation to the distance of the coast.

The exceedance of WHO air quality standards (Section 1.2: Table 2) for NO_2 (Figure 35) is reduced drastically from 6.8 days (EMEP_recent) to 0.5 days (EMEP_mitigation). In the entire domain, except for the shipping routes for which emissions are unchanged, there are no regions in EMEP_mitigation in which the number of exceedance days is more than 4 per summer. The exposure of the inhabitants of the Netherlands decreases by 81%

(EMEP_mitigation) from an exposure of 14.5 days in EMEP_recent as a result of emission controls (Section 5.4: Table 12).

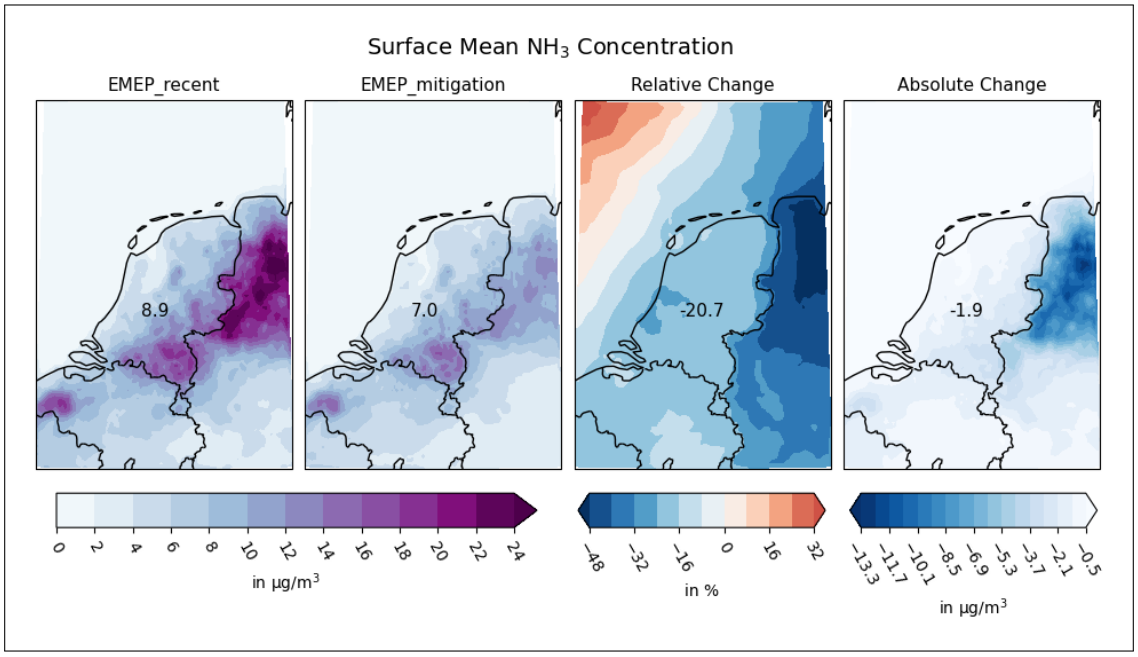

Figure 33: 10-year summertime (JJA) average of daily mean surface ammonia (NH_3) concentrations in µg/m^3 as output for domain 3. The first panel shows EMEP_recent (based on reported emission for 2008-2017), the second panel shows EMEP_mitigation (based on ECLIPSE V6b MFR 2050 emissions) output, both simulations are based on WRF_recent (2008-2017) meteorology. The third panel shows the relative and the fourth panel shows the absolute change between EMEP_mitigation and EMEP_recent. The numbers in the centre represent the respective means for the Netherlands in the same units.

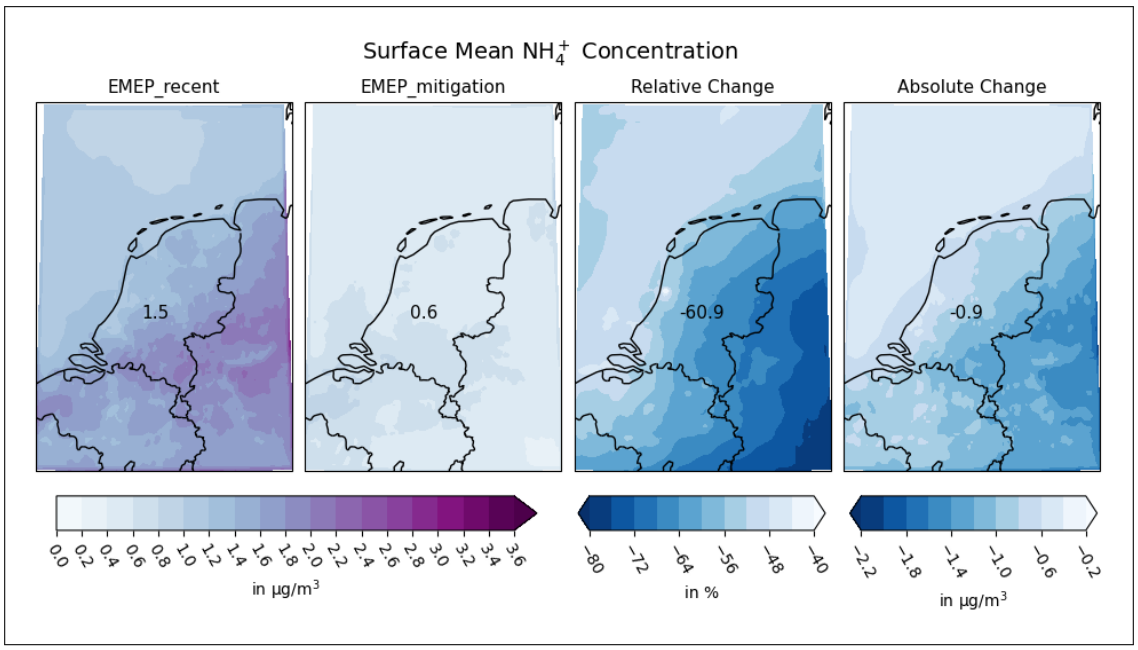

Figure 34: Same as in Figure 33 for ammonium (NH_4^+) in µg/m^3.

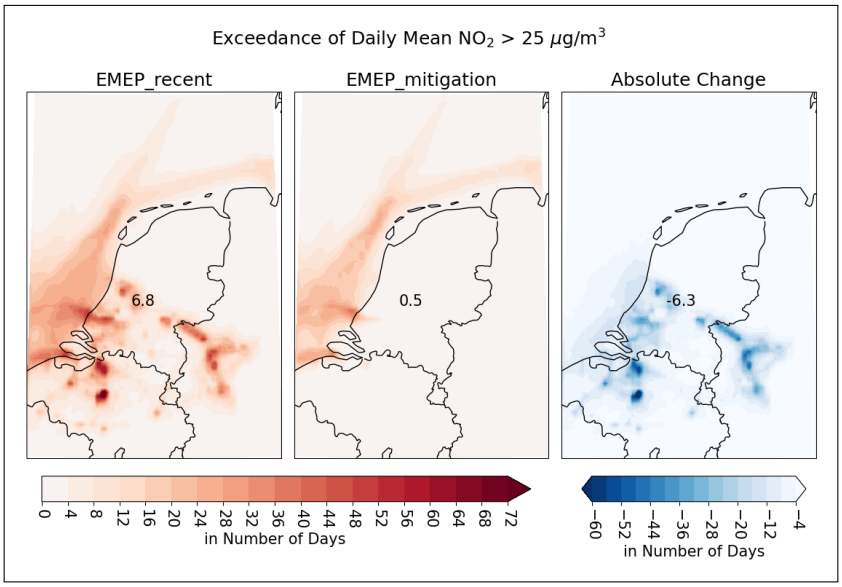

Figure 35: 10-year mean of number of days in summer with surface mean NO_2 concentrations higher than the 25 µg/m^3 WHO daily NO_2 threshold. Panels 1 and 2 show the number of exceedance days for EMEP_recent (based on reported emission for 2008-2017) and EMEP_mitigation (based on ECLIPSE V6b MFR 2050 emissions) output, both simulations are based on WRF_recent (2008-2017) meteorology. Panel 3 displays the absolute change. The numbers in the centre represent the respective mean for the Netherlands.

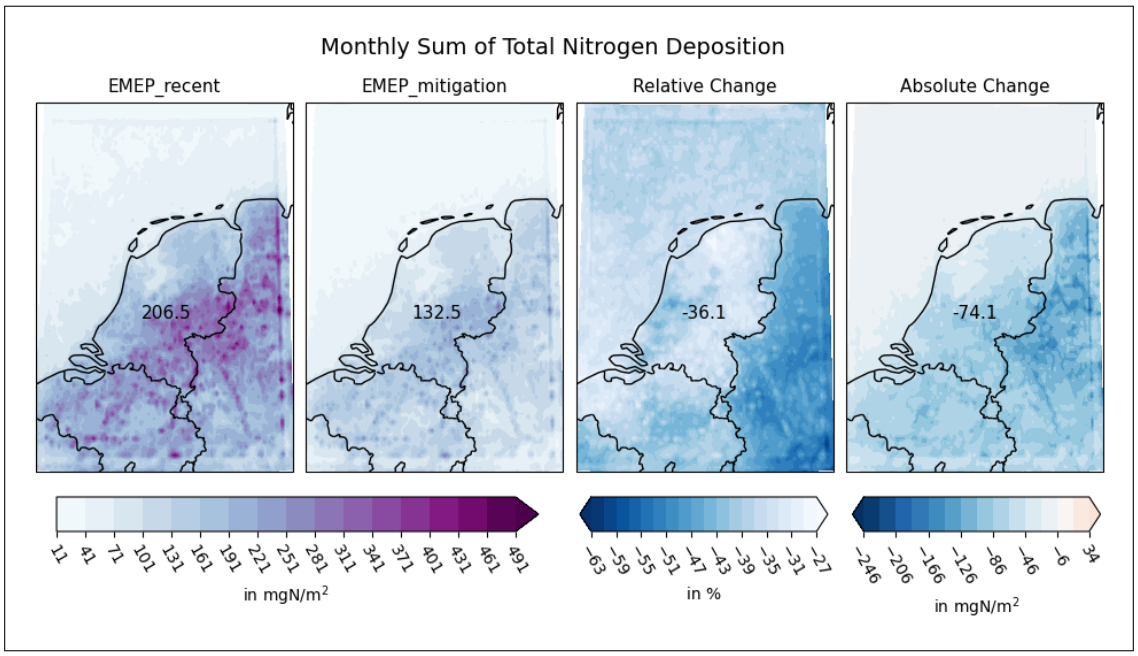

Figure 36: 10-year summertime (JJA) average of monthly sums of wet and dry deposition of reduced and oxidised nitrogen in mgN/m^2 as output for domain 3. The first panel shows EMEP_recent (based on reported emission for 2008-2017), the second panel shows EMEP_mitigation (based on ECLIPSE V6b MFR 2050 emissions) output, both simulations are based on WRF_recent (2008-2017) meteorology. The third panel shows the relative and the fourth panel shows the absolute change between EMEP_mitigation and EMEP_recent. The numbers in the centre represent the respective means for the Netherlands in the same units.

The total nitrogen deposition (Figure 36) decreases by an average of 36.1% in the Netherlands but less strongly in the Netherlands than in the adjacent regions in Germany. Table 10 gives an overview of the role of the wet and dry deposition of reduced and oxidised components in the Netherlands. The deposition of oxidised nitrogen, which makes up only 38% of the total deposition of nitrogen, accounts for 59% of the decrease in total nitrogen deposition.

	EMEP_ recent	EMEP_ mitigation		
	Mean in mgN/m^2	Mean in mgN/m^2	Relative Change in %	Absolute Change in mgN/m^2
Wet deposition of NH_3	50.9	44.9	-11.2	-6.0
Wet deposition of NH_4^+	14.1	5.7	-59.4	-8.4
Wet deposition of reduced nitrogen	65.0	50.6	-22.2	-14.5
Dry deposition of reduced nitrogen	63.7	47.6	-26.6	-16.2
Wet deposition of oxidised nitrogen	35.9	15.9	-55.7	-20.0
Dry deposition of oxidised nitrogen	41.9	18.4	-55.0	-23.5
Total deposition of nitrogen	206.5	132.5	-36.1	-74.1

Table 10: Overview of the 10-year summertime (JJA) mean of monthly sums of nitrogen deposition for the land surface of the Netherlands in its different forms for EMEP_recent and EMEP_mitigation, their relative, and absolute change.

5.3.3 Fine Particulate Matter

Fine particulate matter ($PM_{2.5}$) concentrations decrease by an average of 47.6% in the Netherlands in EMEP_mitigation compared to EMEP_recent (Figure 37). The decrease is strongest in the most polluted areas in the Netherlands. In the Rhine-Ruhr region, $PM_{2.5}$ concentrations decrease less strongly than in the surrounding areas.

The change in emission leads to a change in the mean composition of $PM_{2.5}$ in the Netherlands between EMEP_recent to EMEP_mitigation (Figure 38). The purely meteorologically influenced components sea salt and wind-blown dust stay constant and all other components decrease. The share and absolute concentration of nitrate decreases most strongly from 3.53 µg/m^3 (EMEP_recent) to 0.98 µg/m^3 (EMEP_mitigation). NH_4^+ also decreases strongly from 1.53 µg/m^3 to 0.59 µg/m^3 with emission reductions. Sulphate (SO_4^{2-}) and particulate organic matter also decrease slightly but particulate organic matter becomes the component with the highest fraction of 27.3%.

The number of days in which the WHO air quality standard for daily mean $PM_{2.5}$ (Section 1.2: Table 2) is exceeded decreases from 17.1 days (EMEP_recent) to 2.9 days (EMEP_mitigation) on average per summer (Figure 39). In the entire domain the maximum number of exceedance days decreases from 32 to 8 days per summer with emission reductions. Emission controls decrease the average exposure by 81% (EMEP_mitigation) from 16.4 days in EMEP_recent (Section 5.4: Table 12).

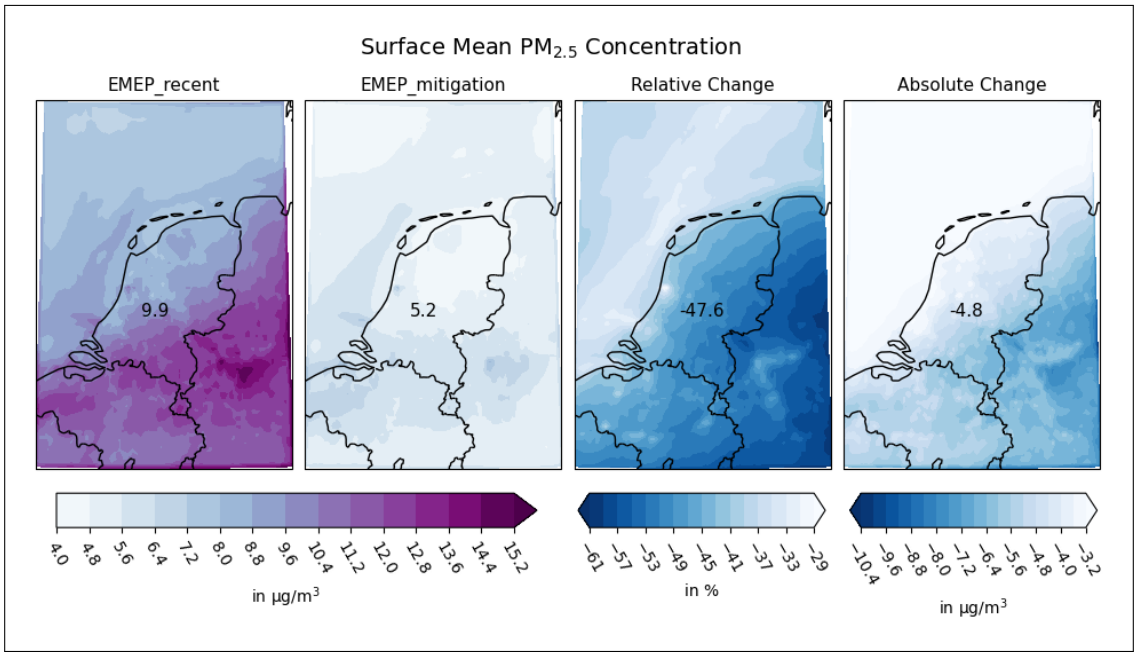

Figure 37: 10-year summertime (JJA) average of daily mean surface $PM_{2.5}$ concentrations in µg/m^3 as output for domain 3. The first panel shows EMEP_recent (based on reported emission for 2008-2017), the second panel shows EMEP_mitigation (based on ECLIPSE V6b MFR 2050 emissions) output, both simulations are based on WRF_recent (2008-2017) meteorology. The third panel shows the relative and the fourth panel shows the absolute change between EMEP_mitigation and EMEP_recent. The numbers in the centre represent the respective means for the Netherlands in the same units.

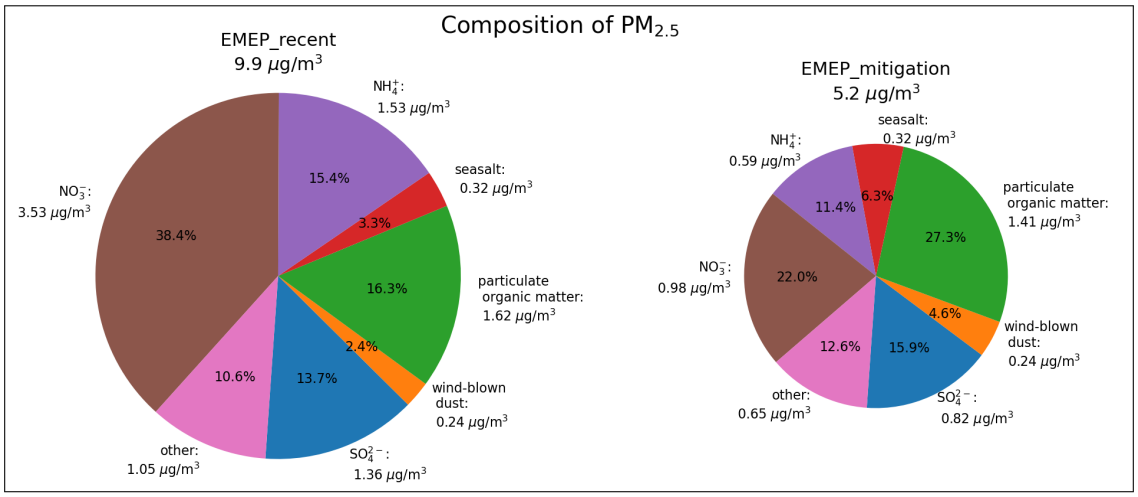

Figure 38: 10-year summertime (JJA) average composition of $PM_{2.5}$ over the Netherlands. The left panel shows the composition for EMEP_recent (based on reported emissions for 2008-2017), the right panel shows EMEP_mitigation (based on ECLIPSE V6b MFR 2050) output, both simulations are based on WRF_recent (2008-2017) meteorology.

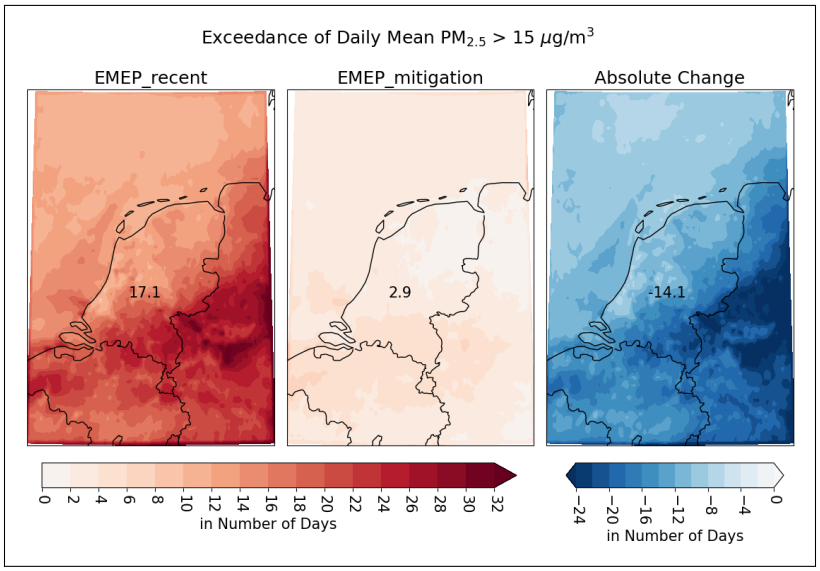

Figure 39: 10-year mean of number of days in summer (JJA) with surface $PM_{2.5}$ concentrations higher than 15 µg/m^3 WHO daily ozone threshold. Panels 1 and 2 show the number of exceedance days for EMEP_recent (based on reported emission for 2008-2017) and EMEP_mitigation (based on ECLIPSE V6b MFR 2050 emissions) output, both simulations are based on WRF_recent (2008-2017) meteorology. Panel 3 displays the absolute change. The numbers in the centre represent the respective mean for the Netherlands.

5.4 Combined Effect of Climate Change and Emission Reductions on Air Quality

This section presents the results of the combined effect of emission reductions under ECLIPSE V6b MFR for 2050 and of climate change under the high climate change scenario RCP8.5 in EMEP_future compared to the base scenario EMEP_recent based on 2008-2017 emissions and meteorology.

By comparing the results in this section with the results in Section 5.2 and Section 5.3 research question 5 (How is the effect of emission controls influenced by climate change and what is the effect of emission controls in a changing climate?) can be assessed in Section 6.2.3.

5.4.1 Ozone

Surface ozone concentrations (Figure 40) are projected to increase in most parts of the Netherlands in EMEP_future compared to EMEP_recent by 5.9% on average. In domain 3 the increase is strongest in the urban areas of Amsterdam, Rotterdam, The Hague, Brussels, Antwerp and the Rhine-Ruhr region. The rural areas located in between those regions show a stronger increase in ozone concentrations than the north of the Netherlands. Ozone concentrations decrease over the North Sea, in western Lower Saxony and the southeast of the domain.

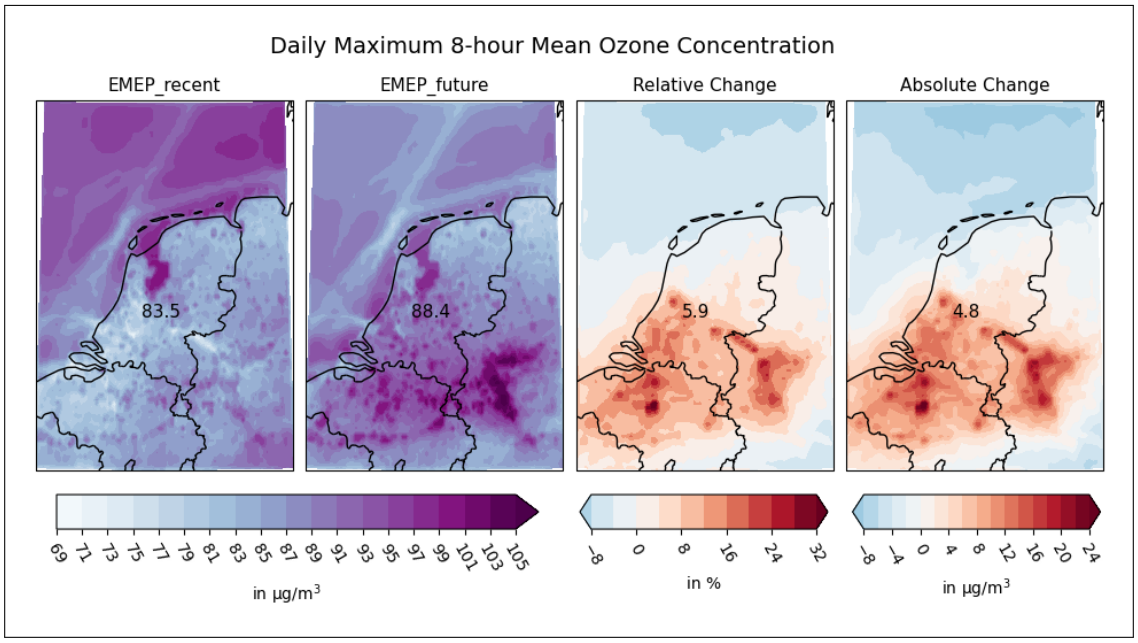

Figure 40: 10-year summertime (JJA) average of daily maximum 8-hour mean surface ozone concentrations in µg/m^3 as output for domain 3. The first panel shows EMEP_recent (based on WRF_recent and reported emission for 2008-2017), the second panel shows EMEP_future (based on WRF_future and ECLIPSE V6b MFR 2050 emissions) output. The third panel shows the relative and the fourth panel shows the absolute change between EMEP_future and EMEP_recent. The numbers in the centre represent the respective means for the Netherlands in the same units.

The density function of 10-year average of the mean over the Netherlands showing the mean concentrations for each day of summer (Figure 41) shifts to higher concentrations from EMEP_recent to EMEP_climate. The temporal variability narrows and the most frequent concentration decreases slightly from EMEP_recent to EMEP_mitigation. The combined effect from EMEP_recent to EMEP_future is a shift to higher concentrations with a broadening of the most common concentrations.

The spatial variability of the number of days in which WHO air quality standards (Section 1.2: Table 2) for ozone are exceeded increases from EMEP_recent to EMEP_future (Figure 42). In urban areas, such as Amsterdam and Brussels and in the Lower Rhine Region, where the number of exceedance days is lower than average in EMEP_recent, the increases to EMEP_future are most pronounced. In addition, the Rhine-Ruhr area with the number of exceedances higher than average in EMEP_recent experiences a strong increase. In areas located in between those areas the exceedances also increase. The number of exceedances decreases in the north of the Netherlands, western Lower Saxony and the southeast of domain 3. The average exposure of the population increases by 36% from 17.2 days in EMEP_recent as the effect of climate change and emission controls. This increase is higher than the effect of emission reductions alone but lower than the effect of climate change (Table 12).

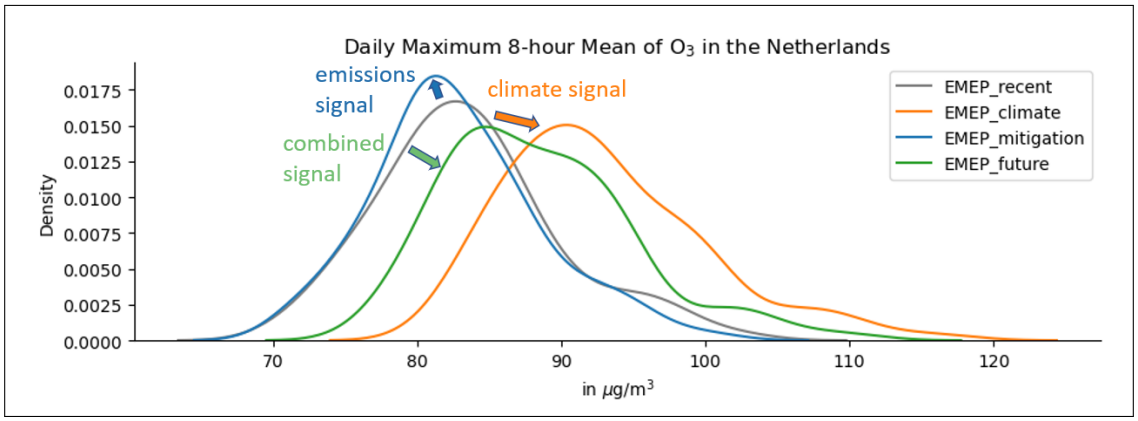

Figure 41: Density function for the daily maximum 8-hour mean ozone concentration for all 92 days of June to August averaged over 10-years and the Netherlands. The shift from the grey to the orange curve depicts the change between EMEP_recent and EMEP_climate with constant emissions (reported emissions for 2008-2017) and a changing climate (WRF_recent to WRF_future). The shift from the grey to the blue curve depicts the change between EMEP_recent and EMEP_mitigation with constant meteorology (WRF_recent) and emissions reductions from the reported emissions for 2008-2017 to ECLIPSE V6b MFR 2050. The shift from the grey to the green curve depicts the combined effect of meteorology and emission changes.

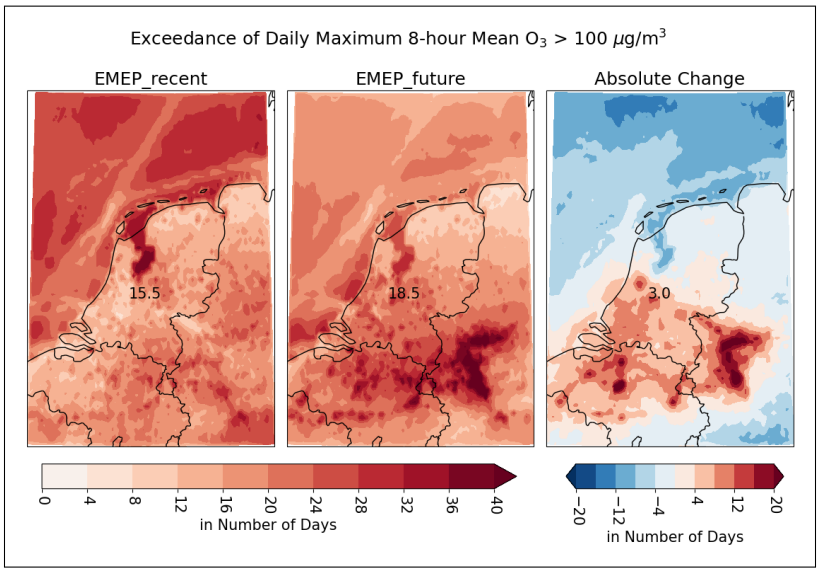

Figure 42: 10-year mean of number of days in summer with daily maximum 8-hour mean surface ozone concentrations higher than 100 µg/m^3 WHO daily ozone threshold. Panels 1 and 2 show the number of exceedance days for EMEP_recent (based on WRF_recent reported emission for 2008-2017) and EMEP_future (based on WRF_future and ECLIPSE V6b MFR 2050 emissions) output. Panel 3 displays the absolute change. The numbers in the centre represent the respective mean for the Netherlands.

The change in mean dry deposition between EMEP_recent and EMEP_future (Figure 43) shows the same spatial pattern as the change in surface maximum 8-hour mean ozone concentrations (Figure 40) with a relative change of similar magnitude.

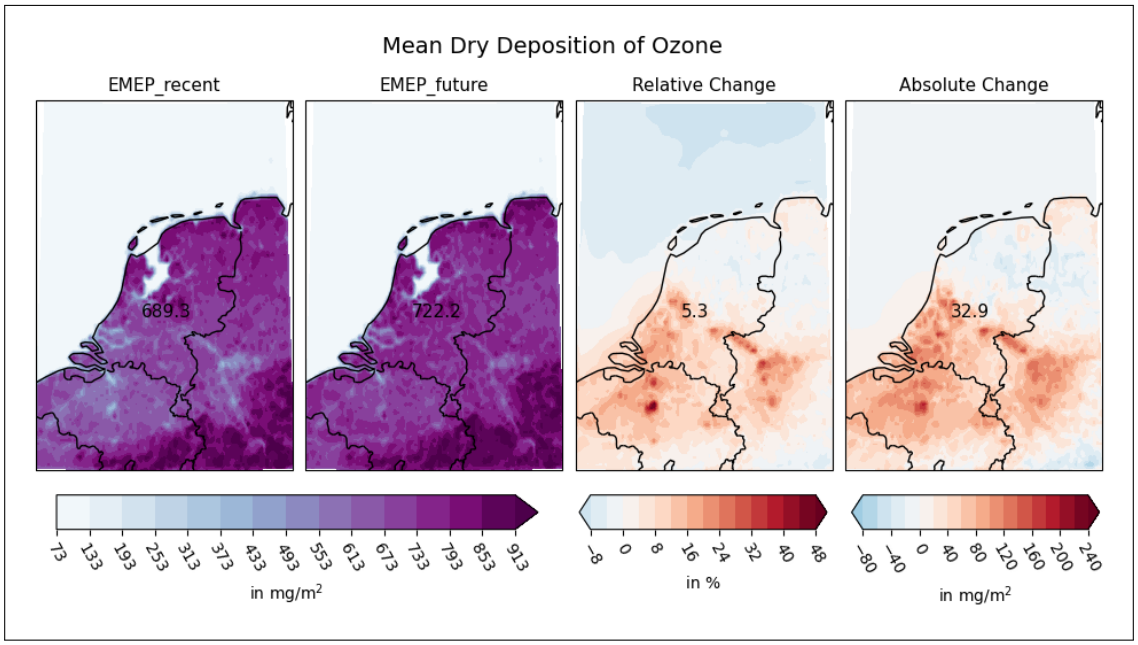

Figure 43: 10-year summertime (JJA) average of total monthly dry deposition of ozone in mg/m^2 as output for domain 3. The first panel shows EMEP_recent (based on WRF_recent and reported emission for 2008-2017), the second panel shows EMEP_future (based on WRF_future and ECLIPSE V6b MFR 2050 emissions) output. The third panel shows the relative and the fourth panel shows the absolute change between EMEP_future and EMEP_recent. The numbers in the centre represent the respective means for the Netherlands in the same units.

5.4.2 Reduced and Oxidised Nitrogen

Surface ammonia (NH_3) decreases by 27.6% on average in the Netherlands (Figure 44). The decrease is more strongly both in absolute and relative measures in western Lower Saxony than in the Netherlands.

The density function of the mean NH_3 concentrations for each day in summer, averaged over 10-years and the Netherlands (Figure 45), shows a shift of the highest concentrations to lower ones from EMEP_recent to EMEP_climate which leads to a narrower distribution. From EMEP_recent to EMEP_mitigation the reduction of concentrations is more pronounced and the distribution is narrowed similarly to the one of EMEP_climate. The combined effect of climate change and emission reductions leads to a stronger decrease of the total values and the seasonal variability of the NH_3 concentrations.

Ammonium (NH_4^+) concentrations decrease by an average of 76.0% in the Netherlands from EMEP_recent to EMEP_future (Figure 46). The decrease in domain 3 is lowest over the North Sea where NH_4^+concentrations are halved and strengthens to the southeast of the domain to up to 90%.

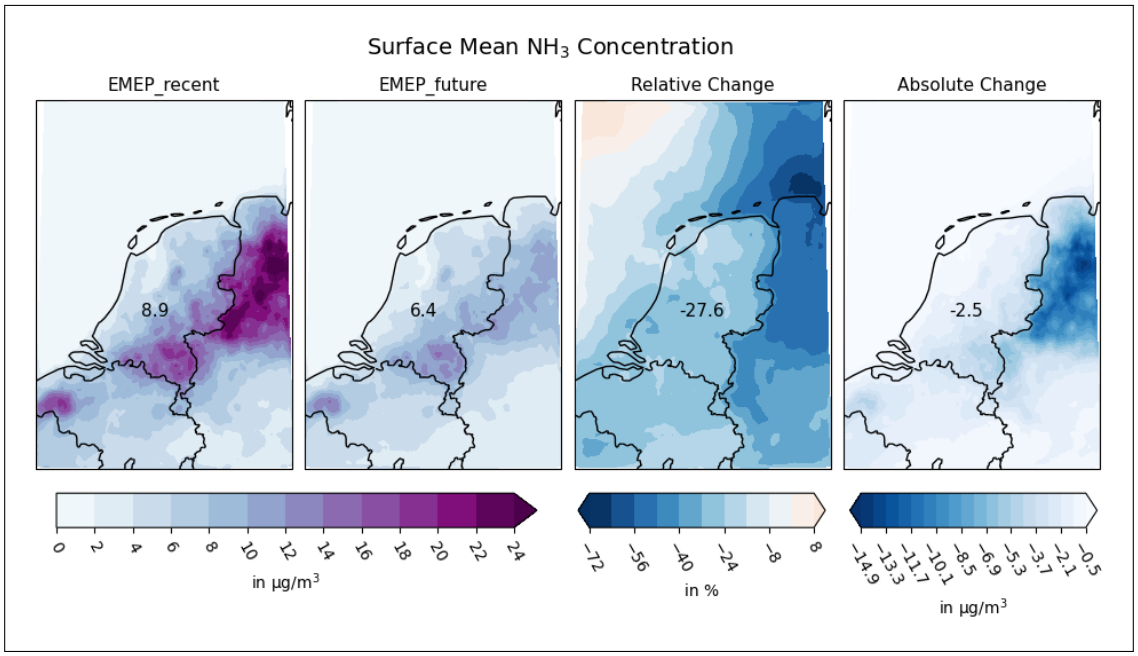

Figure 44: 10-year summertime (JJA) average of daily mean surface ammonia (NH_3) concentrations in µg/m^3 as output for domain 3. The first panel shows EMEP_recent (based on WRF_recentand reported emission for 2008-2017), the second panel shows EMEP_future (based on WRF_future and ECLIPSE V6b MFR 2050 emissions) output. The third panel shows the relative and the fourth panel shows the absolute change between EMEP_future and EMEP_recent. The numbers in the centre represent the respective means for the Netherlands in the same units.

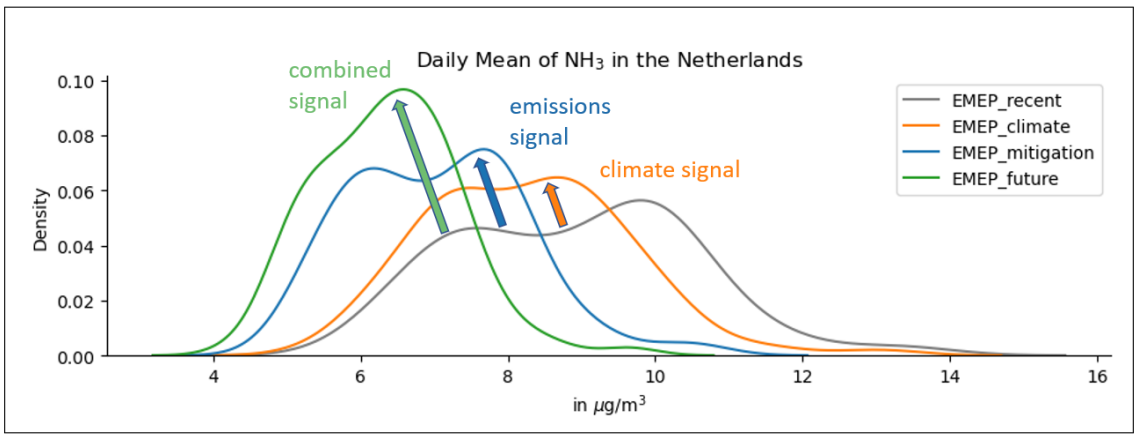

Figure 45: Density function for the daily mean NH_3 concentration in µg/m^3 for all 92 days of June to August averaged over 10-years and the Netherlands. The shift from the grey to the orange curve depicts the change between EMEP_recent and EMEP_climate with constant emissions (reported emissions for 2008-2017) and a changing climate (WRF_recent to WRF_future). The shift from the grey to the blue curve depicts the change between EMEP_recent and EMEP_mitigation with constant meteorology (WRF_recent) and emissions reductions from the reported emissions for 2008-2017 to ECLIPSE V6b MFR 2050. The shift from the grey to the green curve depicts the combined effect of meteorology and emission changes.

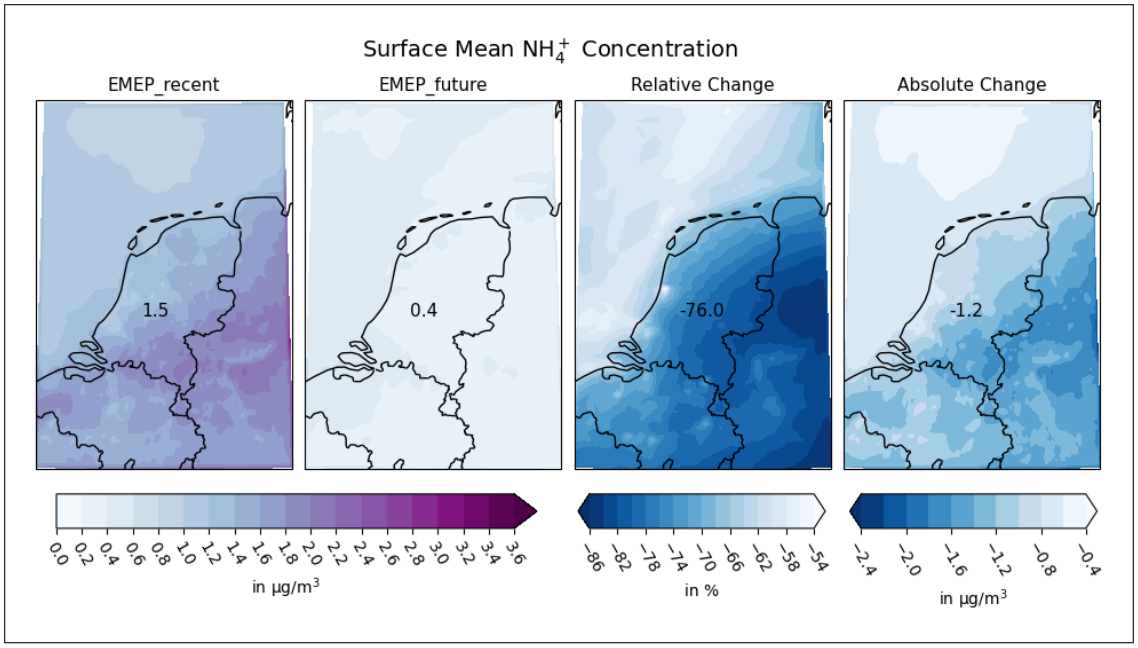

Figure 46: 10-year summertime (JJA) average of daily mean surface ammonium (NH_4^+) concentrations in µg/m^3 as output for domain 3. The first panel shows EMEP_recent (based on WRF_recentand reported emission for 2008-2017), the second panel shows EMEP_future (based on WRF_future and ECLIPSE V6b MFR 2050 emissions) output. The third panel shows the relative and the fourth panel shows the absolute change between EMEP_future and EMEP_recent. The numbers in the centre represent the respective means for the Netherlands in the same units.

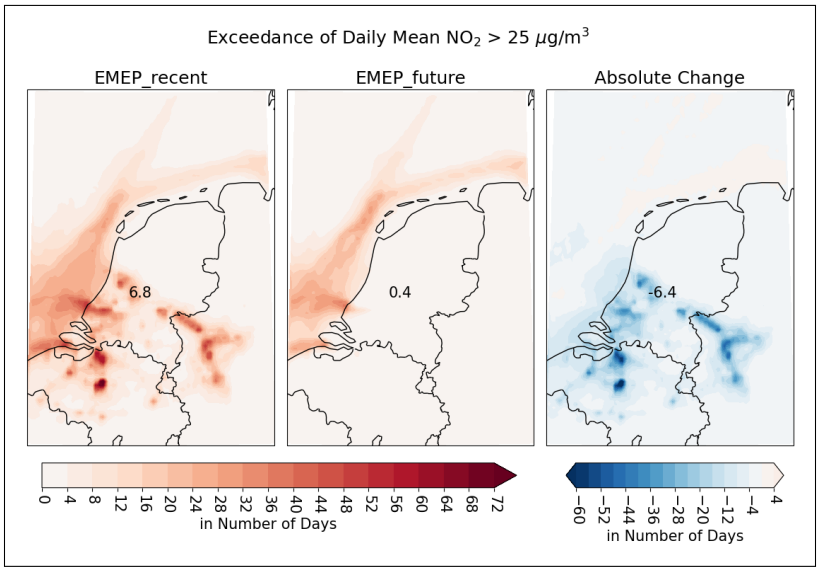

Figure 47: 10-year mean of number of days in summer with surface mean NO_2 concentrations higher than the 25 µg/m^3 WHO daily NO_2 threshold. Panels 1 and 2 show the number of exceedance days for EMEP_recent (based on WRF_recent reported emission for 2008-2017) and EMEP_future (based on WRF_future and ECLIPSE V6b MFR 2050 emissions) output. Panel 3 displays the absolute change. The numbers in the centre represent the respective mean for the Netherlands.

The number of days in which WHO air quality standards (Section 1.2: Table 2) for daily mean NO_2 are exceeded (Figure 47) decreases strongly from an average of 6.8 days (EMEP_recent) to 0.4 days (EMEP_future) per summer averaged over the Netherlands. The maximum local exceedances reduce from 63 days (EMEP_recent) to less than 4 days (EMEP_future) except for the locally influenced areas of unchanged shipping emissions close to Rotterdam. The exposure to harmful levels of NO_2 is 14.5 days on average for every inhabitant in EMEP_recent. It decreases by 94% as the combined effect of climate change and emission controls (Table 12).

The relative change in total nitrogen deposition (Figure 48) is approximately uniform with small local fluctuations in the entire domain 3 and amounts to -43.5% in the Netherlands in EMEP_future compared to EMEP_recent. The relative change in the Netherlands and Belgium is slightly weaker than in Germany and over the North Sea.

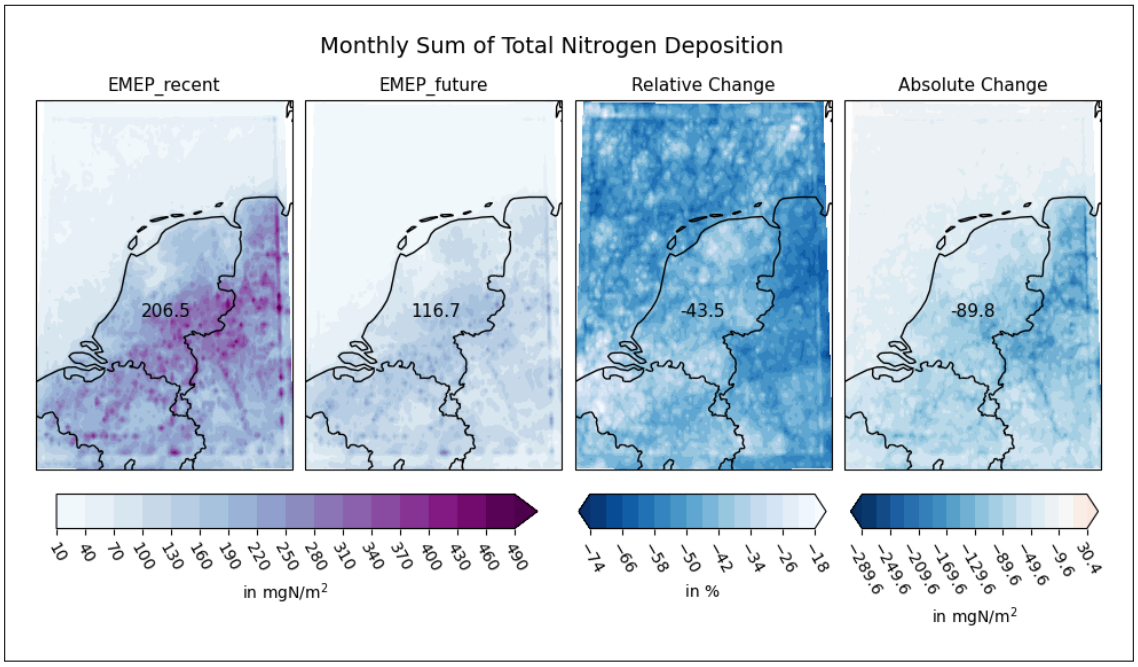

Figure 48: 10-year summertime (JJA) average of monthly sums of wet and dry deposition of reduced and oxidised nitrogen in mgN/m^2 as output for domain 3. The first panel shows EMEP_recent (based on WRF_recent and reported emission for 2008-2017), the second panel shows EMEP_future (based on WRF_future and ECLIPSE V6b MFR 2050 emissions) output. The third panel shows the relative and the fourth panel shows the absolute change between EMEP_future and EMEP_recent. The numbers in the centre represent the respective means for the Netherlands in the same units.

The dry and wet forms of deposition of reduced and oxidised nitrogen (Table 11) all contribute about a quarter of the total decrease in nitrogen deposition between EMEP_recent and EMEP_future. The relative change is highest for the wet deposition of oxidised nitrogen with -61.3%.

	EMEP_ recent	EMEP_ future		
	Mean in mgN/m^2	Mean in mgN/m^2	Relative Change in %	Absolute Change in mgN/m^2
Wet deposition of NH_3	50.9	36.5	-27.4	-14.4
Wet deposition of NH_4^+	14.1	4.8	-65.0	-9.3
Wet deposition of reduced nitrogen	65.0	41.3	-36.0	-23.7
Dry deposition of reduced nitrogen	63.7	42.5	-34.8	-21.3
Wet deposition of oxidised nitrogen	35.9	13.9	-61.3	-22.0
Dry deposition of oxidised nitrogen	41.9	19.1	-53.1	-22.8
Total deposition of nitrogen	206.5	116.7	-43.5	-89.8

Table 11: Overview of the 10-year summertime (JJA) mean of monthly sums of nitrogen deposition for the land surface of the Netherlands in its different forms for EMEP_recent and EMEP_future, their relative, and absolute change.

5.4.3 Fine Particulate Matter

Fine particulate matter ($PM_{2.5}$) decreases by 58.9% in a future climate with emission reductions which leads to a spatial maximum of mean summertime $PM_{2.5}$ concentrations of 7 µg/m^3(Figure 49). In the Netherlands the decrease is strongest in Limburg and North Brabant, both in relative and absolute measures.

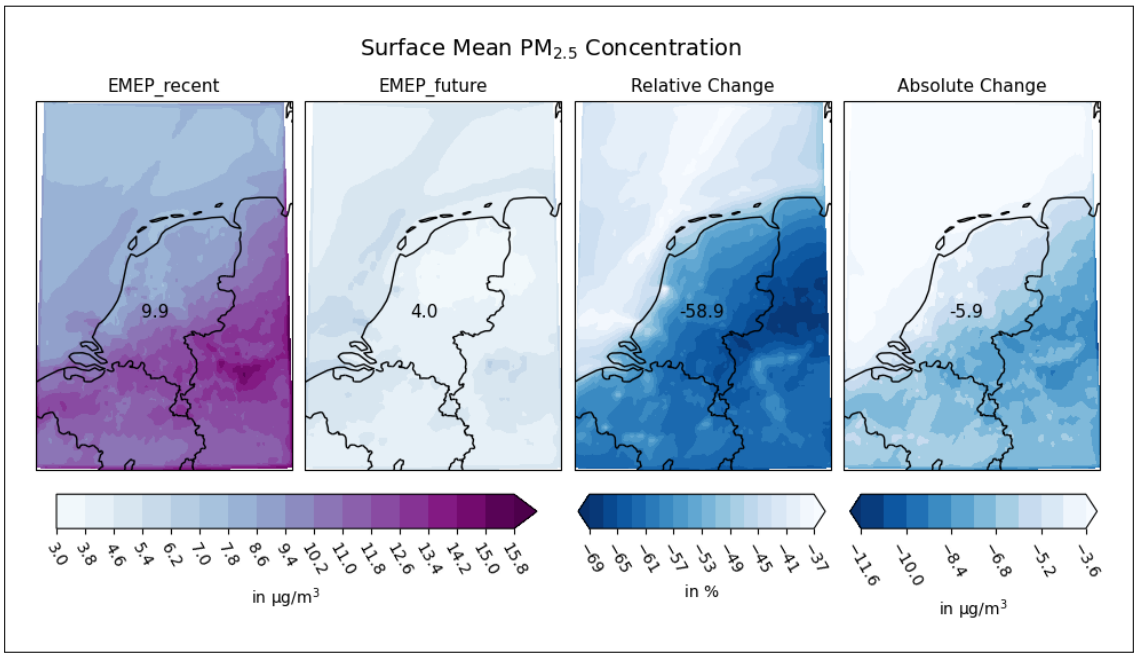

Figure 49: 10-year summertime (JJA) average of daily mean surface $PM_{2.5}$ concentrations in µg/m^3 as output for domain 3. The first panel shows EMEP_recent (based on WRF_recentand reported emission for 2008-2017), the second panel shows EMEP_future (based on WRF_future and ECLIPSE V6b MFR 2050 emissions) output. The third panel shows the relative and the fourth panel shows the absolute change between EMEP_future and EMEP_recent. The numbers in the centre represent the respective means for the Netherlands in the same units.

Between EMEP_recent and EMEP_future the composition of $PM_{2.5}$ changes in the Netherlands (Figure 50). The absolute concentrations of all components decrease. The strongest decreases are in nitrate which is reduced by 91.2% and ammonium (NH_4^+) which is reduced by 87.5%. Particulate organic matter also decreases slightly but becomes the component that makes up the largest share of $PM_{2.5}$ with 36.8%.

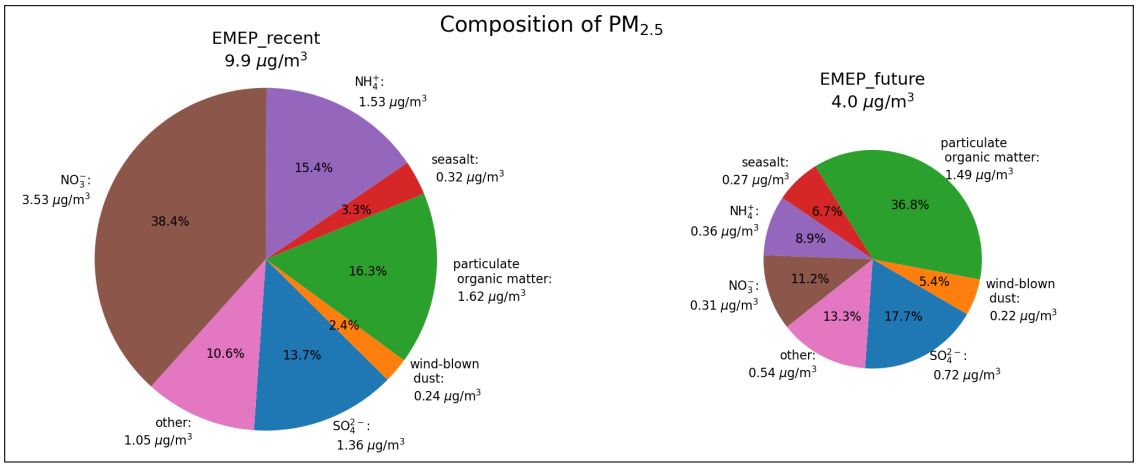

Figure 50: 10-year summertime (JJA) average composition of $PM_{2.5}$ over the Netherlands. The left panel shows the composition for EMEP_recent (based on WRF_recent reported emission for 2008-2017), the right panel shows EMEP_future (based on WRF_future and ECLIPSE V6b MFR 2050 emissions) output.

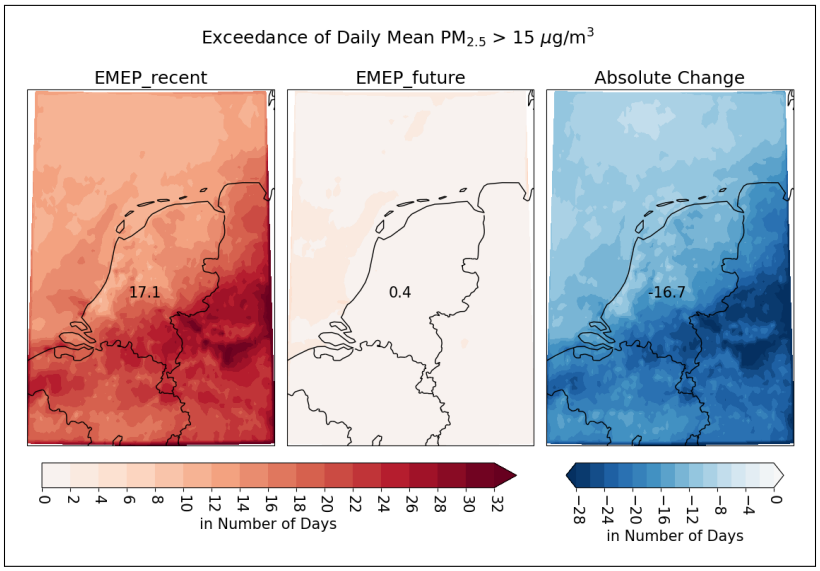

Figure 51: 10-year mean of number of days in summer (JJA) with surface $PM_{2.5}$ concentrations higher than 15 µg/m^3 WHO daily ozone threshold. Panels 1 and 2 show the number of exceedance days for EMEP_recent (based on WRF_recent reported emission for 2008-2017) and EMEP_future (based on WRF_future and ECLIPSE V6b MFR 2050 emissions) output respectively. Panel 3 displays the absolute change. The numbers in the centre represent the respective mean for the Netherlands.

The number of days in which WHO air quality standards for daily mean $PM_{2.5}$ (Section 1.2: Table 2) are exceeded (Figure 51) decreases drastically from 17.1 days (EMEP_recent)

to 0.4 days (EMEP_future) per summer. The absolute decrease is strongest in the most polluted areas. The exposure of the inhabitants of the Netherlands to harmful levels of outdoor $PM_{2.5}$ concentration is expected to be nearly eliminated with a decrease of -98% from an exposure of 16.4 days in EMEP_recent (Table 12).

The density function of 10-year average of the mean over the Netherlands showing the mean $PM_{2.5}$ concentrations for each day of summer (Figure 52) shifts to lower concentrations with climate change from EMEP_recent to EMEP_climate. With emission reduction measures between EMEP_recent and EMEP_mitigation the most frequent $PM_{2.5}$ concentrations decrease more strongly and the variability decreases. The combined effect of climate change and emission reduction measures between EMEP_recent and EMEP_future leads to a stronger decrease of $PM_{2.5}$ concentrations and a narrowing of the temporal variability. Compared to EMEP_mitigation the tail of higher concentrations of the distribution is much shorter with the highest concentrations close to the lowest concentrations in EMEP_recent.

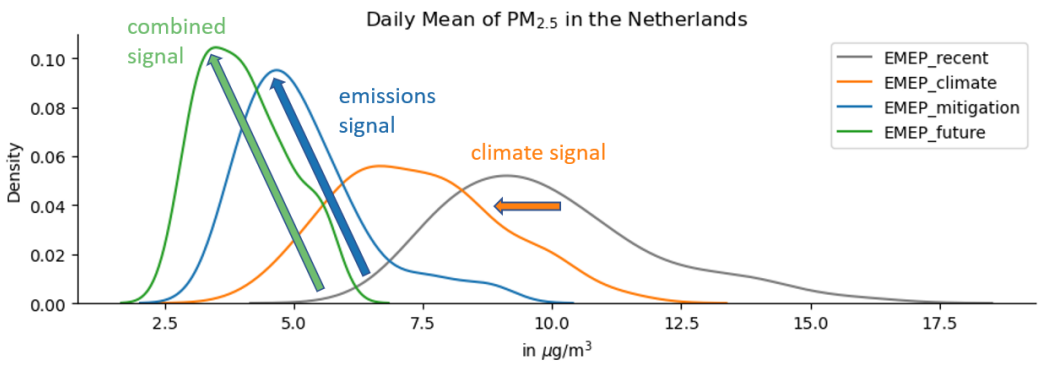

Figure 52: Density function for the daily mean $PM_{2.5}$ concentration in µg/m^3 for all 92 days of June to August averaged over 10-years and the Netherlands. The shift from the grey to the orange curve depicts the change between EMEP_recent and EMEP_climate with constant emissions (reported emissions for 2008-2017) and a changing climate (WRF_recent to WRF_future). The shift from the grey to the blue curve depicts the change between EMEP_recent and EMEP_mitigation with constant meteorology (WRF_recent) and emissions reductions from the reported emissions for 2008-2017 to ECLIPSE V6b MFR 2050. The shift from the grey to the green curve depicts the combined effect of meteorology and emission changes.

Pollutant	Absolute exposure in EMEP_recent	Relative change to EMEP_recent in		
		EMEP_climate	EMEP_mitigation	EMEP_future
O_3	∅ 17.2 days	+52%	+1%	+36%
NO_2	∅ 14.5 days	−15%	−92%	−94%
$PM_{2.5}$	∅ 16.4 days	−55%	−81%	−98%

Table 12: Exposure of the population in the Netherlands (Section 3.7) to harmful concentrations of O_3, NO_2, and $PM_{2.5}$ on average per summer (JJA). Harmful is here defined as the exceedance of the WHO air quality standards for the daily maximum 8-hour mean ozone concentration of 100 µg/m^3, for the daily mean NO_2 concentration of 25 µg/m^3, and for the daily mean $PM_{2.5}$ concentration of 15 µg/m^3. The table displays the average exposure for every inhabitant in EMEP_recent and the relative change of EMEP_climate, EMEP_mitigation, and EMEP_future to EMEP_recent.

6 Discussion

This section discusses the strengths and weaknesses of the study design (Section 6.1). It continues with an interpretation of the results, structured along research questions 3 to 5 and based on the theory outlined in Section 2, and puts the findings into the context of previous work (Section 6.2).

6.1 Study Design

In order to determine the framework in which the results of this study are valid, it is important to consider the strengths, weaknesses, and consequences of choices in the study design in addition to the model validation discussion in Section 4.2. This includes the choice of RCP8.5 (Section 6.1.1), the emission datasets used for the EMEP4NL simulations (Section 6.1.2), and the modelling set-up (Section 6.1.3).

6.1.1 Choice of RCP8.5

In an attempt to determine an upper estimate of the impact of climate change on air quality, the high climate change scenario RCP8.5 is chosen for this study. Whether RCP8.5 is a suitable scenario to study consequences of climate change has been controversially discussed. Schwalm et al. (2020) suggest that cumulative greenhouse gas emissions between 2005 and 2020 and future estimates of emissions in a business-as-usual scenario for 2050 by the IEA agree best with RCP8.5, out of the four RCP scenarios. They argue that RCP8.5, in spite of overestimating the cumulative emissions by mid-century, is a suitable choice for midterm time horizons due to path dependence and a closer agreement with historical emissions. Pedersen et al. (2020) support this choice of high emission scenarios, arguing that a wide range of climate scenarios is needed to account for low probability but high impact effects. Hausfather and Peters (2020) and Burgess et al. (2020) challenge this view by questioning the underlying assumptions in RCP8.5 about land-use emissions and carbon intensity development. Following their assumptions of lower emissions in mid-century than in RCP8.5, it should be considered that the climate system and atmospheric chemistry are complex and interacting systems. Therefore, changes in air quality in a lower climate change scenario would likely but not necessarily be constrained to the bounds determined in this study.

6.1.2 Emissions Input to EMEP4NL

Using invariant spatial distributions and time factors to distribute the total annual emissions per sector and pollutant for all emission years (2008-2017; 2050) may lead to biases in the results. The expected shift in the location of industries (Dekkers et al., 2012) and their relative share on the total emissions could lead to changes in their contributions to air pollution. According to Hendriks et al. (2015), the temporal distribution of emissions

is also expected to change and to affect the effectiveness of emission reductions.

For the emission scenario for 2050, the data from the ECLIPSE V6b MFR for 2050 is only used for the 27 countries of the European Union and for Great Britain. The emissions of other countries within domain 1, such as Switzerland, but also of the shipping tracks of the North Sea along the coast of the Netherlands remain unchanged at 2017 data. This might have an impact on surface concentrations of air pollutants in the Netherlands.

6.1.3 Modelling Set-Up

Nudging WRF with HadGEM2-ES RCP8.5 climate output and using the resulting meteorological fields as input for EMEP4NL has distinct advantages and disadvantages for air quality analysis.

One of the strengths of this set-up is that it enables a high resolution analysis for the Netherlands in spite of coarse climate projection outputs. In addition, the validity of this set-up is supported by a comparison of the meteorological changes with climate change between WRF_recent and WRF_future with the changes in the regional climate scenario W_H (strong warming, high changes in circulation pattern) by the KNMI (KNMI, 2015). The magnitude of the temperature increase, the decrease in relative humidity, and the decrease in precipitation in summer all agree approximately with the output of this scenario. Compared to studies in which only the temperature or sea-surface temperature is adjusted to a future climate projection, this set-up additionally has the capability to translate the full changes in meteorology in a climate projection to high resolution meteorological fields, including changes in wind patterns and initial conditions of soil moisture. Furthermore, the use of EMEP4NL with its explicit chemistry scheme instead of tropospheric chemistry parameterizations within global climate models leads not only to a higher resolution but also to a more complete representation of chemical processes in the atmosphere.

An important limitation of this study's methodology is the offline use of EMEP4NL which means that regional feedbacks of chemistry onto climate are not included. A study by Skjøth and Geels (2013) additionally finds that climate change could increase biogenic ammonia emissions in Europe by up to 40%. This finding is supported by Sutton et al. (2013). The temperature dependence of NH_3 emissions is not included in EMEP4NL. This could impact NH_3 but in extension also $PM_{2.5}$ and O_3 concentrations, as well as $PM_{2.5}$ composition. In addition, the precipitation output of WRF depends highly on the nudging settings (Appendix B) and displays a high spatial variation in the mean of 10-years of summer (Figure 14) which indicates that rainfall is too local in the model.

Lacressonnière et al. (2012) tested the suitability of using climate model forcings in chemistry transport models to analyse future air quality by using the same method for a period in the past. They conclude that measures such as the number of days above a certain air quality threshold are most robust for ozone. Since the meteorology in this study shows

biases to observations (Section 4.1), this induces further biases.

6.2 Discussion of Results

The discussion of the results is subdivided along the research questions 3 to 5. Each question is discussed in the context of theory and literature and the corresponding hypothesis is approved or rejected.

6.2.1 Effect of Climate Change on Air Quality

Based on the results presented in Section 5.2, this subsection aims to answer research question 3: How are summertime levels of ozone, $PM_{2.5}$, and ammonia affected by climate change under the RCP8.5 scenario in the Netherlands until the 2050s?

As hypothesised, surface O_3 concentrations (Figure 17) increase in a future climate due to higher temperatures and more stagnant conditions (Section 2.5). NO_2 photolysis is more pronounced at higher altitudes in the atmosphere. Therefore, with a higher mixing layer height during the day in a future climate (Figure 63), the ozone formed at these higher altitudes is then mixed downward leading to higher ozone concentrations at the surface which reinforces the effect of temperature and stagnant conditions. The increase in O_3 is stronger in a more polluted atmosphere (Figure 20) but in contrast to the finding of Doherty et al. (2013) not locally stronger in the most polluted areas. The validity of these results is supported by Andersson and Engardt (2010). They show that the dependence of dry deposition of ozone on meteorology and of changes in isoprene emissions on meteorology are important processes that need to be included for future ozone projections. Both dependencies on meteorology are included in this study. When comparing the magnitude of the increase in ozone by mid-century with the existing literature, the increase is significant in contrast to Watson et al. (2016) and higher than estimated in Colette et al. (2015). The results align with Lacressonnière et al. (2014) who find a slightly stronger increase for a larger domain of western Europe.

With less precipitation and higher temperatures in a future climate, both surface NH_3 and $PM_{2.5}$ concentrations are hypothesised to increase solely as an effect of climate change. The reason for this is a shift in the chemical equilibrium between NH_3 and NH_4^+ towards NH_3 at higher temperatures and less deposition with less frequent precipitation (Section 2.5). Instead, both NH_3 and $PM_{2.5}$ decrease in the daily mean (Figures 21 and 25). Only during the night NH_3 increases as expected. The decrease during the day and in the daily average is linked to the increase in the mixing layer height during the day (Figure 15) in a future climate. This means that NH_3, as well as the nitrogen species that contribute to $PM_{2.5}$ (NH_4^+ and NO_3^-) are dispersed over a larger volume of air which reduces their surface concentrations (Jacob and Winner, 2009). The shift in the chemical equilibrium leads to a stronger decrease in NH_4^+ than in NH_3 (Figure 22) in this increased mixing volume.

This finding is supported by Colette et al. (2013) who also find the strongest impact of climate change on $PM_{2.5}$ concentrations in NH_4^+ and NO_3^-. Furthermore, it agrees with Jacob and Winner (2009) who speculate that particulate matter could decrease due to the volatilisation of semi-volatile components such as nitrate. Surface SO_4^{2-} concentrations are likely not influenced as strongly as the nitrogen compounds by increase of the mixing layer height since it is formed as a secondary aerosol at higher altitudes in clouds. The decrease in $PM_{2.5}$ in the Netherlands also aligns with the findings of Park et al. (2020). The finding is in contrast to Lacressonnière et al. (2016) who find the largest changes in $PM_{2.5}$ due to climate change in dust, sea salt, and particulate organic matter concentrations.

6.2.2 Effect of Emission Reductions on Air Quality

By comparing the results in Sections 5.2 and 5.3, this section aims to answer research question 4: How does the effect of climate change compare to the effect of strong air pollutant emission reductions on summertime air quality? The hypothesis corresponding to this research question is that the magnitude of O_3, $PM_{2.5}$, and NH_3 changes is smaller in a high climate change scenario than in a strong air pollutant emission reductions scenario.

Under the strong air pollutant reductions scenario ECLIPSE MFR for 2050, the ozone formation regime shifts from a previously VOC-limited regime (EMEP_recent, EMEP_climate) to a NO_x-limited regime (EMEP_mitigation, EMEP_future). Subsequently, surface ozone concentrations do not decrease over the entirety of domain 3 with emission reduction measures but increases in the areas where NO_x emissions were highest before. Therefore, the overall effect of emission reduction measures on ozone concentrations, deposition, days of exceedance, and exposure is small (Section 5.3.1) and smaller than the effect of climate change (Section 5.2.1). Climate change has a stronger isolated effect on the development of summertime ozone concentrations in the Netherlands until the 2050s than strong emission reductions. This finding differs from the results in Tagaris et al. (2007), Colette et al. (2013), and Watson et al. (2016) who find that the effect of emission reduction measures on ozone is larger than the effect of climate change. The reason for this might lie in the VOC-limited ozone formation under recent (2008-2017) emissions in the Netherlands and the regime shift when emission controls are applied (Figure 28). For ozone the hypothesis therefore needs to be rejected.

Both NH_3 and $PM_{2.5}$ decrease under the high climate change scenario and the strong emission reduction measures. The magnitude of the isolated climate change effect is smaller than the effect of strong emission reduction measures but with approximately one third of their effect for NH_3 and one half of their effect for $PM_{2.5}$ not negligibly small. The hypothesis can be approved for these components.

6.2.3 Combined Effect of Climate Change and Emission Reductions for Air Quality

This subsection discusses research question 5: How is the effect of emission controls influenced by climate change and what is the effect of emission controls in a changing climate? The hypothesis corresponding to this research question states that the effectiveness of air pollutant emission reductions weakens for ozone. The effect of climate change on O_3 is expected to be mitigated when emission reduction measures are applied in addition. Since NH_3 and $PM_{2.5}$ are found to decrease solely as an effect of climate change in Section 6.2.1, the effect is expected to amplify.

The combination of air pollutant emission reductions and climate change leads to a small decrease of daily maximum 8-hour mean concentrations of ozone on the northern coast of the Netherlands but to increases in the rest of the country with the strongest changes in urban areas. The effect of air pollutant emission reductions is weakened by climate change. The "climate change penalty" on ozone (Wu et al., 2008) is thus confirmed, as in Jacob and Winner (2009), Colette et al. (2013), and Colette et al. (2015). However, emission reduction measures still play an important role in a warming climate to limit air pollution since emission reduction measures approximately halve the effect of climate change on daily maximum 8-hour mean concentrations of ozone and reduce the increase in exposure from +52% (EMEP_climate) to +36% (EMEP_future). The hypothesis can therefore be approved for ozone.

For NH_3 and $PM_{2.5}$, both climate change and emission reduction measures lead to a decrease in surface concentrations. Therefore, the effect of emission reduction measures is reinforced by climate change and vice versa. The former constitutes a climate change benefit. This finding agrees with Colette et al. (2013) who also find a "climate change benefit" for surface concentrations of $PM_{2.5}$. The hypothesis can be approved.

7 Outlook

For future studies the use of regional climate scenarios, such as the KNMI scenarios G_L, G_H, W_L, and W_H (KNMI, 2015), instead of the coarse global HadGEM2-ES RCP8.5 output as input for WRF could improve the meteorological fields and therefore the representation of chemical processes in the Netherlands. A comparison of the air quality responses to different climate scenarios could additionally help to determine the sensitivity of the air quality changes to different degrees of warming and wind field changes.

Furthermore, nudging WRF more frequently, i.e., every 6 instead of every 24 hours, towards the climate scenario data could improve the representation of processes in the weather model. However, the larger the step in resolution from the climate scenario to the weather model, the more the spatial variability is decreased by each nudging step. So,

the benefits and drawbacks of a higher nudging frequency for a given ratio of resolutions should be analysed first.

In addition, it would be interesting to simulate the impact of climate change on air quality over a longer period, e.g., April to September. This would allow for an analysis of the impact of high ozone concentrations on crops and forests with the measures $AOT40_{crops}$ and $AOT40_{forests}$ (EEA, 2022) and could capture all days in which ozone concentrations exceed WHO air quality thresholds for human health in the Netherlands. An analysis of other seasons might bring further insights about the impact of climate change on air quality.

The reliability of the concentrations but also of the number of exceedance days could be improved by applying a bias-correction with the Delta-method (Copernicus Climate Change Service, 2021) to the temperature and wind output fields of WRF. This would minimise the effect of the biases in the meteorological input of WRF. By comparing the new results to this study, this would also help to determine the relative importance of meteorological biases to emission biases and biases caused by the modelling approach.

The validation of the EMEP4NL output could be improved by comparing the results not only to measured station data but also to air quality reanalysis data of the Netherlands.

Concerning the EMEP4NL output analysis, it might be interesting to extend the deposition analysis by looking at how the deposition velocity and the deposition to forests and crops change.

8 Conclusion

The modelling approach of this study does not reproduce the absolute values of the observed meteorological variables (temperature and wind) and air pollutant concentrations (O_3, NH_3, and $PM_{2.5}$) but it does show how an increased occurrence of stagnant conditions and a higher mixing layer height influences air pollutant concentrations in a changing climate. This study finds that climate change alone leads to an increase of 11.3% in the daily maximum 8-hour mean of O_3 concentrations and a decrease of 5.9% in daily mean NH_3 and of 25.4% in daily mean $PM_{2.5}$ concentrations. Emission reduction measures alone lead to a decrease of 20% in NH_3 and of 47.6% in $PM_{2.5}$ concentrations, to a shift in the O_3 formation regime, and local increases of O_3 in urban areas. The combination of climate change and emission reduction measures reinforces the reductions in daily mean NH_3 (-27.6%) and $PM_{2.5}$ (-58.9%) concentrations. For O_3 climate change has a detrimental effect on the benefit of emission reduction measures, and emission reduction measures half the mean effect of climate change on O_3 concentrations in the Netherlands.

9 References

Akimoto, H. (2016). *Atmospheric Reaction Chemistry.* Springer Atmospheric Sciences. Springer Japan, Tokyo.

Amann, M., Klimont, Z., and Wagner, F. (2013). Regional and global emissions of air pollutants: Recent trends and future scenarios. *Annual Review of Environment and Resources*, 38:31–55. doi: 10.1146/annurev-environ-052912-173303.

Andersson, C. and Engardt, M. (2010). European ozone in a future climate: Importance of changes in dry deposition and isoprene emissions. *Journal of Geophysical Research: Atmospheres*, 115(D2). doi: 10.1029/2008JD011690.

Burgess, M. G., Ritchie, J., Shapland, J., and Pielke, R. (2020). IPCC baseline scenarios have over-projected CO2 emissions and economic growth. *Environmental Research Letters*, 16(1):014016. doi: 10.1088/1748-9326/abcdd2.

Centraal Bureau voor de Statistiek (CBS) (2022). Kaart van 500 meter bij 500 meter met statistieken. https://www.cbs.nl/nl-nl/dossier/nederland-regionaal/geografische-data/kaart-van-500-meter-bij-500-meter-met-statistieken, Accessed: 2022-11-12.

Colette, A., Andersson, C., Baklanov, A., Bessagnet, B., Brandt, J., Christensen, J. H., Doherty, R., Engardt, M., Geels, C., Giannakopoulos, C., Hedegaard, G. B., Katragkou, E., Langner, J., Lei, H., Manders, A., Melas, D., Meleux, F., Rouïl, L., Sofiev, M., Soares, J., Stevenson, D. S., Tombrou-Tzella, M., Varotsos, K. V., and Young, P. (2015). Is the ozone climate penalty robust in Europe? *Environmental Research Letters*, 10(8):084015. doi: 10.1088/1748-9326/10/8/084015.

Colette, A., Bessagnet, B., Vautard, R., Szopa, S., Rao, S., Schucht, S., Klimont, Z., Menut, L., Clain, G., Meleux, F., Curci, G., and Rouïl, L. (2013). European atmosphere in 2050, a regional air quality and climate perspective under CMIP5 scenarios. *Atmospheric Chemistry and Physics*, 13(15):7451–7471. doi: 10.5194/acp-13-7451-2013.

Compendium voor de Leefomgeving (CLO) (2020). Temperatuur in Nederland en mondiaal, 1907 - 2019. https://www.clo.nl/indicatoren/nl0226-temperatuur-mondiaal-en-in-nederland, Accessed: 2022-11-01.

Copernicus Climate Change Service (2021). What is bias correction? https://climate.copernicus.eu/sites/default/files/2021-01/infosheet7.pdf, Accessed: 2022-11-20.

Dekkers, J., Koomen, E., Jacobs-Crisioni, C., and Rijken, B. (2012). *Scenario-Based Projections of Future Land Use in the Netherlands; A Spatially-Explicit Knowledge Base for the Knowledge for Climate Programme.* (Spinlab Research Memorandum; No. 11). VU University. Link.

Deutsches Klimarechenzentrum (DKRZ) (2015). CMIP5 Archive. https://esgf-data.dkrz.de/search/cmip5-dkrz/, Accessed: 2022-11-01.

Dodge, M. C. (1977). Combined use of modeling techniques and smog chamber data to derive ozone-precursor relationships. In *International Conference on Photochemical Oxidant Pollution and Its Control: Proceedings*, volume 2, pages 881–889. US Environmental Protection Agency.

Doherty, R. M., Wild, O., Shindell, D. T., Zeng, G., MacKenzie, I. A., Collins, W. J., Fiore, A. M., Stevenson, D. S., Dentener, F. J., Schultz, M. G., Hess, P., Derwent, R. G., and Keating, T. J. (2013). Impacts of climate change on surface ozone and intercontinental ozone pollution: A multi-model study. *Journal of Geophysical Research: Atmospheres*, 118(9):3744–3763. doi: 10.1002/jgrd.50266.

Dudhia, J. (1989). Numerical Study of Convection Observed during the Winter Monsoon Experiment Using a Mesoscale Two-Dimensional Model. *Journal of the Atmospheric Sciences*, 46(20):3077–3107. doi: 10.1175/1520-0469(1989)046¡3077:NSOCOD¿2.0.CO;2.

Dutch National Institute for Public Health and the Environment (RIVM) (2022a). Grootschalige concentratie- en depositiekaarten nederland (gcn en gdn). https://data.rivm.nl/apps/gcn/, Accessed: 2022-11-11.

Dutch National Institute for Public Health and the Environment (RIVM) (2022b). Luchtmeetnet. https://www.luchtmeetnet.nl/, Accessed: 2022-11-01.

EMEP Centre on Emission Inventories and Projections (CEIP) (2022). Emissions as used in EMEP models. https://www.ceip.at/webdab-emission-database/emissions-as-used-in-emep-models, Accessed: 2022-11-01.

EMEP/European Environment Agency (EEA) (1999). *EMEP/CORINAIR Atmospheric Emission Inventory Guidebook: Index to Methodology Chapters*. 2. edition.

European Commission (EC) (2022). Europe's Air Quality Status 2022. https://environment.ec.europa.eu/strategy/zero-pollution-action-plan_en#documents, Accessed: 2022-11-01.

European Environment Agency (EEA) (2022a). Exceedance of air quality standards in Europe. https://www.eea.europa.eu/ims/exceedance-of-air-quality-standards, Accessed: 2022-11-01.

European Environment Agency (EEA) (2022b). Exposure of Europe's ecosystems to ozone. https://www.eea.europa.eu/ims/exposure-of-europes-ecosystems-to-ozone, Accessed: 2022-11-20.

European Union (EU) (2022). Environment: EU Air Quality Standards.

https://environment.ec.europa.eu/topics/air/air-quality/eu-air-quality-standards_en, Accessed: 2022-11-01.

Finlayson-Pitts, B. J. and Pitts, James N., J. (1999). *Chemistry of the Upper and Lower Atmosphere: Theory, Experiments, and Applications.* Elsevier Science & Technology, San Diego, US.

Geiß, A., Wiegner, M., Bonn, B., Schäfer, K., Forkel, R., von Schneidemesser, E., Münkel, C., Chan, K. L., and Nothard, R. (2017). Mixing layer height as an indicator for urban air quality? *Atmospheric Measurement Techniques*, 10(8):2969–2988. doi: 10.5194/amt-10-2969-2017.

Guenther, A. B., Zimmerman, P. R., Harley, P. C., Monson, R. K., and Fall, R. (1993). Isoprene and monoterpene emission rate variability: Model evaluations and sensitivity analyses. *Journal of Geophysical Research: Atmospheres*, 98(D7):12609–12617. doi: 10.1029/93JD00527.

Hausfather, Z. and Peters, G. P. (2020). RCP8.5 is a problematic scenario for near-term emissions. *Proceedings of the National Academy of Sciences*, 117(45):27791–27792. doi: 10.1073/pnas.2017124117.

Hendriks, C., Kuenen, J., Kranenburg, R., Scholz, Y., and Schaap, M. (2015). A shift in emission time profiles of fossil fuel combustion due to energy transitions impacts source receptor matrices for air quality. *Environmental Science: Processes & Impacts*, 17(3):510–524. doi: 10.1039/C4EM00444B.

Hofmann, D. J., Butler, J. H., Dlugokencky, E. J., Elkins, J. W., Masarie, K., Montzka, S. A., and Tans, P. (2006). The role of carbon dioxide in climate forcing from 1979 to 2004: Introduction of the Annual Greenhouse Gas Index. *Tellus B: Chemical and Physical Meteorology*, 58(5):614–619. doi: 10.1111/j.1600-0889.2006.00201.x, Updated version at https://gml.noaa.gov/aggi/aggi.html, Accessed: 2022-11-01.

Hole, L. and Engardt, M. (2008). Climate Change Impact on Atmospheric Nitrogen Deposition in Northwestern Europe: A Model Study. *Ambio*, 37(1):9–17. doi: 10.1579/0044-7447(2008)37[9:ccioan]2.0.co;2 .

Hoogerbrugge, R., Geilenkirchen, G., den Hollander, H., van der Swaluw, E., Visser, S., de Vries, W., and Wichink Kruit, R. (2019). Grootschalige concentratie- en depositiekaarten Nederland Rapportage 2019.

Intergovernmental Panel on Climate Change (IPCC), Masson-Delmotte, V., Zhai, P., Pirani, A., Connors, S. L., Péan, C., Berger, S., Caud, N., Chen, Y., Goldfarb, L., Gomis, M. I., Huang, M., Leitzell, K., Lonnoy, E., Matthews, J. B. R., Maycock, T. K., Waterfield, T., Yelekçi, Ö., Yu, R., and Zhou, B., editors (2021). *Climate Change 2021: The Physical Science Basis. Contribution of Working Group I to the Sixth Assessment*

Report of the Intergovernmental Panel on Climate Change. Cambridge University Press, Cambridge, United Kingdom and New York, NY, USA. doi: 10.1017/9781009157896.

International Energy Agency (IEA) (2018). World Energy Outlook 2018. https://www.iea.org/reports/world-energy-outlook-2018, Accessed: 2022-11-01.

International Institute for Applied Systems Analysis (IIASA) (2019). Eclipse v6b global emission fields. ECLIPSE V6b MFR totals per SNAP sector accessed from: https://gains.iiasa.ac.at/models/gains_models4.html, more information: https://previous.iiasa.ac.at/web/home/research/researchPrograms/air/Global_emissions.html, https://previous.iiasa.ac.at/web/home/research/researchPrograms/air/ECLIPSEv6b.html, Accessed: 2022-11-01.

Jacob, D. J. (1999). *Introduction to Atmospheric Chemistry*. Princeton University Press.

Jacob, D. J. and Winner, D. A. (2009). Effect of climate change on air quality. *Atmospheric Environment*, 43(1):51–63. doi: 10.1016/j.atmosenv.2008.09.051.

Jiménez, P. A., Dudhia, J., González-Rouco, J. F., Navarro, J., Montávez, J. P., and García-Bustamante, E. (2012). A Revised Scheme for the WRF Surface Layer Formulation. *Monthly Weather Review*, 140(3):898–918. doi: 10.1175/MWR-D-11-00056.1.

Jones, C. D., Hughes, J. K., Bellouin, N., Hardiman, S. C., Jones, G. S., Knight, J., Liddicoat, S., O'Connor, F. M., Andres, R. J., Bell, C., Boo, K.-O., Bozzo, A., Butchart, N., Cadule, P., Corbin, K. D., Doutriaux-Boucher, M., Friedlingstein, P., Gornall, J., Gray, L., Halloran, P. R., Hurtt, G., Ingram, W. J., Lamarque, J.-F., Law, R. M., Meinshausen, M., Osprey, S., Palin, E. J., Parsons Chini, L., Raddatz, T., Sanderson, M. G., Sellar, A. A., Schurer, A., Valdes, P., Wood, N., Woodward, S., Yoshioka, M., and Zerroukat, M. (2011). The HadGEM2-ES implementation of CMIP5 centennial simulations. *Geoscientific Model Development*, 4(3):543–570. doi: 10.5194/gmd-4-543-2011.

Kain, J. S. and Fritsch, J. M. (1993). Convective parameterization for mesoscale models: The Kain–Fritsch scheme. *Amer. Meteor. Soc.*, (No.24):165–170. doi: 10.1007/978-1-935704-13-3_16.

Klimont, Z., Höglund-Isaksson, L., Heyes, C., Rafaj, P., Schöpp, W., Cofala, J., Purohit, P., Borken-Kleefeld, J., Kupiainen, K., Kiesewetter, G., Winiwarter, W., Amann, M., Zhao, B., Wang, S., Bertok, I., and Sander, R. (2022). Global scenarios of air pollutants and methane: 1990-2050. In preparation.

Klimont, Z., Kupiainen, K., Heyes, C., Purohit, P., Cofala, J., Rafaj, P., Borken-Kleefeld, J., and Schöpp, W. (2017). Global anthropogenic emissions of particulate matter including black carbon. *Atmospheric Chemistry and Physics*, 17(14):8681–8723. doi: 10.5194/acp-17-8681-2017.

Koninklijk Nederlands Meteorologisch Instituut (KNMI) (2015). KNMI'14 Klimaatscenario's voor Nederland. https://cdn.knmi.nl/knmi/pdf/bibliotheek/klimaatbrochures/Brochure_KNMI14_NL.pdf, English version: https://cdn.knmi.nl/system/data_center_publications/files/000/070/807/original/Brochure_KNMI14_EN_2015.pdf?1653079346, Accessed: 2022-11-15.

Koninklijk Nederlands Meteorologisch Instituut (KNMI) (2021). Windrozen van de nederlandse hoofdstations: Langjarig gemiddelde (1991-2020). https://www.knmi.nl/nederland-nu/klimatologie/grafieken/maand/windrozen, Accessed: 2022-11-10.

Koninklijk Nederlands Meteorologisch Instituut (KNMI) (2022). Klimaatdashboard. https://www.knmi.nl/klimaatdashboard, Accessed: 2022-11-01.

Lacressonnière, G., Foret, G., Beekmann, M., Siour, G., Engardt, M., Gauss, M., Watson, L., Andersson, C., Colette, A., Josse, B., Marécal, V., Nyiri, A., and Vautard, R. (2016). Impacts of regional climate change on air quality projections and associated uncertainties. *Climatic Change*, 136(2):309–324. doi: 10.1007/s10584-016-1619-z.

Lacressonnière, G., Peuch, V.-H., Arteta, J., Josse, B., Joly, M., Marécal, V., Saint Martin, D., Déqué, M., and Watson, L. (2012). How realistic are air quality hindcasts driven by forcings from climate model simulations? *Geoscientific Model Development*, 5(6):1565–1587. doi: 10.5194/gmd-5-1565-2012.

Lacressonnière, G., Peuch, V. H., Vautard, R., Arteta, J., Déqué, M., Joly, M., Josse, B., Marécal, V., and Saint-Martin, D. (2014). European air quality in the 2030s and 2050s: Impacts of global and regional emission trends and of climate change. *Atmospheric Environment*, 92:348–358. doi: 10.1016/j.atmosenv.2014.04.033.

Lammel, G. and Graßl, H. (1995). Greenhouse effect of NO_x. *Environmental Science and Pollution Research International*, 2(1):40–45. doi: 10.1007/BF02987512.

Lin, Y. and Colle, B. A. (2011). A New Bulk Microphysical Scheme That Includes Riming Intensity and Temperature-Dependent Ice Characteristics. *Monthly Weather Review*, 139(3):1013–1035. doi: 10.1175/2010MWR3293.1.

Manders, A. M. M., van Meijgaard, E., Mues, A. C., Kranenburg, R., van Ulft, L. H., and Schaap, M. (2012). The impact of differences in large-scale circulation output from climate models on the regional modeling of ozone and PM. *Atmospheric Chemistry and Physics*, 12(20):9441–9458. doi: 10.5194/acp-12-9441-2012.

Martin, G. M., Bellouin, N., Collins, W. J., Culverwell, I. D., Halloran, P. R., Hardiman, S. C., Hinton, T. J., Jones, C. D., McDonald, R. E., McLaren, A. J., O'Connor, F. M., Roberts, M. J., Rodriguez, J. M., Woodward, S., Best, M. J., Brooks, M. E., Brown, A. R., Butchart, N., Dearden, C., Derbyshire, S. H., Dharssi, I., Doutriaux-Boucher, M., Edwards, J. M., Falloon, P. D., Gedney, N., Gray, L. J., Hewitt, H. T., Hobson, M.,

Huddleston, M. R., Hughes, J., Ineson, S., Ingram, W. J., James, P. M., Johns, T. C., Johnson, C. E., Jones, A., Jones, C. P., Joshi, M. M., Keen, A. B., Liddicoat, S., Lock, A. P., Maidens, A. V., Manners, J. C., Milton, S. F., Rae, J. G. L., Ridley, J. K., Sellar, A., Senior, C. A., Totterdell, I. J., Verhoef, A., Vidale, P. L., and Wiltshire, A. (2011). The HadGEM2 family of Met Office Unified Model climate configurations. *Geoscientific Model Development*, 4(3):723–757. doi: 10.5194/gmd-4-723-2011.

Meinshausen, M., Smith, S. J., Calvin, K., Daniel, J. S., Kainuma, M. L. T., Lamarque, J.-F., Matsumoto, K., Montzka, S. A., Raper, S. C. B., Riahi, K., Thomson, A., Velders, G. J. M., and van Vuuren, D. P. (2011). The RCP greenhouse gas concentrations and their extensions from 1765 to 2300. *Climatic Change*, 109(1-2):213–241. doi: 10.1007/s10584-011-0156-z, Data available at: http://www.pik-potsdam.de/~mmalte/rcps/, Accessed: 2022-11-01.

Miller, R. L., Schmidt, G. A., Nazarenko, L. S., Bauer, S. E., Kelley, M., Ruedy, R., Russell, G. L., Ackerman, A. S., Aleinov, I., Bauer, M., Bleck, R., Canuto, V., Cesana, G., Cheng, Y., Clune, T. L., Cook, B. I., Cruz, C. A., Del Genio, A. D., Elsaesser, G. S., Faluvegi, G., Kiang, N. Y., Kim, D., Lacis, A. A., Leboissetier, A., LeGrande, A. N., Lo, K. K., Marshall, J., Matthews, E. E., McDermid, S., Mezuman, K., Murray, L. T., Oinas, V., Orbe, C., Pérez García-Pando, C., Perlwitz, J. P., Puma, M. J., Rind, D., Romanou, A., Shindell, D. T., Sun, S., Tausnev, N., Tsigaridis, K., Tselioudis, G., Weng, E., Wu, J., and Yao, M.-S. (2021). CMIP6 Historical Simulations (1850–2014) With GISS-E2.1. *Journal of Advances in Modeling Earth Systems*, 13(1):e2019MS002034. doi: 10.1029/2019MS002034.

Mitchell, D. (2021). Climate attribution of heat mortality. *Nature Climate Change*, 11(6):467–468. doi: 10.1038/s41558-021-01049-y.

Mlawer, E. J., Taubman, S., Brown, P., Clough, S., and Iacono, M. (1997). Radiative transfer for inhomogeneous atmospheres: RRTM, a validated correlated-k model for the longwave. *J. Geophys. Res*, 102(16):663–16. doi: 10.1029/97JD00237.

Mölders, N. and Kramm, G. (2014). *Lectures in Meteorology*. Springer Atmospheric Sciences. Springer International Publishing, Cham. doi: 10.1007/978-3-319-02144-7.

Murray, F. W. (1967). On the Computation of Saturation Vapor Pressure. *Journal of Applied Meteorology and Climatology*, 6(1):203–204. doi: 10.1175/1520-0450(1967)006¡0203:OTCOSV¿2.0.CO;2.

National Center for Atmospheric Research (NCAR) (2017). Weather Research and Forecasting ARW Version 3 Modeling System User's Guide.

Niu, G.-Y., Yang, Z.-L., Mitchell, K. E., Chen, F., Ek, M. B., Barlage, M., Kumar, A., Manning, K., Niyogi, D., Rosero, E., Tewari, M., and Xia, Y. (2011). The commu-

nity Noah land surface model with multiparameterization options (Noah-MP): 1. Model description and evaluation with local-scale measurements. *Journal of Geophysical Research: Atmospheres*, 116(D12). doi: 10.1029/2010JD015139.

Norwegian Meteorological Institute (MET Norway) (2020). Open source emep msc-w model. Open source code for the EMEP CTM v4.36 available at: https://github.com/metno/emep-ctm, Accessed: 2022-11-01.

Park, S., Allen, R. J., and Lim, C. H. (2020). A likely increase in fine particulate matter and premature mortality under future climate change. *Air Quality, Atmosphere & Health*, 13(2):143–151. doi: 10.1007/s11869-019-00785-7.

Pedersen, J. S. T., van Vuuren, D. P., Aparício, B. A., Swart, R., Gupta, J., and Santos, F. D. (2020). Variability in historical emissions trends suggests a need for a wide range of global scenarios and regional analyses. *Communications Earth & Environment*, 1(1):1–7. doi: 10.1038/s43247-020-00045-y.

Riahi, K., Rao, S., Krey, V., Cho, C., Chirkov, V., Fischer, G., Kindermann, G., Nakicenovic, N., and Rafaj, P. (2011). RCP 8.5—A scenario of comparatively high greenhouse gas emissions. *Climatic Change*, page 25. doi: 10.1007/s10584-011-0149-y.

Rombout, P. J. A., Lioy, P. J., and Goldstein, B. D. (1986). Rationale for an Eight-Hour Ozone Standard. *Journal of the Air Pollution Control Association*, 36(8):913–917. doi: 10.1080/00022470.1986.10466130.

Royal Netherlands Meteorological Institute (KNMI) (2022). Uurgegevens van het weer in Nederland. https://www.knmi.nl/nederland-nu/klimatologie/uurgegevens, Accessed: 2022-11-01.

Schwalm, C. R., Glendon, S., and Duffy, P. B. (2020). RCP8.5 tracks cumulative CO2 emissions. *Proceedings of the National Academy of Sciences*, 117(33):19656–19657. doi: 10.1073/pnas.2007117117.

Seinfeld, J. H. and Pandis, S. N. (2016). *Atmospheric Chemistry and Physics: From Air Pollution to Climate Change*. Wiley, Hoboken, New Jersey, 3. edition.

Simpson, D., Benedictow, A., Berge, H., Bergström, R., Emberson, L. D., Fagerli, H., Flechard, C. R., Hayman, G. D., Gauss, M., Jonson, J. E., Jenkin, M. E., Nyíri, A., Richter, C., Semeena, V. S., Tsyro, S., Tuovinen, J.-P., Valdebenito, Á., and Wind, P. (2012). The EMEP MSC-W chemical transport model – technical description. *Atmospheric Chemistry and Physics*, 12(16):7825–7865. doi: 10.5194/acp-12-7825-2012.

Skamarock, W. C., Klemp, J. B., Dudhia, J., Gill, D. O., Barker, D. M., Duda, X.-Y., Huang, M. G., Wang, W., and Powers, J. G. (2008). A Description of the Advanced Research WRF Version 3.

Skjøth, C. A. and Geels, C. (2013). The effect of climate and climate change on ammonia emissions in Europe. *Atmospheric Chemistry and Physics*, 13(1):117–128. doi: 10.5194/acp-13-117-2013.

Stelson, A., Friedlander, S., and Seinfeld, J. (1979). A note on the equilibrium relationship between ammonia and nitric acid and particulate ammonium nitrate. *Atmospheric Environment (1967)*, 13(3):369–371. doi: 10.1016/0004-6981(79)90293-2.

Stohl, A., Aamaas, B., Amann, M., Baker, L. H., Bellouin, N., Berntsen, T. K., Boucher, O., Cherian, R., Collins, W., Daskalakis, N., Dusinska, M., Eckhardt, S., Fuglestvedt, J. S., Harju, M., Heyes, C., Hodnebrog, Ø., Hao, J., Im, U., Kanakidou, M., Klimont, Z., Kupiainen, K., Law, K. S., Lund, M. T., Maas, R., MacIntosh, C. R., Myhre, G., Myriokefalitakis, S., Olivié, D., Quaas, J., Quennehen, B., Raut, J.-C., Rumbold, S. T., Samset, B. H., Schulz, M., Seland, Ø., Shine, K. P., Skeie, R. B., Wang, S., Yttri, K. E., and Zhu, T. (2015). Evaluating the climate and air quality impacts of short-lived pollutants. *Atmospheric Chemistry and Physics*, 15(18):10529–10566. doi: 10.5194/acp-15-10529-2015.

Sutton, M. A., Reis, S., Riddick, S. N., Dragosits, U., Nemitz, E., Theobald, M. R., Tang, Y. S., Braban, C. F., Vieno, M., Dore, A. J., Mitchell, R. F., Wanless, S., Daunt, F., Fowler, D., Blackall, T. D., Milford, C., Flechard, C. R., Loubet, B., Massad, R., Cellier, P., Personne, E., Coheur, P. F., Clarisse, L., Van Damme, M., Ngadi, Y., Clerbaux, C., Skjøth, C. A., Geels, C., Hertel, O., Wichink Kruit, R. J., Pinder, R. W., Bash, J. O., Walker, J. T., Simpson, D., Horváth, L., Misselbrook, T. H., Bleeker, A., Dentener, F., and de Vries, W. (2013). Towards a climate-dependent paradigm of ammonia emission and deposition. *Philosophical Transactions of the Royal Society B: Biological Sciences*, 368(1621):20130166. doi: 10.1098/rstb.2013.0166.

Tagaris, E., Manomaiphiboon, K., Liao, K.-J., Leung, L. R., Woo, J.-H., He, S., Amar, P., and Russell, A. G. (2007). Impacts of global climate change and emissions on regional ozone and fine particulate matter concentrations over the United States. *Journal of Geophysical Research: Atmospheres*, 112(D14). doi: 10.1029/2006JD008262.

Taylor, K. E., Stouffer, R. J., and Meehl, G. A. (2012). An Overview of CMIP5 and the Experiment Design. *Bulletin of the American Meteorological Society*, 93(4):485–498. doi: 10.1175/BAMS-D-11-00094.1.

van der Eerden, L. J., Dueck, T. A., Berdowski, J. J. M., Greven, H., and van Dobben, H. F. (1991). Influence of NH_3 and $(NH_4)_2SO_4$ on heathland vegetation. *Acta botanica neerlandica*, 40(4):281–296.

van der Swaluw, E., de Vries, W., Sauter, F., Wichink Kruit, R., Vieno, M., Fagerli, H., and van Pul, A. (2021). Trend analysis of reduced nitrogen components over the Netherlands

with the EMEP4NL and OPS model. *Atmospheric Environment*, 248:118183. doi: 10.1016/j.atmosenv.2021.118183.

Varotsos, K. V., Giannakopoulos, C., and Tombrou, M. (2013). Assessment of the Impacts of Climate Change on European Ozone Levels. *Water, Air, & Soil Pollution*, 224(6):1596. doi: 10.1007/s11270-013-1596-z.

Velders, G. J. M., Maas, R. J. M., Geilenkirchen, G. P., de Leeuw, F. A. A. M., Ligterink, N. E., Ruyssenaars, P., de Vries, W. J., and Wesseling, J. (2020). Effects of European emission reductions on air quality in the Netherlands and the associated health effects. *Atmospheric Environment*, 221:117109. doi: 10.1016/j.atmosenv.2019.117109.

Vieno, M., Dore, A. J., Stevenson, D. S., Doherty, R., Heal, M. R., Reis, S., Hallsworth, S., Tarrason, L., Wind, P., Fowler, D., Simpson, D., and Sutton, M. A. (2010). Modelling surface ozone during the 2003 heat-wave in the UK. *Atmospheric Chemistry and Physics*, 10(16):7963–7978. doi: 10.5194/acp-10-7963-2010.

Watson, L., Lacressonnière, G., Gauss, M., Engardt, M., Andersson, C., Josse, B., Marécal, V., Nyiri, A., Sobolowski, S., Siour, G., Szopa, S., and Vautard, R. (2016). Impact of emissions and +2 °C climate change upon future ozone and nitrogen dioxide over Europe. *Atmospheric Environment*, 142:271–285. doi: 10.1016/j.atmosenv.2016.07.051.

Westervelt, D. M., Horowitz, L. W., Naik, V., Tai, A. P. K., Fiore, A. M., and Mauzerall, D. L. (2016). Quantifying PM2.5-meteorology sensitivities in a global climate model. *Atmospheric Environment*, 142:43–56. doi: 10.1016/j.atmosenv.2016.07.040.

World Health Organization (WHO) (2021). *WHO Global Air Quality Guidelines: Executive Summary*. World Health Organization, Geneva. https://apps.who.int/iris/handle/10665/346168, Accessed: 2022-11-01.

World Health Organization (WHO) (2022). World Health Statistics 2022. https://www.who.int/publications/i/item/9789240051157, Accessed: 2022-11-01.

World Meteorological Organization (WMO (1966). International meteorological tables. WMO-No.188. TP. 94, https://library.wmo.int/doc_num.php?explnum_id=7997, Accessed: 2022-11-13.

World Meteorological Organization (WMO) (2021). Air Quality and Climate Bulletin, No.1. https://library.wmo.int/doc_num.php?explnum_id$=$10887, Accessed: 2022-11-01.

World Meteorological Organization (WMO) (2022a). Air Quality and Climate Bulletin, No. 2. https://library.wmo.int/doc_num.php?explnum_id$=$11300, Accessed: 2022-11-01.

World Meteorological Organization (WMO) (2022b). *State of the Global Climate 2021*

(WMO-No. 1290). WMO. WMO, Geneva. https://library.wmo.int/index.php?lvl=notice_display&id=22080#.Y2FqBWmZPEY, Accessed: 2022-11-01.

Wu, S., Mickley, L. J., Leibensperger, E. M., Jacob, D. J., Rind, D., and Streets, D. G. (2008). Effects of 2000–2050 global change on ozone air quality in the United States. *Journal of Geophysical Research*, 113(D6):D06302. doi: 10.1029/2007JD008917.

Appendices

A Updating SST in WRF

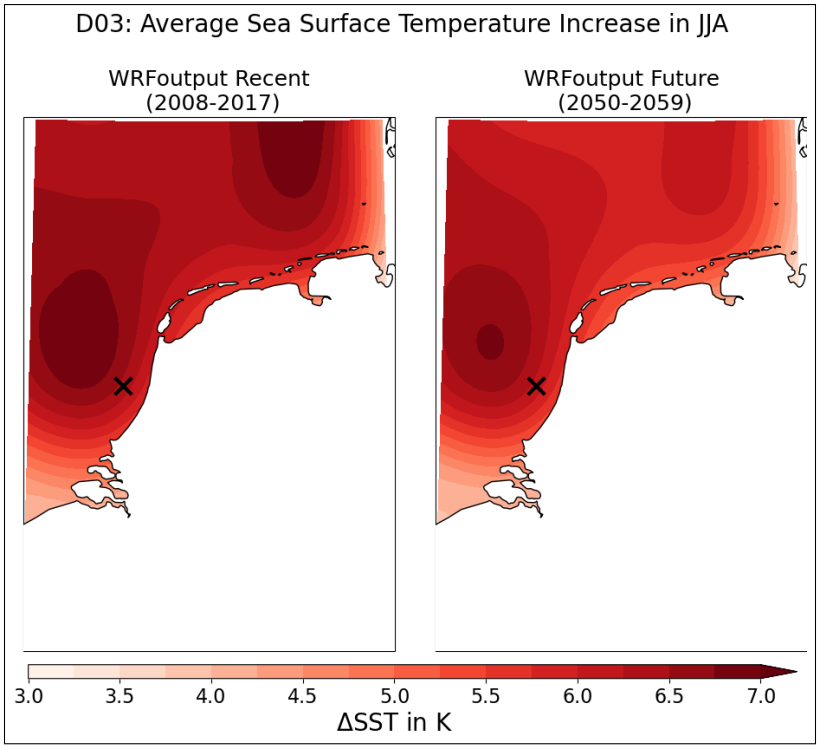

Figure 53: This figure shows the mean difference between the highest and lowest Sea Surface Temperature (SST) in June to August for the 10-years of WRF_recent (2008-2017, first panel) and WRF_future (2050-2059, second panel) in K. The cross marks the position of the SST shown in Figure 54.

Since one of WRF's main applications is short-term weather forecasting, sea-surface temperature, vegetation fractions, sea-ice, and albedo are not updated within a simulation when using the standard setting. Instead their value is kept constant at the initial value throughout the simulation.

For the purpose of this study, simulations spanning the entire summer season at once were performed. To reach a more realistic representation of physical variable fields, SST is included in the HadGEM2-ES RCP8.5 input for WRF (interpolated from monthly values) and added to the Vtable for WPS. In WRF, the SST update option is activated by adding:

`sst_update = 1` in the `&physics` section,

and by adding:

```
auxinput4_inname = "wrflowinp_d<domain>",
auxinput4_interval = 1440,1440,1440,
io_form_auxinput4 = 2,
auxinput5_end_h = 2400
```

in the `&time_control` section both in namelist.input.

Within the summer period, sea surface temperature in the simulated parts of the North Sea and Atlantic increase inhomogenously by up to 11.8°/10.3° in domain 1 and up to 7.0°/6.8° in domain 3 in the recent/future period (see Figure 53).

Figure 54 shows the increase of SST in the 10 years of simulation for WRF_recent and WRF_future at 52.50°N and 4.20°E in the North sea. This shows that while the increase in temperatures over the summer is similar for both time periods, the SST is approximately 2 K higher in WRF_future than in WRF_recent.

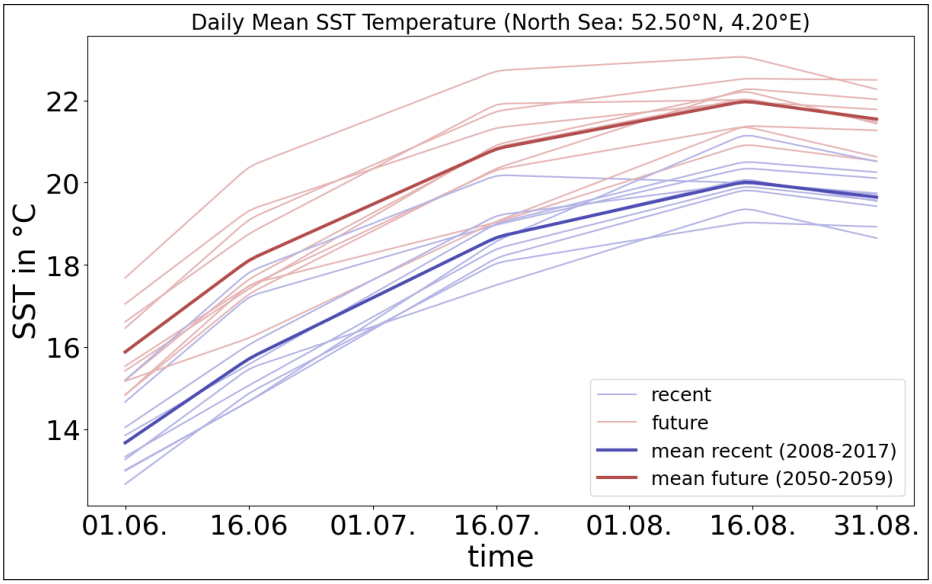

Figure 54: This plot displays the daily mean Sea Surface Temperature at 52.50°N and 4.20°E for June to August. The thin blue/red lines show SST for each year of the recent/future. The thick line represents the respective mean SST.

B The Effect of Humidity Nudging in WRF

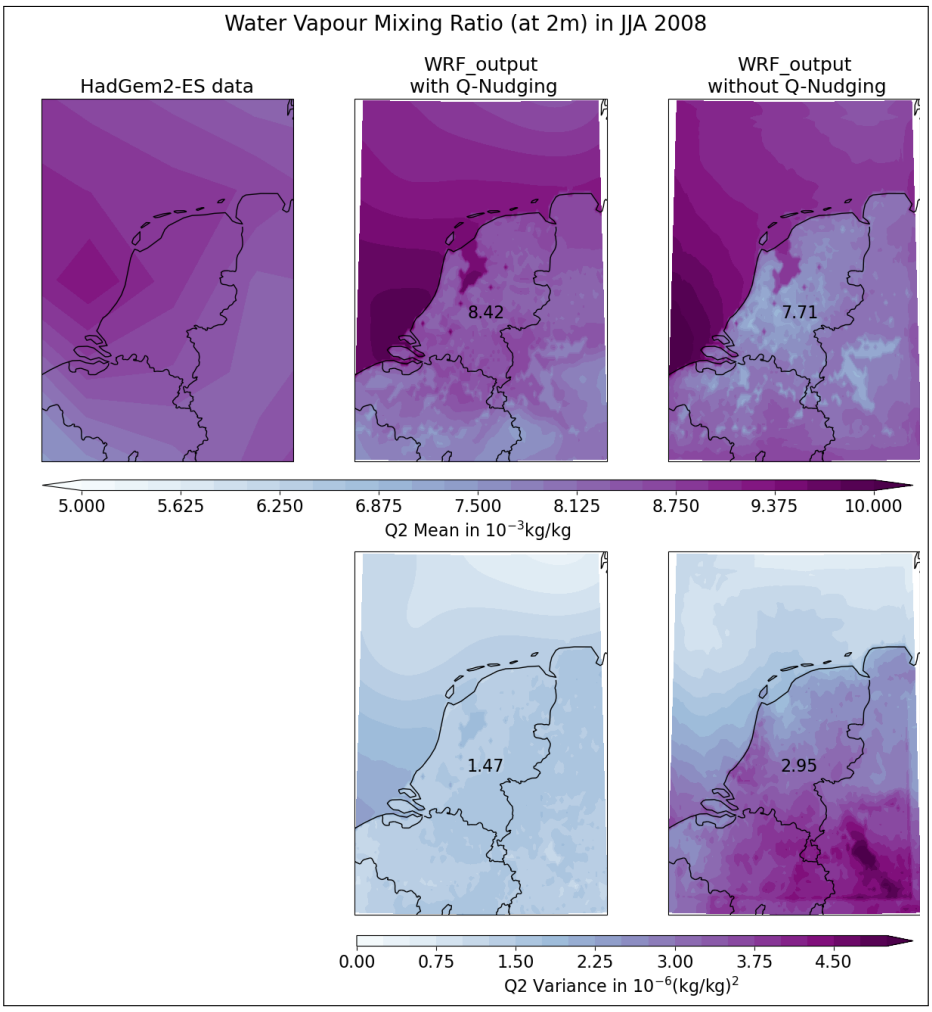

Figure 55: This plot displays the mean (top row) water vapour mixing ratio and its variance (based on hourly values, bottom row) for June to August in 2008. Panel 1 shows the specific humidity in the HadGEM2-ES input for comparison. For the WRF simulation shown in column 2, the humidity nudging coefficient is set to 0.003 s^{-1}. For the WRF simulation shown in column 3, humidity nudging is off. The numbers plotted within the Netherlands show the respective means for the Netherlands in the same respective units.

Newtonian Nudging can be applied in WRF for temperature, wind, and humidity. Using the water vapour nudging option leads to slightly higher mean humidity values, especially in urban areas, but halves its variance. This difference in variance is most pronounced over land areas.

As shown in Figure 56, this change in variability is linked to a major difference in the amount of rainfall. With humidity nudging there is close to no precipitation in the Netherlands (on average 21 mm) and surrounding regions. Without humidity nudging the amount of summertime rainfall increases to 187 mm. The 30-year mean of summertime precipitation between 1991 and 2020 in the Netherlands (KNMI, 2022), is 249 mm with an interannual variance that covers the range between 77 mm (in 2003) to 405 mm

(in 2011). 187 mm fall well within this range.

This effect is likely due to a homogenising effect of low-resolution water vapour nudging on its spatial and temporal distribution in WRF so that the necessary threshold for precipitation is not reached.

Therefore the humidity nudging is disabled for all WRF simulations performed for this study.

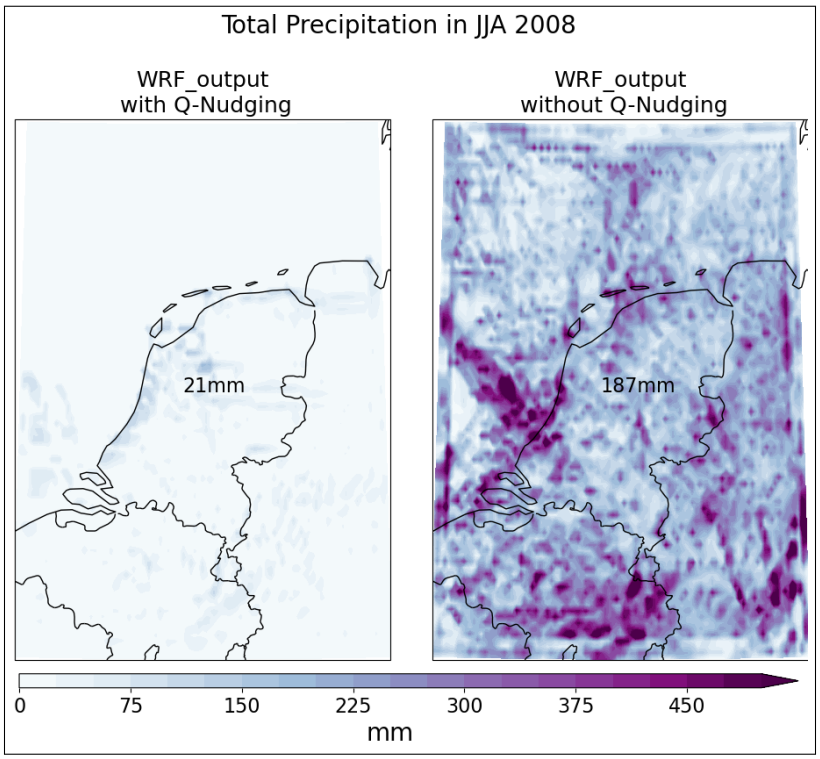

Figure 56: This plot shows the total precipitation for June to August (JJA) in 2008 for one simulation with the humidity nudging coefficient set to 0.0003 s^{-1} (Panel 1) and with humidity nudging off (Panel 2). The values plotted within the Netherlands show the mean total JJA precipitation in 2008 for the Netherlands.

C Extra Figures Model Validation

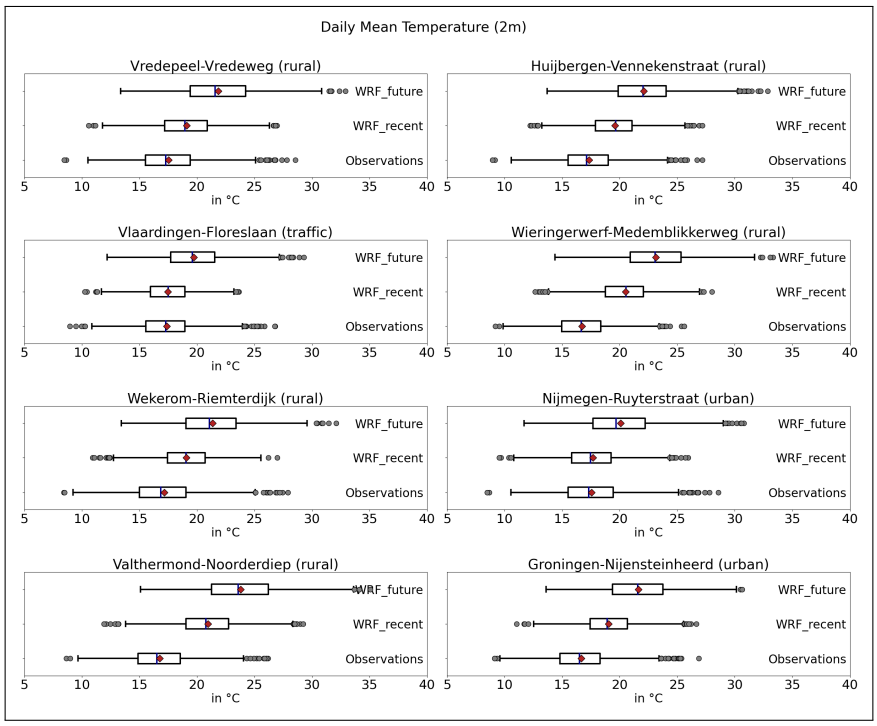

Figure 57: Boxplots of 10-years of daily mean temperatures in summer (JJA) in °C at KNMI stations close by the respective RIVM air quality stations and at the respective locations in WRF_recent (2008-2017) and WRF_future (2050-2059).

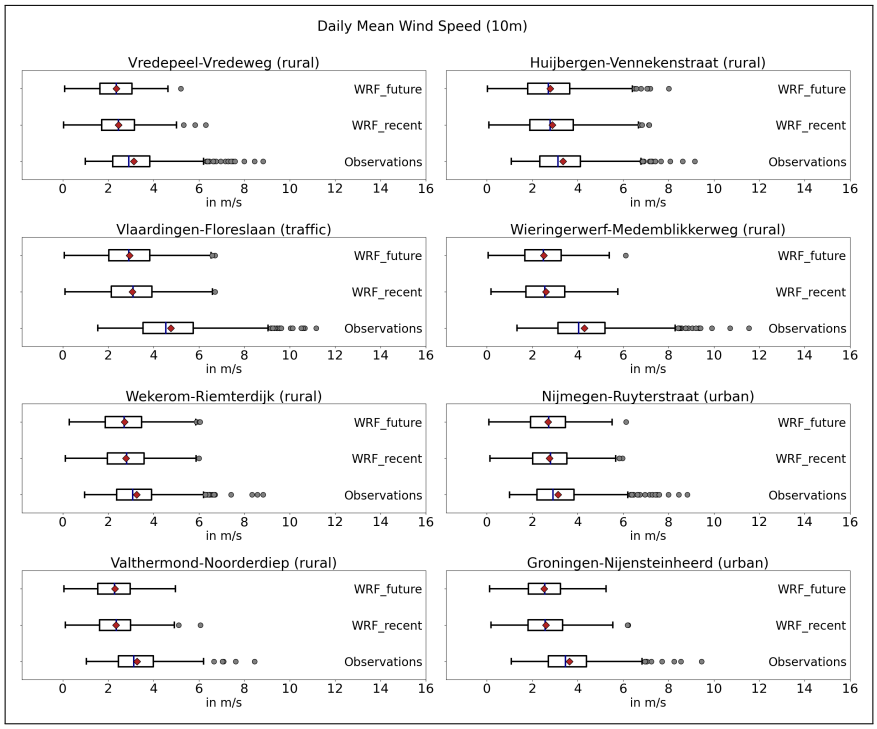

Figure 58: Boxplots of 10-years of daily mean wind speed in summer (JJA) in m/s at KNMI stations close by the respective RIVM air quality stations and at the respective locations in WRF_recent (2008-2017) and WRF_future (2050-2059).

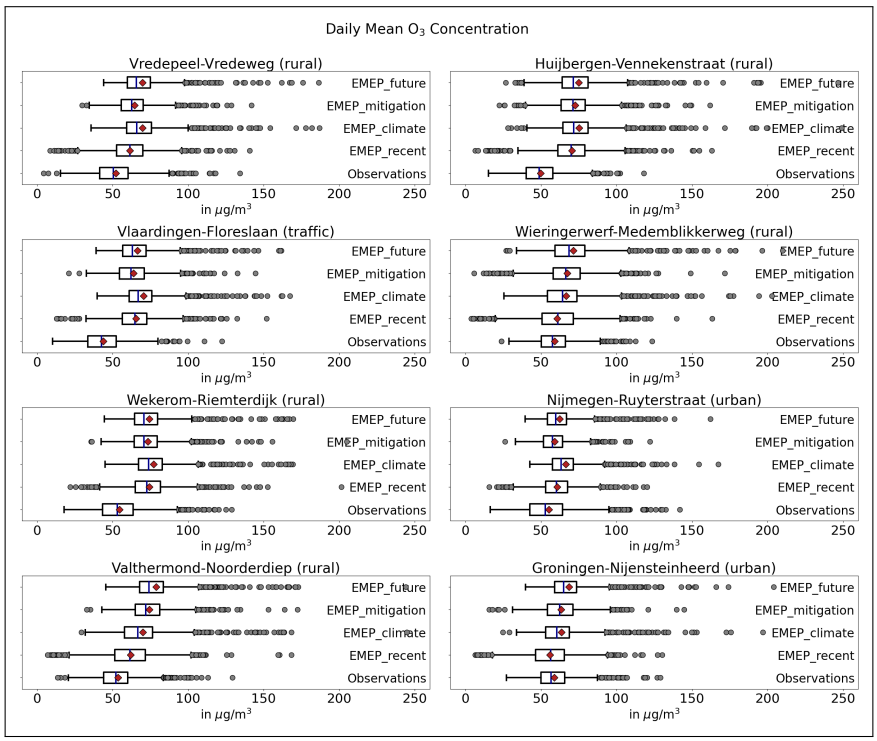

Figure 59: Boxplots of 10-years of daily mean ozone (O_3) concentrations in summer (JJA) in µg/m^3 at RIVM air quality stations and at the respective locations in EMEP_recent, EMEP_climate, EMEP_mitigation, and EMEP_future.

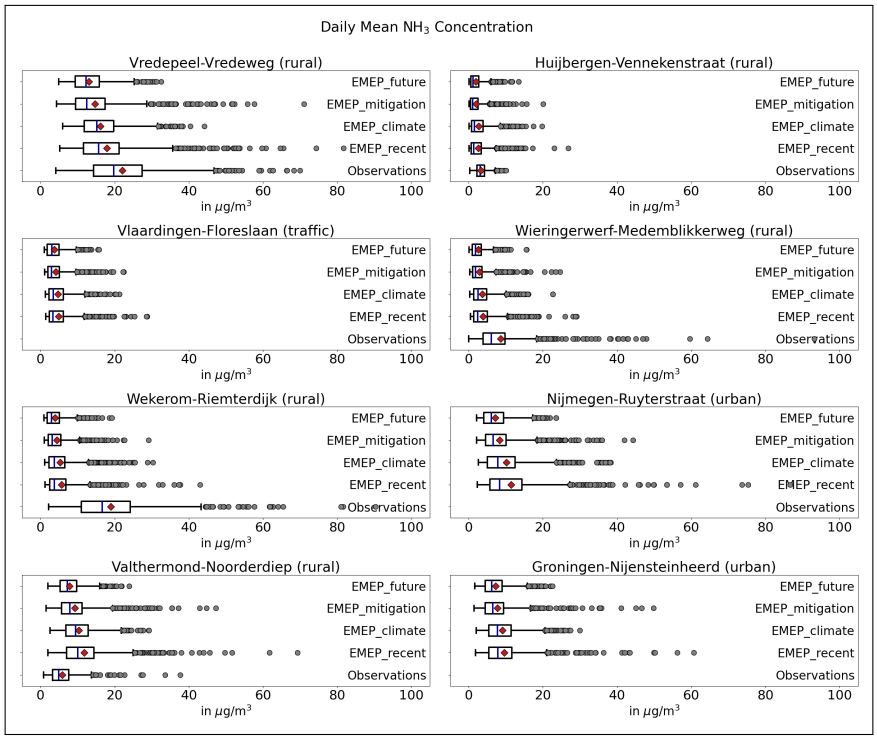

Figure 60: Boxplots of 10-years of daily mean ammonia (NH_3) concentrations in summer (JJA) in µg/m^3 at RIVM air quality stations and at the respective locations in EMEP_recent, EMEP_climate, EMEP_mitigation, and EMEP_future.

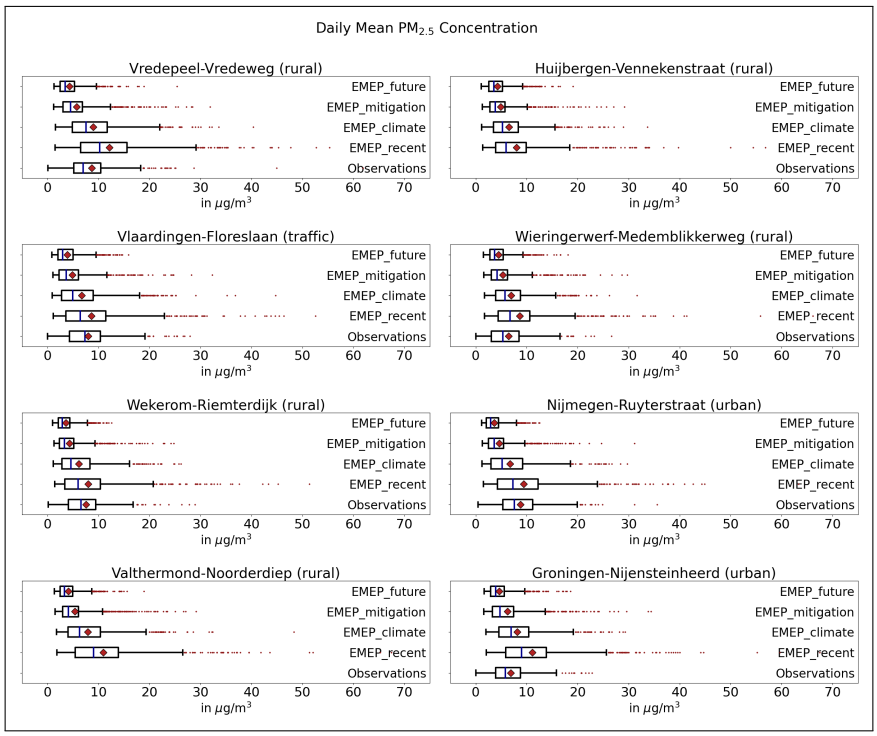

Figure 61: Boxplots of 10-years of daily mean fine particulate matter ($PM_{2.5}$) concentrations in summer (JJA) in µg/m^3 at RIVM air quality stations and at the respective locations in EMEP_recent, EMEP_climate, EMEP_mitigation, and EMEP_future.

D Additional Figures for Results Section

D.1 Changes in Meteorology

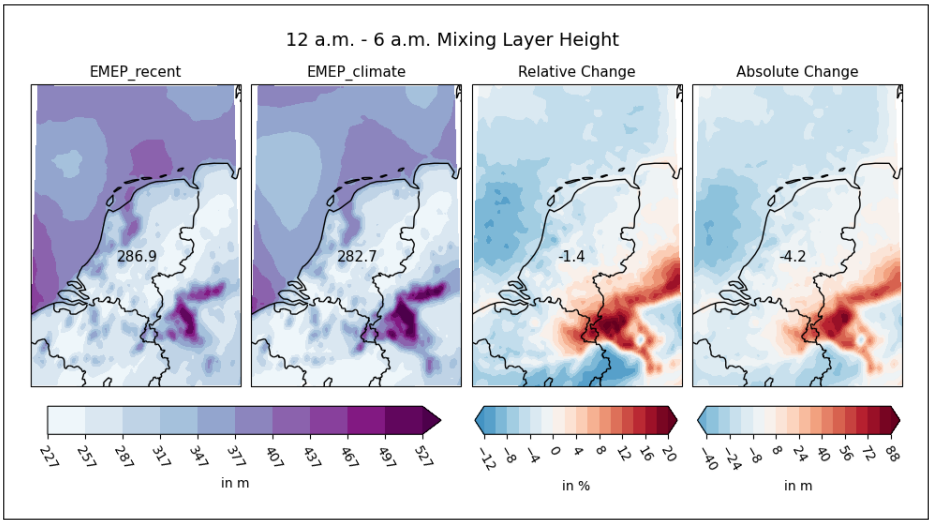

Figure 62: 10-year summertime (JJA) average of the mixing layer height in m between 12 a.m. and 6 a.m. at night as output for domain 3. The first panel shows EMEP_recent (based on WRF_recent: 2008-2017). The second panel shows EMEP_climate (based on WRF_future: 2050-2059). The third panel shows the relative and the fourth panel shows the absolute change between EMEP_recent and EMEP_climate. The numbers in the centre represent the respective means for the Netherlands in the same units.

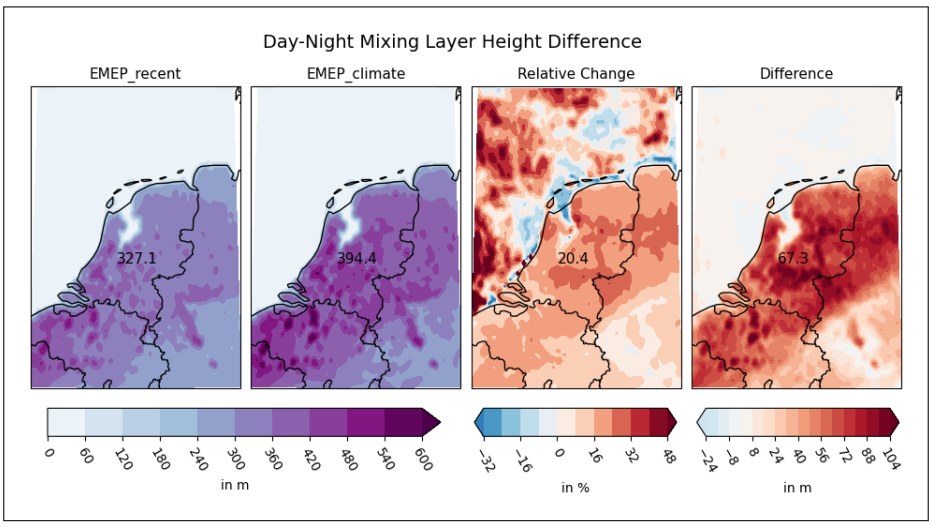

Figure 63: 10-year summertime (JJA) mean mixing layer height difference in m between the afternoon (12 p.m. and 6 p.m.) and night (12 a.m. and 6 a.m.) as output for domain 3 from EMEP_recent and EMEP_climate simulations based on WRF_recent and WRF_future meteorology respectively. Panel 1 displays the difference for EMEP_recent (2008-2017), panel 2 for EMEP_climate (2050-2059). In panel 3 the relative change and in panel 4 the total difference between EMEP_climate and EMEP_recent is shown. The numbers in the centre represent the respective means for the Netherlands in the same units.

D.2 Effect of Climate Change on Air Quality

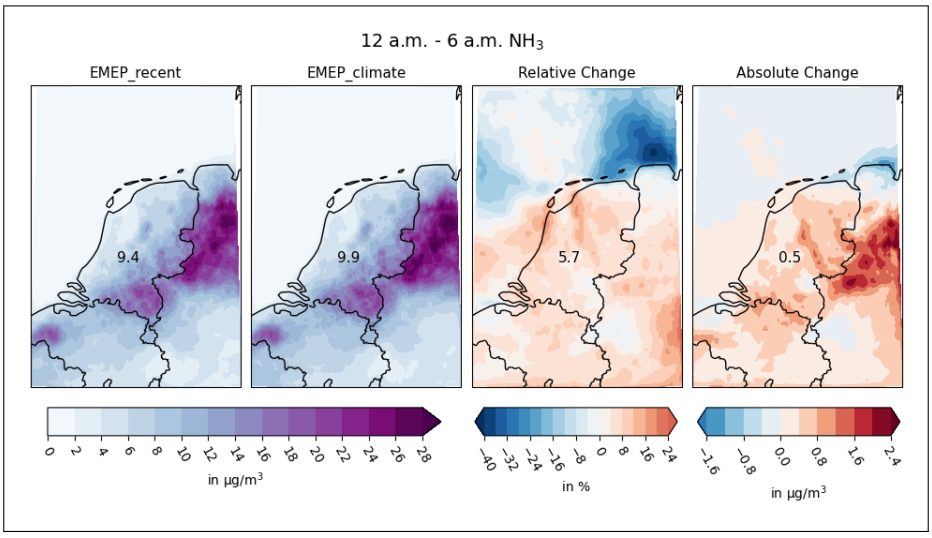

Figure 64: 10-year summertime (JJA) average of the surface NH_3 concentrations in µg/m^3 12 a.m. and 6 a.m. at night as output for domain 3. The first panel shows EMEP_recent (based on WRF_recent: 2008-2017). The second panel shows EMEP_climate (based on WRF_future: 2050-2059). The third panel shows the relative and the fourth panel shows the absolute change between EMEP_recent and EMEP_climate. The numbers in the centre represent the respective means for the Netherlands in the same units.

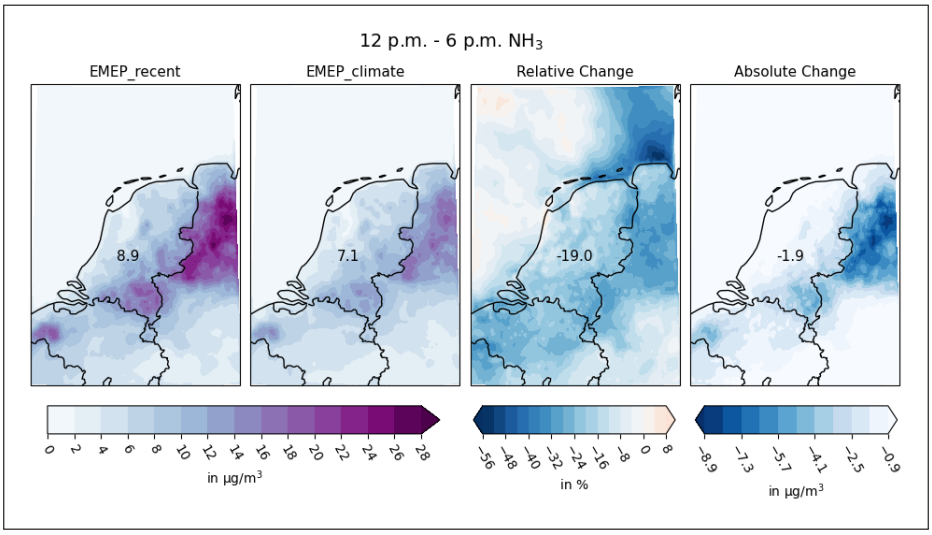

Figure 65: 10-year summertime (JJA) average of the surface NH_3 concentrations in µg/m^3 between 12 p.m. and 6 p.m. at night as output for domain 3. The first panel shows EMEP_recent (based on WRF_recent: 2008-2017). The second panel shows EMEP_climate (based on WRF_future: 2050-2059). The third panel shows the relative and the fourth panel shows the absolute change between EMEP_recent and EMEP_climate. The numbers in the centre represent the respective means for the Netherlands in the same units.

D.3 Effect of Emission Reduction Measures on Air Quality

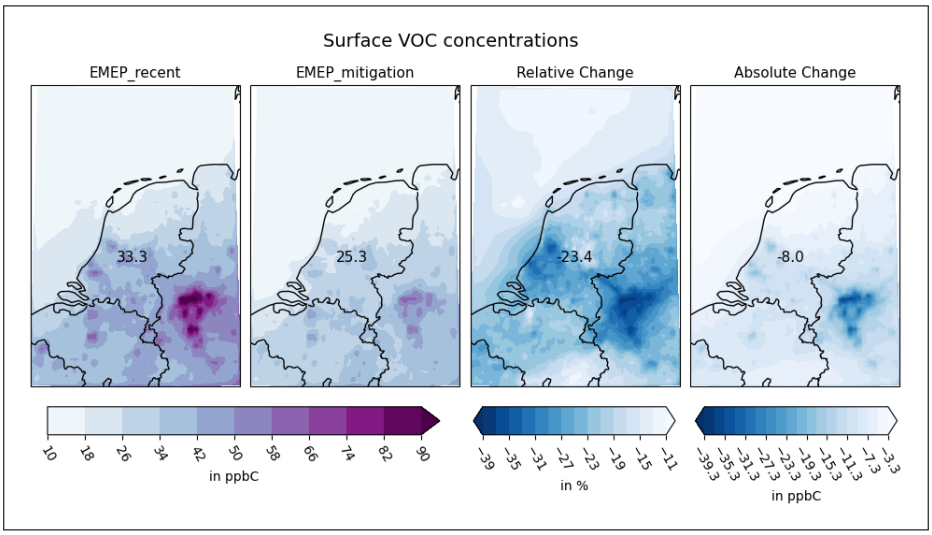

Figure 66: 10-year summertime (JJA) average of daily maximum 8-hour mean surface VOC concentrations in ppbC as output for domain 3. The first panel shows EMEP_recent (based on reported emission for 2008-2017), the second panel shows EMEP_mitigation (based on ECLIPSE V6b MFR 2050 emissions) output, both simulations are based on WRF_recent (2008-2017) meteorology. The third panel shows the relative change and the fourth panel shows the difference between EMEP_mitigation and EMEP_recent. The numbers in the centre represent the respective means for the Netherlands in the same units.

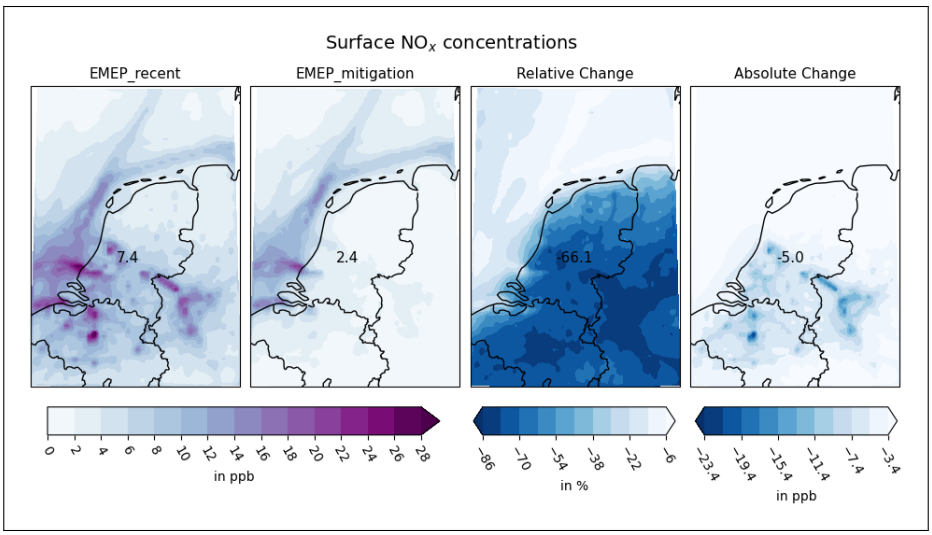

Figure 67: 10-year summertime (JJA) average of daily maximum 8-hour mean surface NO_x concentrations in ppb as output for domain 3. The first panel shows EMEP_recent (based on reported emission for 2008-2017), the second panel shows EMEP_mitigation (based on ECLIPSE V6b MFR 2050 emissions) output, both simulations are based on WRF_recent (2008-2017) meteorology. The third panel shows the relative change and the fourth panel shows the difference between EMEP_mitigation and EMEP_recent. The numbers in the centre represent the respective means for the Netherlands in the same units.